Seychelles Climate Change Scenarios for Vulnerability and Adaptation Assessments

Denis Chang-Seng

BSc (Oceanography and Meteorology)

MSc (Climate)

Prepared for the Seychelles Second National Communication (SNC) Under the United Nations Framework Convention of Climate Change (UNFCCC), and with the Guidance of the National Climate Change Committee (NCCC)

Ministry of Environment and Natural Resources
Republic of Seychelles
October 2007

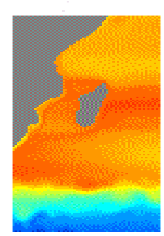

Seychelles Climate Change Scenarios for Vulnerability and Adaptation Assessment

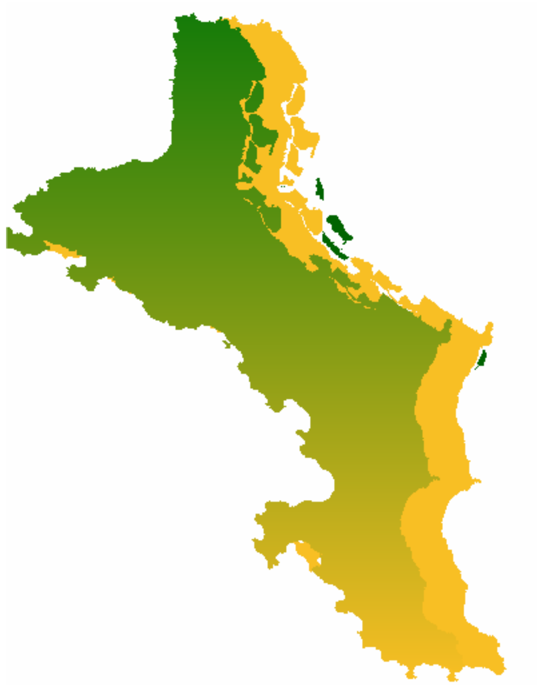

Seychelles Second National Communication
Under the UNFCCC

Ministry of Environment and Natural Resources
Government of Seychelles

Denis Chang-Seng
October 2007

Reviewers

Theodore Marguerite, Antoine Marie Moustache

CONTENTS

Abbreviations

INC	Initial National Communication
SNC	Second National Communication
IPCC	Intergovernmental Panel on Climate Change
TAR	Third Assessment Report
FAR	Fourth Assessment Report
UNFCCC	United Nations Framework Convention on Climate Change
NCEP	National Center of Environmental Prediction
GCM	General Circulation Model
SCENGEN	SCENario GENerator
SRES	Standard Range Emission Scenarios
GPM	Guided Perturbation Method
RCPM	Regional Climate-Change Projection from Multi-Model Ensembles
NCAR	National Center for Atmospheric Research
UCAR	University Corporation for Atmospheric Research
SO_2	Sulphur Dioxide
CO_2	Carbon Dioxide
PDF	Probability Density Function
BM	B2 mid-range emission with mid-range climate sensitivity
AH	A1 high-range emission with high-range climate sensitivity
(DJF)	December, January, February
(MAM)	March, April, May
(JJA)	June, July, August
(SON)	September, October, November
ENSO	EL Nino Southern Oscillation
ITCZ	Inter Tropical Convergence Zone
MJO	Madden Julian Oscillation
TC	Tropical Cyclone
QBO	Quazi Biennial Oscillation
AMO	Atlantic Multi-Decadal Oscillation
IODM	Indian Ocean Dipole Mode
SST	Sea Surface Temperature
O_{18}	Oxygen isotope

Chapter 1

Introduction, Background, Data and Methodologies

1.0 Introduction, Background, Data and Methodologies

1.1 Introduction and Background

Climate is always changing. However, accelerated climate change brought about by human emission of green house gases are of global concern as it threatens ecosystem, sustainable development and human capacities to cope and adapt. The IPCC Fourth Assessment Report (FAR) in 2007 concludes that the observed widespread warming of the atmosphere and ocean, together with ice mass loss, support the conclusion that it is extremely unlikely ((<5%) that global climate change of the past fifty years can be explained without external forcing, and very unlikely (<10%) that it is not due to known natural causes alone. Below is a summary of the climate trends and the characteristics extracted from the Climate Variability and Climate Change Assessment for Seychelles (Chang-Seng, 2007), under the Second National Communication of the IPCC (2007).

"*The trends and characteristics of the Seychelles climate are assessed by analyzing various short terms (1972-2006) and longer term data sets. Overall, the latest temperature trends based on maximum and minimum temperature show warming between +0.33 and +0.82°C respectively and are significantly warmer than previously assessed in the Initial National Communication. The minimum temperature is warming faster than maximum temperature as a result of the 'urban island heat' effect and the warming is higher during the southeast monsoon. The 2007 monthly average maximum temperature observations show record warming of +1.7, +2.5 and +1.3°C for January, February and March respectively compared to the 1972-1990 periods. The record warming in temperature is attributed to a number of factors such as the development of a moderate El Nino late in 2006, an active cyclone season to the northeast of Madagascar, a pronounced positive phase of the Madden Julian Oscillation (MJO) suppressing cloud development in the southwest Indian Ocean and the potential increasing background effect of the green house global warming. The ENSO influence on global rise in air temperature is complex and not clearly* *understood. The warming in air temperature is also reflected in the longer-term data sets.*

The linear trend of the SST data available at the Seychelles International Airport suggests a gradual cooling in SST since 2000; however no firm conclusions can be drawn from such limited data set. The Climate Research Unit's (CRU) SST data and observed air temperature have a strong positive relationship at a 3-4 year cycle rather than a decadal relationship as suggested initially (Payet et al., 1998). The governing force is found to be linked to both the ENSO and the Rossby wave mechanisms (Chang-Seng, 2005). Paleo-climate studies support the hypothesis that drier rather than wetter conditions prevailed during the late Pleistocene period (Heirtzler, 1977). Recently, it was found that the coral isotope (O18) extracted from corals at Beau-Vallon Bay, Mahe, Seychelles and the CRU SST have a consistent upward trend suggesting a warming and a potentially wetter climate trend.

The annual sea level trend anomaly is +1.46 mm per year with a standard error of ± 2.11 mm per year. Most stations in the southwest Indian Ocean are reporting a similar positive trend particularly in the Mauritius and Reunion area. On the other hand, satellite altimetry shows negative sea level in the southwest Indian Ocean from 1993. Therefore, there is no firm evidence of forced sea level rise. The local sea level trends are rather consistent with the global average sea level rise with an average rate of +1.8 mm (1.3 to 2.3 mm) per year over the 1961 to 2003 period. According to the FAR (2007), the underlying cause of sea level rise is due to the decline of mountain glaciers and snow cover in both hemispheres and expansion through thermal warming of the ocean. The 1997-98 periods abnormal extreme events in sea level and rainfall were not only due to the El Nino (Payet et al., 1998), but there was a coupling between the El Nino and Indian Ocean Dipole Mode (Chang-Seng, 2002). It was characterized by a drop in SST in the southeastern part of the Indian Ocean while the SST rose in the western equatorial Indian Ocean, causing ocean thermal expansion and rise in regional and local sea level. Therefore, coastal erosion and inundation impacts may also be viewed as a result of EL Nino, Indian Ocean Dipole (IOD) superimposed on other normal phenomena such as "cyclonic"' generated swell-storm surges and spring tides; all colluding coincidentally to create an abnormal impact as was the case towards in the end of the second week of May 2007.

On the other hand, the lack of expertise to integrate modeling and detailed assessment in increasing coastal developments may change coastal dynamics and processes which may only have negative impacts on the environment.

In addition, the impact of ENSO (El Nino/ La Nina) causes a significant shift in seasonal rainfall pattern rather than an overall increase in both seasons as suggested by Payet et al.,in 1998. The rainy season is more likely than not to be relatively dryer while the dry season is more likely than not to be wetter during El Nino and vice versa for La Nina years (Chang-Seng, 2002).

The dry season is characterized by wetter conditions compared to the 1972-90 periods. The spatial variability of rainfall shows that most areas are wetter than normal in both seasons and annually, with the exception towards the southwest of Mahe. Heavy rainfall events have been the major contributor to the increase in rainfall (Lajoie, 2004). However, the filtered annual rainfall data have a surprising downward rainfall trend. The long term trend of a merged 119-year monthly rainfall data confirms strong rainfall variability over Mahe, Seychelles. It is characterized by distinct 2-4, 10 and 30-year cycles. The 2-4 year cycles are linked to the ENSO, biennial cyclone variability and the QBO (Chang-Seng, 2005). The decadal rainfall cycle is linked to the sunspot cycle (Marguerite, 2001) and the decadal variability in intense tropical cyclone (Chang-Seng, 2005). One of the most interesting and important findings of this assessment is the detection of the 30-year cycle characterized by periods of abnormally high and low rainfall trends operating as a background low climate signal. It is suggested that the 30-year natural cycle has gradual, but significant influence on the long term climate variability in the Seychelles. It is proposed that the 30-year cycle in rainfall is tele-connected to the Atlantic Multi-Decadal Oscillation in sea surface temperature through the ocean thermohaline circulation which distributes heat globally. Although the long term annual rainfall shows an upward trend in rainfall of +2mm per year, it is also clear that the upward trend is not consistent or maintained when the data is filtered further.

Studies by Hoareau (1999) have suggested an increase in intense TCs in the SWIO for the decades 1970-79 and 1990-99, while a decrease in the1980-90s. However, in a recent study (Chang-Seng, 2005) it was shown that the decade 1960-69 was the most active in intense tropical cyclone days in the SWIO. In addition, the linear trend is negative with a decreasing rate of 0.14 intense tropical cyclone day per year in the *southwest Indian Ocean from 1960 to 2005. It was also found that intense TCs are characterized by biennial to decadal cycles that are related by Quasi Biennial Oscillation and the decadal variability in the deep ocean thermohaline circulation respectively. Furthermore, tropical cyclone has decreased at a rate of -0.023 tropical cyclone day per year. In contrast, the number of tropical depression has an upward trend of +0.025 tropical depression per year possibly linked with a warming in SST in the south central Indian Ocean. The recent tropical cyclone direct impacts in the Seychelles portrays that the cyclonic belt and risks area is widening possibly associated with global warming. However, there is simply no firm evidence to draw such conclusions due to lack of data and scientific research. There were similar TC strike probabilities in the past caused by 'anomalous' variation in weather patterns (Parker and Jury, 1999; Chang-Seng, 2005) occurring at the time. The ENSO impact on tropical cyclone activity shows that EL Nino characterized by anomalous SST warming favours less intense tropical cyclone while mild La Nina is favourable for an increase in intense tropical cyclone in the SWIO. There is a compromise between SST and wind shear effect on intense TC development (Gray 1984 a, b; Shapiro, 1987; Chang-Seng, 2005). TCs are likely to track westward during La Nina and southwards during El Nino"*.

The immediate concern is a need to address the growing global climate-environmental risks, though uncertainties and climate complexities such as the effects of climate feedbacks remain unclear. In that context, the United Nations Framework Convention on Climate Change (UNFCCC) requires non-annex 1 parties to prepare Vulnerability and Adaptation Assessments for climate change. These assessments explore and, where possible, quantify the vulnerability of various systems and sectors to climate variability and climate change. Thus, it is crucial to identify critical thresholds of regional climate change beyond which whole systems or sectors may be unsustainable, ineffectively or collapse. Thus, it is not only important to asses past and recent climate (part 1), but also to actually asses, through robust methods and techniques, climate scenario and its impacts at the finest spatial and time resolution as possible. Though daunting and challenging, as there are many uncertainties, climate scenarios help in the vulnerability and adaptation assessments. Complex experiments or research to generate regional and national climate scenarios are simply not available to all countries. On this premise, simple climate scenario generators (CSGs) are useful if it can address the behaviour of complex models; explore rapidly and efficiently climate predictions and their uncertainties for many regions. The MAGICC-SCENGEN forms one such scenario model. It is of low cost and a flexible tool for generating regional and national climate scenarios. It has been used extensively by the IPCC and member countries.

The Seychelles Initial National Communication (INC) adopted the Intergovernmental Panel on Climate Change (IPCC) publications of 1996 on global climate scenarios in its assessment on the identified sectors. Thus, the assessment did not use climate scenarios to carry out national vulnerability and adaptation assessments of climate change. As a consequence, there was a lack of confidence in the magnitude, time and location of potential future climate change impacts. The uncertainties of climate change and its impacts were also not assessed. As a result of these general global projections, national policy makers and decision makers might not have responded effectively.

1.2 Data and Methodology

1.2.1 MAGICC SCENGEN

The MAGICC SCENGEN software tool is employed to carry out a climate scenario for vulnerability and adaptation assessments towards the Seychelles' Second National Communication (SNC). MAGICC/SCENGEN is a coupled gas-cycle/climate model (MAGICC) that drives a spatial climate-change scenario generator (SCENGEN). MAGICC has been the primary model used by IPCC to produce projections of future global-mean temperature and sea level rise. The climate model in MAGICC is an upwelling-diffusion energy-balance model that produces global- and hemispheric-mean output. The 4.1 version of the software uses the IPCC TAR (Third Assessment Report) version of MAGICC.

Global-mean temperatures from MAGICC are used to drive SCENGEN. SCENGEN uses a version of the pattern scaling method described in Santer et al. (1990) to produce spatial patterns of change from an extensive data base of atmosphere/ocean GCM (AOGCM) data from the CMIP data set. The pattern scaling method is based on the separation of the global-mean and spatial-pattern components of future climate change, and the further separation of the latter into greenhouse-gas and aerosol components. Spatial patterns in the data base are 'normalized' and expressed as changes per 1^{o}C change in global-mean temperature. For the SCENGEN scaling component, the user can select from a number of different AOGCMs for the patterns of greenhouse-gas-induced climate.

SCENGEN is a climate SCENario GENerator that uses the output from MAGICC to produce maps showing the regional details of future climate. The MAGICC and SCENGEN outputs are gas concentrations; radiative forcing breakdown; global-mean temperature and sea level while the SCENGEN outputs are baseline climate data; model validation results; changes in mean climate; changes in variability; signal-to - noise ratios and probabilities of precipitation increase. The overall purpose of using MAGICC-SCENGEN software tool is to conduct climate scenario development for expert and non-expert users, 'hands on' education for climate change issues and access to climate model and observed climate data bases. The MAGICC SCENGEN tool does not provide all the solutions but it can address the following issues:

- Global-mean temperature change for a given emissions scenarios;
- The uncertainties in climate projections;
- Management to stabilize greenhouse-gas concentrations;
- Details of changes in regional climate patterns;
- Changes in climate variability;
- Assess model differences;
- Assessment of the probability of an increase/decrease in precipitation at a given location.

The new version of MAGICC/SCENGEN is designed to serve the following purposes:

(1) To update MAGICC to the version used in the IPCC TAR;
(2) To include the SRES emissions scenarios (with the attendant expansion of the range of gases for which future emissions can be specified) in MAGICC's emissions data base, and to add new emissions scenarios for the stabilization of CO_2 concentration allowing for the effects of climate feedbacks on the carbon cycle (see below);
(3) To improve SCENGEN's baseline observed climate data base to give full global coverage rather than, as in version 2.4, land coverage only;
(4) To employ new and more up-to-date climate model results in the SCENGEN data base;
(5) To allow users to investigate changes in variability;
(6) To quantify uncertainties in terms of inter-model differences, and use these to give probabilistic outputs;

(7) To quantify uncertainties in the time domain through standard signal-to-noise ratios, where the signal is the change in the mean state and the noise is the baseline inter-annual variability;

(8) To provide area-average outputs for user-definable regions and for a library of standard regions.

The assessment also compares the two possible future climate change scenarios using the Standard Range Emission Scenarios (SRES) mid-range emission scenario i.e B2 mid-range emission with a mid range climate sensitivity of 2.6°C and the A1 high-range emission with high range climate sensitivity of 4.6°C. It is advantageous to consider more than one emission scenarios and climate sensitivities in a V & A assessment, given the uncertainty associated with future climate greenhouse gas and SO2 emissions. The IPCC 2000 published four SRES storylines can be summarised as follows:

1. SRES A1: The pursuit of personnel wealth is more important than environmental quality. There is very rapid economic growth, low population growth, and new and more efficient energy technologies are rapidly introduced;
2. SRES A2: Strengthening of regional cultures, an emphasis on family values, and local traditions, high population growth, and less concern for rapid economic development;
3. SRES B1: A move towards less materialistic values and the introduction of clean technologies are emphasized. Global solutions to environmental and social sustainability are sought, including concerted efforts for rapid technology development dematerialisation of the economy and improving equity;
4. SRES B2: The emphasis is on local or regional solutions to economic, social, and environmental sustainability.

In MAGICC SCENGEN 4.1, the IS92a emission scenario is replaced by the P50 emission scenario.

The assessment considers spatial and temporal patterns at seasonal to annual climate change pattern for the two identified climatic regions consisting of the Mahe group and the Aldabra group for the years 2025, 2050 and 2100. The reference baseline climate condition is from 1972 to 90.

The input model parameters include aerosols, carbon dioxide feedback effects, variable ocean thermocline, ocean and atmospheric vertical diffusion, and ice melt which is the result of glacier melt within the process. A selection of seven Global Circulation Models (GCMs) is employed to assess regional climate changes. The GCMs used are as follows: CSM (); ECH3 (Germany); ECH4 (Germany/European); GFD (Manabe et al., (1991) and Stouffer et al., (1994)); HAD2 (UK); HAD3 (UK); and MODBAR ().The local parameters assessed are average maximum temperature, average minimum temperature and rainfall. The assessment also explores for a single future 'national' climate pattern by constructing GCMs composite fields. Climate scenario uncertainties are also addressed.

Scaling of GCM change fields with local data was applied since Global Circulation Models (GCM) is at a 5 degree resolution (500 km) while local data is at less than 1 degree resolution. In order to determine those changes at a particular location within the selected GCM boundary, the changes in mean precipitation at GCM resolution of 5 degree were applied to the observed mean seasonal or annual precipitation data for Mahe, Seychelles.

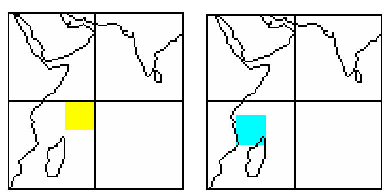

(a) (b)

Fig 1.1: Modeled area (a) Mahe (b) Aldabra

1.2.2 General Circulation Model (GCM)-Guided Perturbation Method (GPM)

The GCM-Guided Perturbation Method (GPM) for regional climate change scenarios developed by Hewitson, University of Cape Town is investigated as a possible methodology for integration in the climate change scenario generation, and adaptation assessments. It is not a GCM downscaled methodology, but it does represent a regional scale perturbation in accordance with the GCM first order response to greenhouse gas forcing. Consequently, this allows one to undertake an assessment of fundamental regional sensitivities to climate change in a manner that is not arbitrary but guided by GCMs.

1.2.3 Regional Climate-Change Projection from Multi-Model Ensembles (RCPM)

Regional Climate-Change Projection from Multi-Model Ensembles (RCPM) is a statistical analysis of the projections made by different climate models developed by the National Center for Atmospheric Research (NCAR) and the University Corporation for Atmospheric Research (UCAR) in 2006. The Bayesian statistical model is used to synthesize the information in an ensemble of global climate models (GCMs) into a probability density function (PDF) of change in temperature or precipitation for a given geographic region. A PDF describes the likelihood that an unknown variable will take on a value found within a particular range. Bayesian analysis uses known data to infer probabilistic values for unknown data that are consistent with the known values. This allows one to infer the reliability of the models' forecasts for the future (which is unknown) based on their ability to reproduce observed data and their agreement with one another (both of which are known).

In generating the PDF, the analysis assigns an implicit weight to each model's contribution based on two factors: bias and convergence. A model's bias is assessed by comparing its reproduction of the current climate to observed historical data, averaged over a region and season of interest. Convergence among models is rewarded by giving relatively more weight to projections that agree with the other members of the ensemble than to outliers. Because agreement between models may be due to model dependence, the analysis down weighs the convergence criterion relative to the bias criterion.

The analysis is performed at a regional scale, area-averaging data from several grid points into regional means of temperature and precipitation. For any given season and emissions scenario, the Bayesian model is used to determine a PDF of temperature and precipitation change. The emission scenarios selected is the SRES A1B (mid-range); and change is the difference between two 20-year averages, for example the 1980-1990 periods. This analysis covers a region that is represented in the climate models as Open Ocean. Because the models are too coarse-grained to include any islands in the region, the climate projections given here only apply over open water, and do not necessarily reflect the effects of climate change over any islands. In order to understand the implications of ocean climate change for islands in this region, one would need to apply local expertise and understanding of how ocean climate is related to and influences island climate.

1.2.3.1 Caveats and Cautions

- The uncertainty range as represented by the PDFs does not encompass all the uncertainties that characterize climate change projections, especially at regional scales. In particular:
    - The PDFs are conditional on the specified emissions scenario. Probabilities are not assigned to the different scenarios;
    - Generally speaking, the projections are conditional on the GCMs used. The GCMs are acquired from the PCMDI archive organized by IPCC Fourth Assessment Report (FAR) participants. These GCMs are state-of-the-art coupled climate models, but each of them carries considerable uncertainty in its parameterizations and in its representation of processes and dynamics, especially at regional scales. These uncertainties have not been explicitly incorporated into the analysis;
    - For regions of complex topography and small extent, the preceding caveat is even more significant than it is for large areas over smooth terrain. Consequently, an area encompassing 4 grid points (a grid point is approximately 2.8 degrees on each side) is the minimum extent to comfortably address the issue using this framework;
- PDFs are normalized so the area under the curve integrates to 1**.** It is only meaningful to speak of probabilities for a range of possible values (e.g. 60% probability of warming between 2 and 4 ^{o}C) and not for a single value;
- Changes in temperature and precipitation are derived separately; the quantiles of one distribution should not be associated with the corresponding quantiles of the other;
- Change in precipitation is presented in both absolute and relative amounts. The percentage change values for areas with low precipitation can be very large even though the absolute change is small;

- Each model's grid has been interpolated to the median resolution of the available models, the T42 Gaussian grid. This grid covers the globe with 64 grid points in latitude and 128 grid points in longitude.

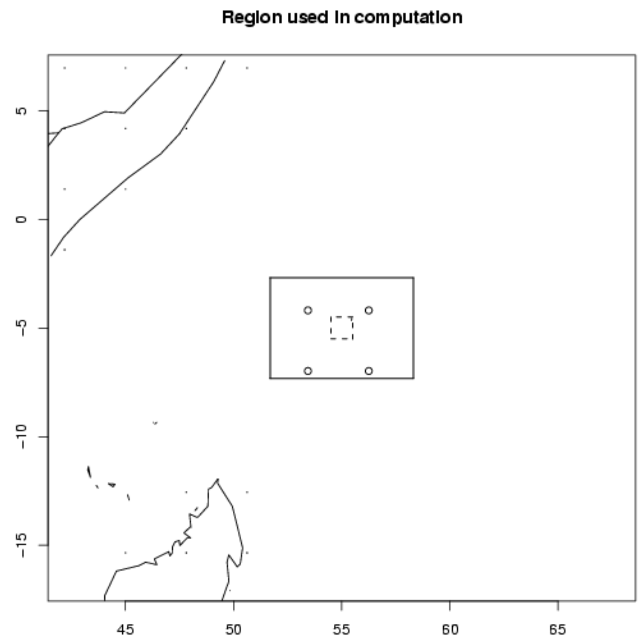

Fig1.2: RCPM modeled area

Chapter 2

Global-Scale Climate Changes

2.0 Global-Scale Climate Changes

The assessment of global-scale climate changes in this section of the V&A compares two possible future climate change scenarios using the B2 mid-range emission with a mid range climate sensitivity of 2.6 ^{o}C and the A1 high range emission with a high range climate sensitivity of 4.6 ^{o}C. It is also valuable to consider more than one emission scenarios and climate sensitivities in a V & A assessment, given the uncertainty associated with future climate greenhouse gas and sulphur dioxide (SO_2) emissions. Figures 2.1 to 2.6 are the MAGICC output comparisons between the global carbon dioxide concentrations (ppmv), mean temperature (^{o}C) and the mean sea level changes (cm) derived from the two climate scenarios abbreviated as BM and AH scenarios respectively.

2.1 Global Carbon Dioxide Concentrations

Table 2.0 summarises the differences between the two scenarios. In brief, the BM policy best guess scenario for carbon dioxide concentration is projected to increase from 430, 480 and 620 ppmv for the years 2025, 2050 and 2100 respectively. In contrast, the AH policy best guess shows an increase from 430, 530 and 730 ppmv respectively for the above cited years.

2.2 Global Mean Temperature

The corresponding temperature change for the BM policy best guess scenario shows global warming from 0.7, 1.3 and 2.5 ^{o}C while the AH policy best guess warming range from 0.8, 1.7 and 3.0 ^{o}C for the years 2025, 2050 and 2100 respectively.

2.3 Global Sea Level

The BM policy best guess average global sea level rise are 7, 15 and 35 cm while 8, 17 and 40 cm for the case of the AH scenarios for the years 2025, 2050 and 2100 respectively.

Overall, the A1 high-range emission with high climate sensitivity simulates higher global mean temperatures and sea level changes. The mean global temperature changes range from 0.7-3.0 ^{o}C, while sea level changes range from 7 to 40 cm from the years 2025 to 2100. The next step is to use SCENGEN as the climate SCENario GENerator. SCENGEN requires the output from MAGICC to produce maps showing the regional and national details of future climate. As discussed in chapter 1, the SCENGEN outputs include baseline climate data, model validation results, changes in mean climate, and changes in variability, signal-to noise ratios, and probabilities of increase.

2.3.1 Regional Sea Level

Sea level scenarios for specific region or location are not available in MAGICC-SCENGEN. However, the Hadley Center for Climate Prediction and Research has published the change in annual sea level from the 1960-1990 and the 2070-2100 periods using the IS92 or P50 emission scenario. Sea level rise for the period 2070-2100 is expected to be in the range of 0.5-0.6 meter for HadCM2 (fig 2.7 a), but it is 0.4 -0.5 meter for the HadCM3 model (fig 2.7b).

Thus, the next chapter discusses the B2 mid-range emission scenario with a mid-range climate sensitivity at a national level.

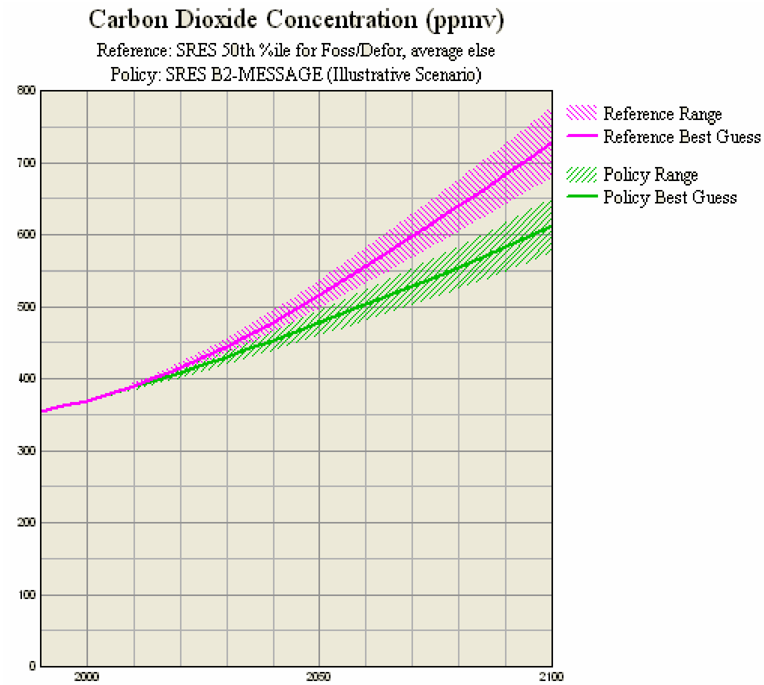

Fig 2.1: Global carbon dioxide concentration for the B2 mid-range emission with mid-range climate sensitivity.

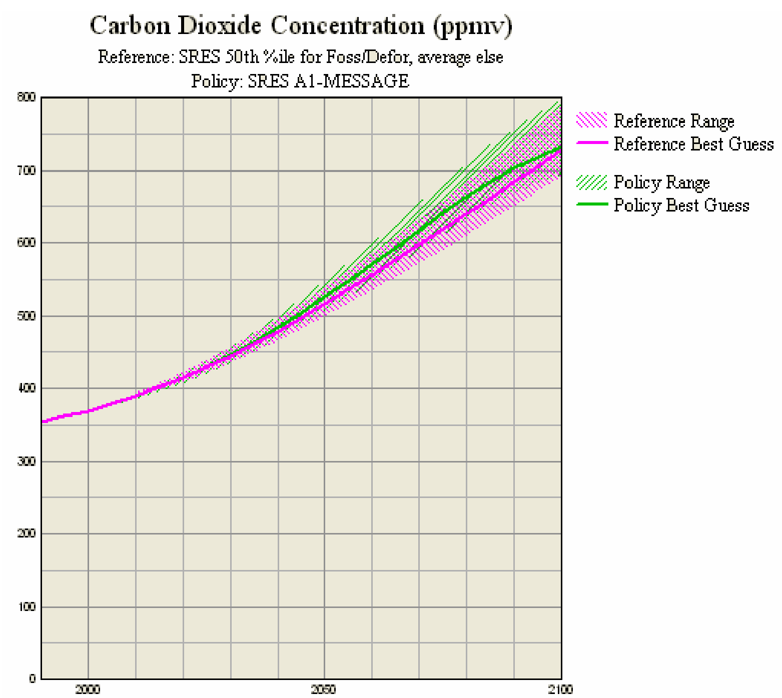

Fig 2.2: Global carbon dioxide concentration for the A1 high-range emission with high- range climate sensitivity.

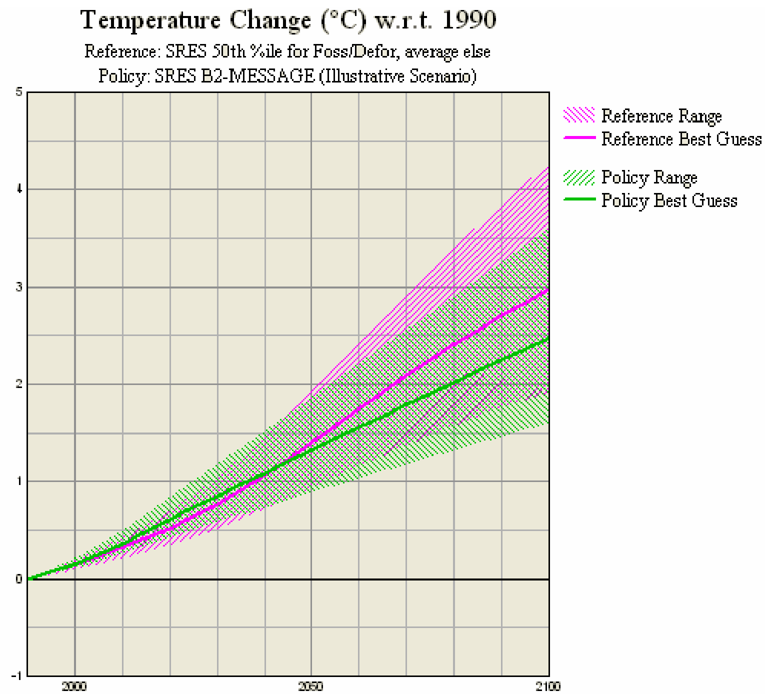

Fig 2.3: Global mean temperature change for the B2 mid-range emission with mid-range climate sensitivity.

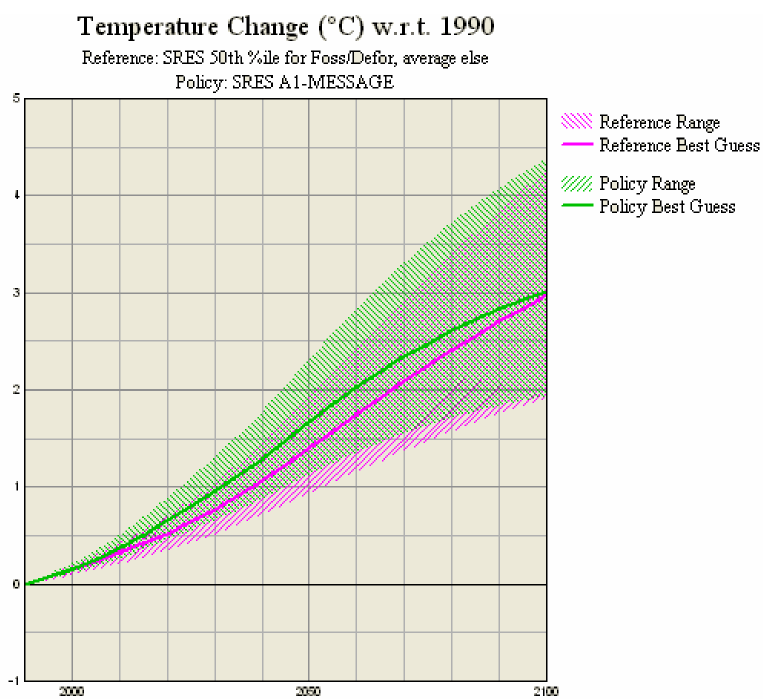

Fig 2.4: global mean temperature change for the A1 high- range emission with high-range climate sensitivity.

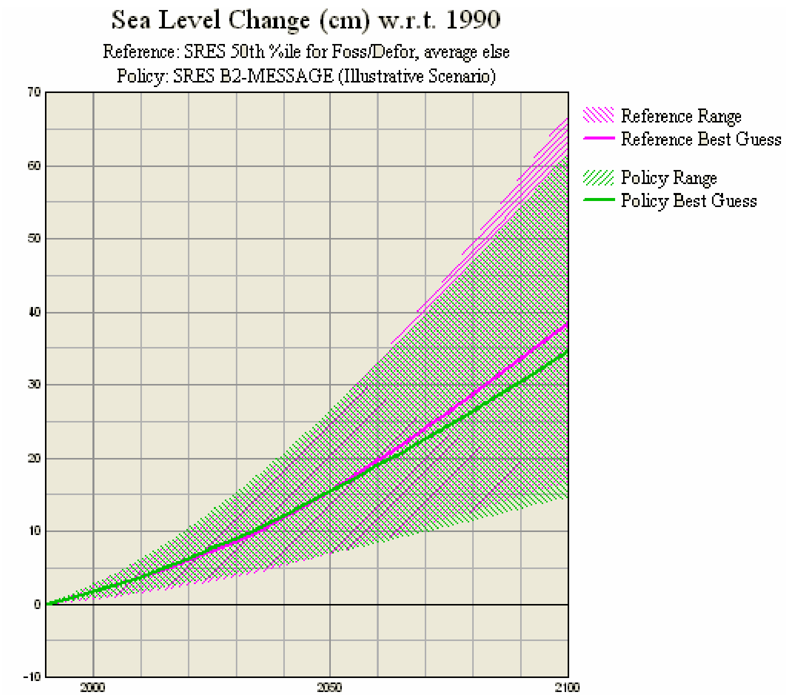

Fig 2.5: Global mean sea level change for the B2 mid-range emission with mid-range climate sensitivity.

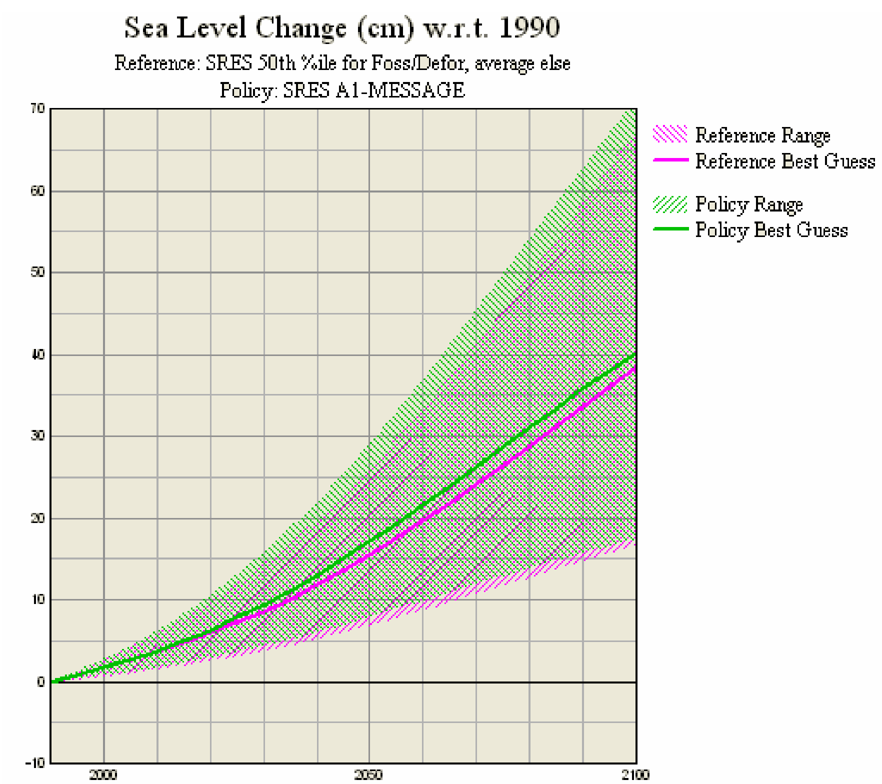

Fig 2.6: Global mean sea level change for the A1 high-range emission with high-range climate sensitivity.

	2025		2050		2100	
Climate Scenario	**BM**	**AH**	**BM**	**AH**	**BM**	**AH**
CO_2 (Policy Range) Policy Best Guess	(420-440) 430	(425-450) 430	(460-500) 480	(500-550) 530	(580-650) 620	(690-800) 730
Temp (Policy Range) (Policy Best Guess) ^{o}C	(0.5-1.0) 0.7	(0.7-1.3) 0.8	(0.8-1.8) 1.3	(1.2-2.3) 1.7	(1.6-3.6) 2.5	(1.9-4.3) 3.0
Sea Level (Policy Range) Policy Best Guess	(3-12) 7	(4-13) 8	(7-27) 15	(8-29) 17	(14-62) 35	(17-70) 40

Table 2.0: Summary of global carbon dioxide (ppmv), change in average global temperature (^{o}C) and average global change in sea level (cm) values for the policy range and policy best guess for the B2 mid-range emission with mid range climate sensitivity of 2.6 ^{o} C and the A1 high-range emission with high-range climate sensitivity of 4.6^{o}C, abbreviated as BM and AH

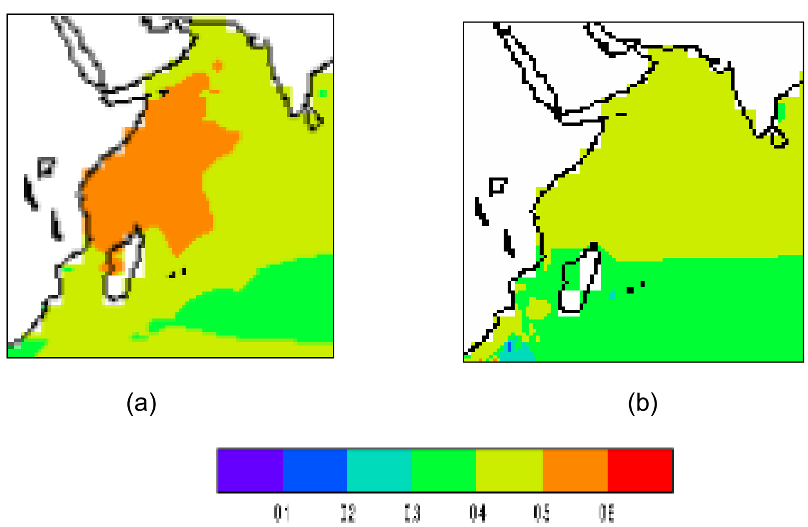

Fig 2.7: Regional sea level projections for the year 2100
(a) HadCM2 (b) HadCM3

Chapter 3

Climate Changes for B2 Mid-Range Emission with a Mid- Range Climate Sensitivity for the Mahe Area

3.0 Climate Changes for B2 Mid-Range Emission with a Mid -Range Climate Sensitivity for the Mahe Area

This section analyses climate changes for the B2 mid-range emission with mid range climate sensitivity at national level for the Mahe group using a simple downscaling procedure. The analyses concentrate on examining individual GCMs output with the objective of targeting climate extremes (i.e. maximum or lowest rainfall) which may indicate critical thresholds for the quantification of risks and vulnerability. The analyses provide a comprehensive assessment of model differences in simulating spatial and temporal time scales. On the other hand, the composite analysis is simply an average of the seven GCMs outputs. This technique is useful as it simplifies analyses by generating a single climate pattern at a particular location.

3.1.1 Spatial Rainfall Changes

The Standardized-Average GCMs (CSM; ECH3, ECH4, GFD, HAD2, HAD3, MODBAR) graphical spatial percentage change in rainfall projections for the B2 mid-range emission with a mid-range climate sensitivity at a 5-degree grid size resolution are shown in figure 3.1 for December, January, February (DJF), March, April, May (MAM), June, July, August (JJA) and September, October, November (SON) seasons of the projected years 2025, 2050 and 2100. It also includes the annual percentage change (%) in precipitation. The scale indicates the average changes in model precipitation for the area centered over Mahe and the inner islands. In principle, one can apply the percentage change to any observed rainfall data set located within this defined boundary. In summary, the spatial analysis shows positive (wetter climate) changes for DJF, MAM and SON while negative (dryer climate) for the JJA seasons respectively. In addition, the respective changes increase from the years 2025 to 2100. However, the changes are not very clearly indicated due to the variation of the pixels. This indeed reflects the normal characteristics of rainfall spatial variability. Thus, further detailed analyses exploit the SCENGEN output files which give full statistical details of the greenhouse-induced climatic values of the defined area.

Table 3.1 shows the detailed statistics of the emission scenario, by the season, and the projected years 2025, 2050 and 2100. In addition, the composite GCMs values are given by the averaged values. In addition, Table 3.1 shows the simple downscaling to adjust the percentage changes to actual location rainfall values and the equivalent anomaly in rainfall with reference to the base line climate condition from 1972 to 1990.

3.1.2 Extremes of Seasonal Rainfall

It is important to note that one may derive a number of useful information from the Table 3.1. Individual GCMs simulations indicate the extreme maximum or minimum values of rainfall. This implies that individual GCM output has the potential to show worst and best case scenarios i.e. extremes. For instance, the individual GCM projected change in seasonal rainfall for the DJF season shows a minimum of +0.6 % (0.1 mm) and a maximum change of +5.9 % (19 mm) for the year 2025. In the case of the year 2050, individual model shows a minimum change of -0.3 % (-10.6 mm) and a maximum change of 9.3 % (+25.4 mm).The minimum change in rainfall for the year 2100 is -5.6 % (-17.5 mm) while the maximum change is +12.4 % (+38.6 mm).

In the case of the MAM season, the lowest change in rainfall is -5.4 % (-9.3 mm) while the maximum change is +9.4 % (+17.5 mm) for the year 2025. A minimum change of -9.2% (-15.2 mm) and a maximum of +17.7 % (+35.6 mm) is expected for the year 2050 while -14.8 % (-24.6 mm) and +35.7 % (+59.2 mm) for the year 2100.

Similarly for JJA, the change in rainfall is -12.7 % (-9.9 mm) and +2.3% (+ 4.1 mm), for the year 2025, -7.7 % (- 6.2 mm) and +22.7 % (+18.4 mm) for the year 2050. In the case of JJA of the year 2100 the minimum change in rainfall simulated is -36.3 % (-31.1 mm) and the maximum is +14.9 % (+12.8 mm). .

Lastly, the change in minimum and maximum rainfall for the SON season is 5.2 % (-0.4 mm) and +6.4 % (+12.7 mm) respectively for the year 2025. The lowest change in rainfall for SON of the year 2050 is -10.4% (-11.1 mm) while the maximum change is10.7 % (+13.9 mm). The lowest change in rainfall predicted by individual model is -13.1 % (-13.6 mm) while the maximum change is +26.6 % (+27.6 mm), for 2100. Figures 3.2.1 to 3.2.3 show the GCMs projected seasonal rainfall.

3.1.3 Composite of Seasonal Rainfall

The composite model is simply an average of the individual GCMs to simplify and generate a single regional climate pattern. The composite changes in rainfall for DJF, MAM, JJA, and SON seasons for the year 2025 are +3.7 %, +2.0 %, -3.3% and +3.8 % respectively (Table 3.1) The year 2050 composite changes in rainfall for the same respective months are +5.3%, + 4.3%, +7.3 % and +2.4 %. The year 2100 composite rainfall changes are +4.9%, +10.5%, -10.8 %, and +11.8 % for the DJF, MAM, JJA and SON seasons respectively.

Therefore, the largest increase in rainfall is expected during the DJF and SON seasons, whereas JJA will have a negative change in the year 2025. It is surprising to note that models are simulating a wetter climate during JJA season around the 2050s with a +7.3 % increase in rainfall. This is an important future climate change pattern to be noted. Lastly, the composite values show a wetter-like season during SON with an increase of +11.8 % in rainfall, while JJA becomes dryer with an expected decrease in precipitation of -10.8 % for the year 2100. The composite graph (Fig 3.2.4) shows clearly the rainfall trends as discussed earlier, i.e. wetter rainy season and dryer dry season respectively for the years 2025 and 2100. In contrast, rainfall projection for JJA of the year 2050 suggests relatively wetter dry season.

The predicted composite rainfall anomaly for DJF when compared to the 1972-1990 periods mean of 311 mm is +11.6, +16.6, +15.4 mm respectively for the years 2025, 2050 and 2100. The rainfall anomalies for the MAM season compared to the base line mean of 157.9 mm are +2.5, +6.1, +15.1 mm respectively. Similarly, the rainfall anomaly with reference to the baseline mean of 81.1 mm for JJA is -4.2, +5.9, and -8.7 mm respectively for the years 2025, 2050 and 2100. The SON rainfall anomalies with reference to the 1972-1990 periods of 98.3 mm are +2.0, +2.7 and +11.6 mm respectively.

3.1.4 Extremes of Annual Rainfall

The extreme annual change in precipitation is predicted by the ECH4 and HAD GCMs (Table 3.2). For instance, the ECH4 GCM simulates maximum annual rainfall changes of +4.9 %, +8.5 %, +16.3 % while the Had3 GCM simulates lowest rainfall changes of - 2.4 %, -4.8 % and -8.6 % for the years 2025, 2050 and 2100 respectively.

Thus, the annual maximum rainfall is predicted to range between +107 and +355 mm while the lowest model predicted rainfall ranges between -51.7 and -187 mm annually.

3.1.5 Composite of Annual Rainfall

Table 3.2 also shows GCMs composites of annual rainfall. For example, the average percentage change in average annual rainfall are +1.7 %, +2.7 %, and 5.5 % for the years 2025, 2050 and 2100 respectively. Figure 3.2.8 shows the composite GCM scenario of the annual precipitation values for the Mahe, Seychelles International Airport for the years 2025, 2050 and 2100. The projected increases in annual rainfall relative to the 1972-1990 periods mean of 2177.9 mm are +37.9, +58.2, and +118.7 mm for the years 2025, 2050 and 2100 respectively. Thus, rainfall is projected to increase to a total of 2215.8, 2236.1 and 2296.6 mm annually by 2025, 2050 and 2100 correspondingly.

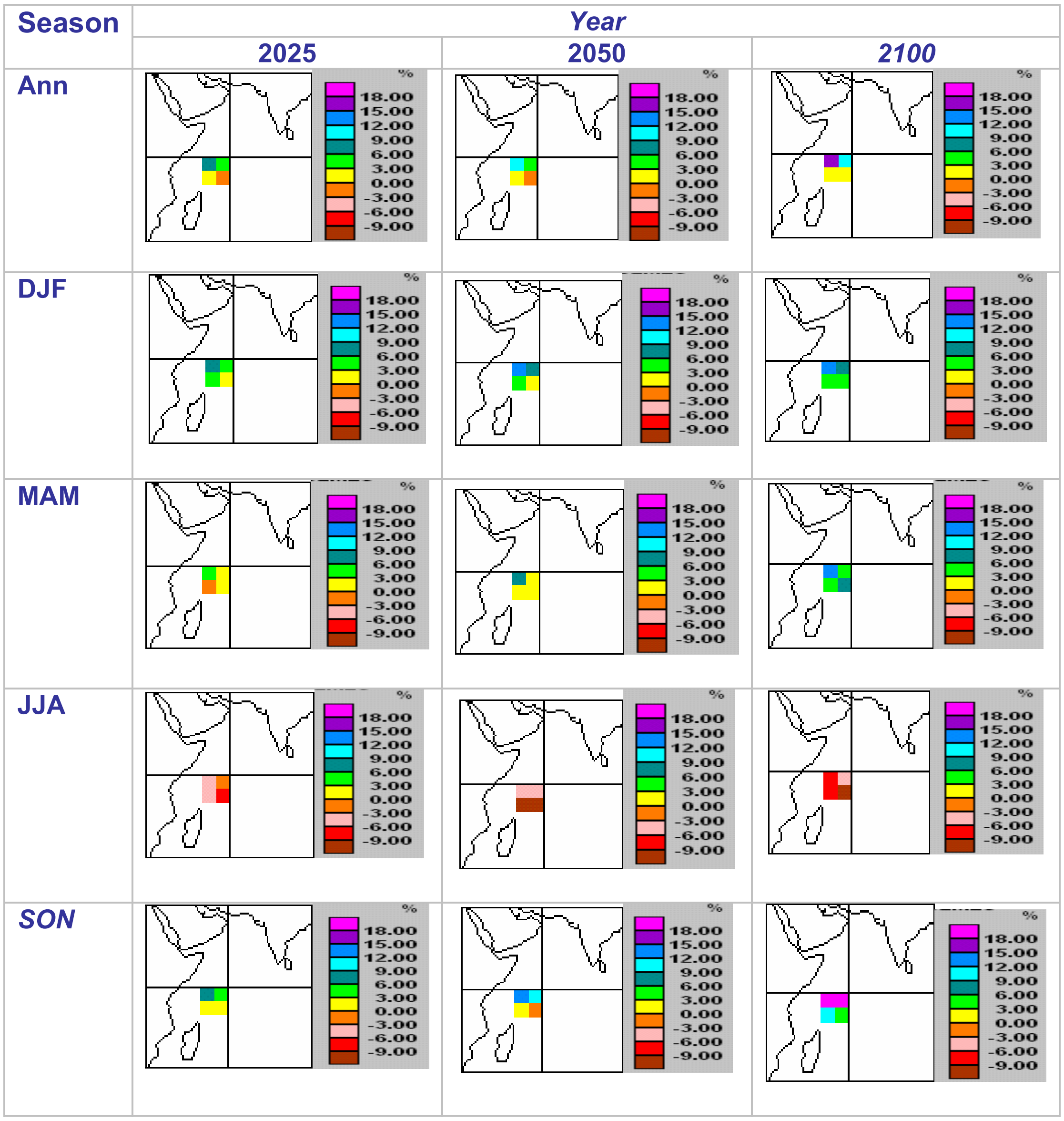

Figure 3.1: Standardized -Average GCMs (CSM, ECH3, ECH4, GFD, HAD2, HAD3, MODBAR) percentage change (%) in rainfall projections (for B2 mid-range emission with a mid-range climate sensitivity at 5-degree grid size resolution.

Year	GCM Model	Season											
		DJF			MAM			JJA			SON		
		% Change in Rf	Predicted Rf (mm)	Change in Rf (mm)	% Change in Rf	Predicted Rf (mm)	Change in Rf (mm)	% Change in Rf	Predicted Rf (mm)	Change in Rf (mm)	% Change in Rf	Predicted Rf (mm)	Change in Rf (mm)
	Base Rf	**0.0**	311.0	0	**0**	157.3	0		81.13	0		98.3	0
2025	**CSM_D2**	5.3	327.6	16.6	2.9	163.1	5.8	-3.9	79.4	-1.73	-5.2	97.9	-0.4
	ECH3D2	0.6	311.1	0.1	-0.3	157.3	0	1.5	84.5	3.37	5.9	110.4	12.1
	ECH4D2	2.8	318.9	7.9	9.4	174.8	17.5	2.3	85.2	4.07	6.4	111.0	12.7
	GFDLD2	4.5	324.8	13.8	1.7	160.9	3.6	-9.5	74.2	-6.93	3.4	107.6	9.3
	HAD2D2	5.9	330.0	19	4.6	166.3	9	-10.0	73.7	-7.43	3.4	107.6	9.3
	HAD3D2	2.4	317.4	6.4	-5.4	148.0	-9.3	-12.7	71.2	-9.93	-3.2	100.2	1.9
	MODBAR	4.6	325.3	14.3	1.1	159.9	2.6	-4.5	78.9	-2.23	3.8	108.1	9.8
	Compo-Site Model	3.7	322.6	11.6	2.0	160.4	3.1	-5.3	76.9	-4.23	2.1	100.3	2
2050	**CSM_D2**	8.1	331.9	20.9	5.9	170.7	13.4	-6.7	75.7	-5.4	-10.4	87.2	-11.1
	ECH3D2	-0.3	300.4	-10.6	0.1	159.6	2.3	3.3	83.8	2.6	9.8	111.1	12.8
	ECH4D2	3.7	315.3	4.3	17.7	192.9	35.6	4.6	84.8	3.7	10.7	112.2	13.9
	GFDLD2	6.7	326.6	15.6	3.7	166.4	9.1	16.8	94.7	13.6	5.3	105.8	7.5
	HAD2D2	9.3	336.4	25.4	9.1	176.7	19.4	17.8	95.6	14.4	5.3	105.8	7.5
	HAD3D2	2.9	312.5	1.5	-9.2	142.1	-15.2	22.7	99.6	18.4	-6.7	91.6	-6.7
	MODBAR	6.9	327.4	16.4	2.7	164.6	7.3	-7.7	74.9	-6.2	6.1	106.7	8.4
	Compo-Site Model	5.3	327.6	16.6	4.3	164	6.7	7.3	87	5.9	2.9	101.1	2.8
2100	**CSM_D2**	10.1	342.5	31.5	13.6	179.8	22.5	-6.2	75.8	-5.33	-13.1	84.7	-13.6
	ECH3D2	-5.6	293.5	-17.5	2.6	161.5	4.2	12.4	91.8	10.67	24.9	124.1	25.8
	ECH4D2	1.8	316.6	5.6	35.7	216.5	59.2	14.9	93.9	12.77	26.6	125.9	27.6
	GFDLD2	7.5	334.3	23.3	9.4	172.8	15.5	-25.2	59.6	-21.53	16.4	115.3	17
	HAD2D2	12.4	349.6	38.6	19.6	189.7	32.4	-27.1	57.9	-23.23	16.4	115.3	17
	HAD3D2	0.4	312.4	1.4	-14.8	181.9	24.6	-36.3	50.0	-31.13	-6.1	91.9	-6.4
	MODBAR	7.9	335.6	24.6	7.6	169.9	12.6	-8.1	74.2	-6.93	17.9	116.8	18.5
	Comp-Site Model	4.9	326.4	15.4	10.5	173.8	16.5	-10.8	72.4	-8.73	11.8	109.9	11.6

Table 3.1: Seasonal model percentage change (%), change (mm) and actual predicted rainfall (mm) for the years 2025, 2050 and 2100 for B2 mid-range emission with a mid-range climate sensitivity.

Year	Model	Change in Rf (%)	Change (Anomaly) in Rf (mm)	Annual Rf (mm)
	OBSERVED	0	0	2177.9
2025	**CSM_D2**	1.525	33.2	2211.1
	ECH3D2	1.676	36.5	2214.4
	ECH4D2	4.916	107.1	2285.0
	GFDLD2	1.579	34.4	2212.3
	HAD2D2	2.407	52.4	2230.3
	HAD3D2	-2.376	-51.7	2126.2
	MODBAR	2.461	53.6	2231.5
	Composite Model	**1.741**	**37.9**	**2215.8**
2050	**CSM_D2**	2.277	49.6	2227.5
	ECH3D2	2.553	55.6	2233.5
	ECH4D2	8.459	184.2	2362.1
	GFDLD2	2.377	51.8	2229.7
	HAD2D2	3.886	84.6	2262.5
	HAD3D2	-4.833	-105.3	2072.6
	MODBAR	3.985	86.8	2264.7
	Composite Model	**2.672**	**58.2**	**2236.1**
2100	**CSM_D2**	4.709	102.6	2280.5
	ECH3D2	5.225	113.8	2291.7
	ECH4D2	16.305	355.1	2533.0
	GFDLD2	4.896	106.6	2284.5
	HAD2D2	7.726	168.3	2346.2
	HAD3D2	-8.63	-188.0	1989.9
	MODBAR	7.912	172.3	2350.2
	Composite Model	**5.449**	**118.7**	**2296.6**

Table 3.2: Percentage change (%) in rainfall, anomaly in rainfall (mm), actual average annual rainfall (mm) and equivalent composite model rainfall for the years 2025, 2050 and 2100 for B2 mid-range emission with a mid-range climate sensitivity

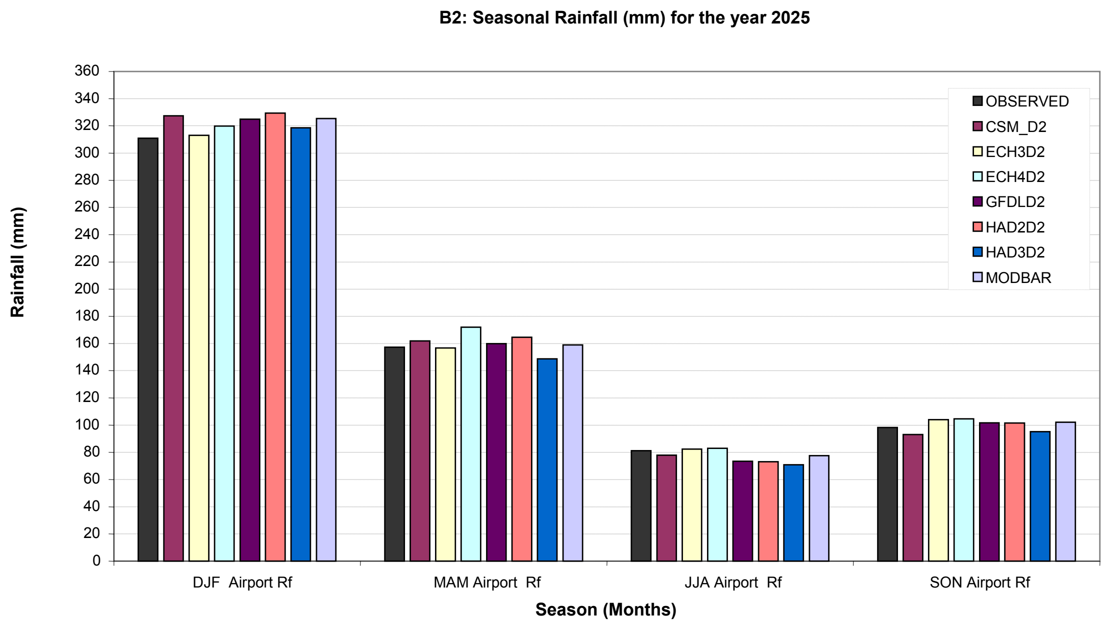

Fig 3.2.1: Observed (1972-1990 –Grey color) and scenarios of seasonal precipitation values (mm) for the International Airport, for B2 mid-range emissions with a mid-range climate sensitivity for the year 2025

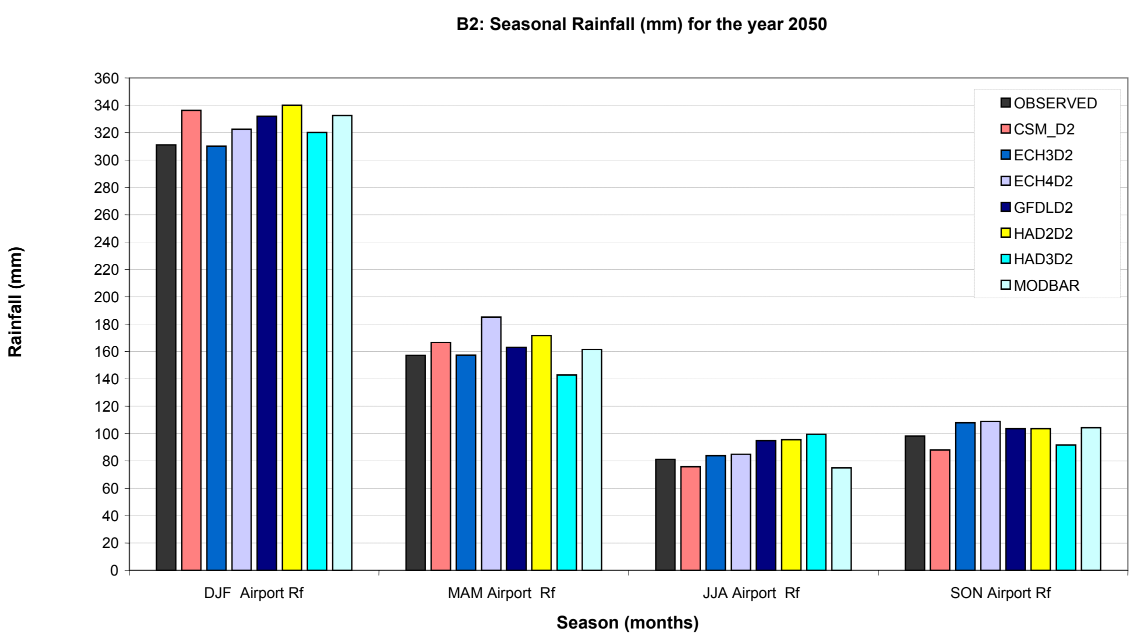

Fig 3.2.2: Observed (1972-1990 –Grey color) and scenarios of seasonal precipitation values (mm) for the International Airport, for B2 mid-range emission with a mid-range climate sensitivity for the year 2025

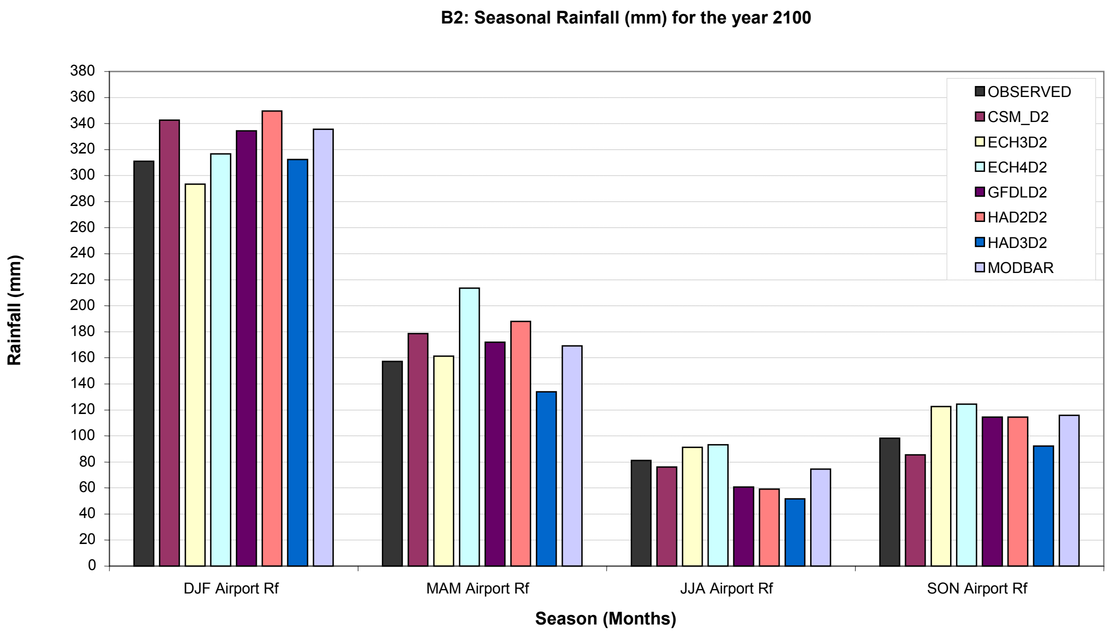

Fig 3.2.3: Observed (1972-1990-Grey color) and scenarios of seasonal precipitation values (mm) for the International Airport for B2 mid-range emission with a mid-range climate sensitivity for the year 2100

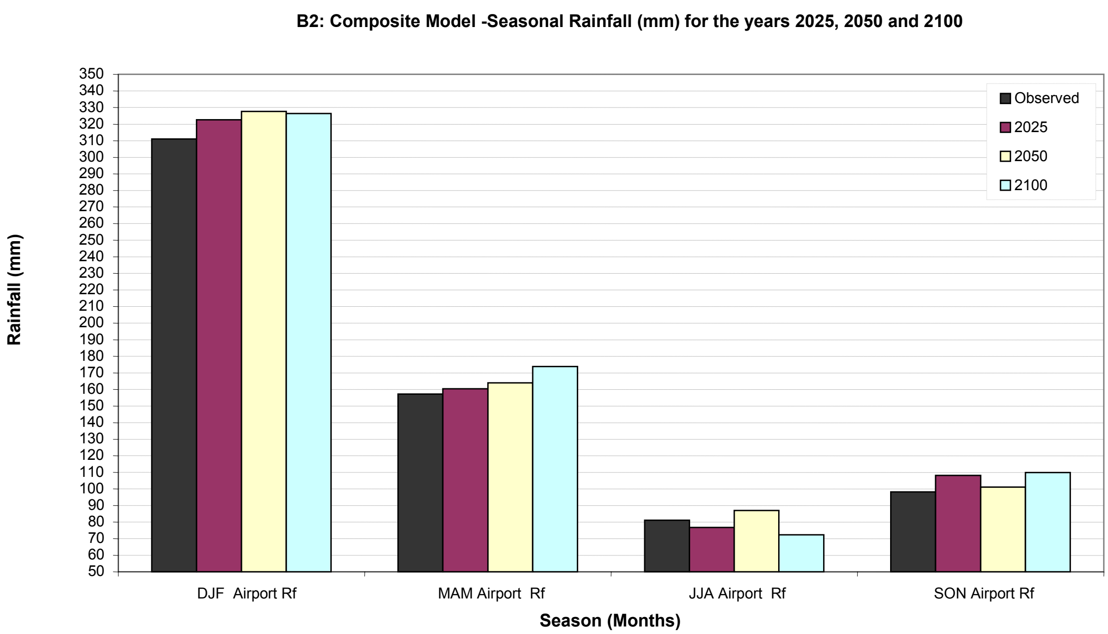

Fig 3.2.4: Observed (1972-1990-Grey color) and composite model scenarios of seasonal precipitation values (mm) for the International Airport for the years 2025, 2050 and 2100 for B2 mid-range emission with a mid-range climate sensitivity.

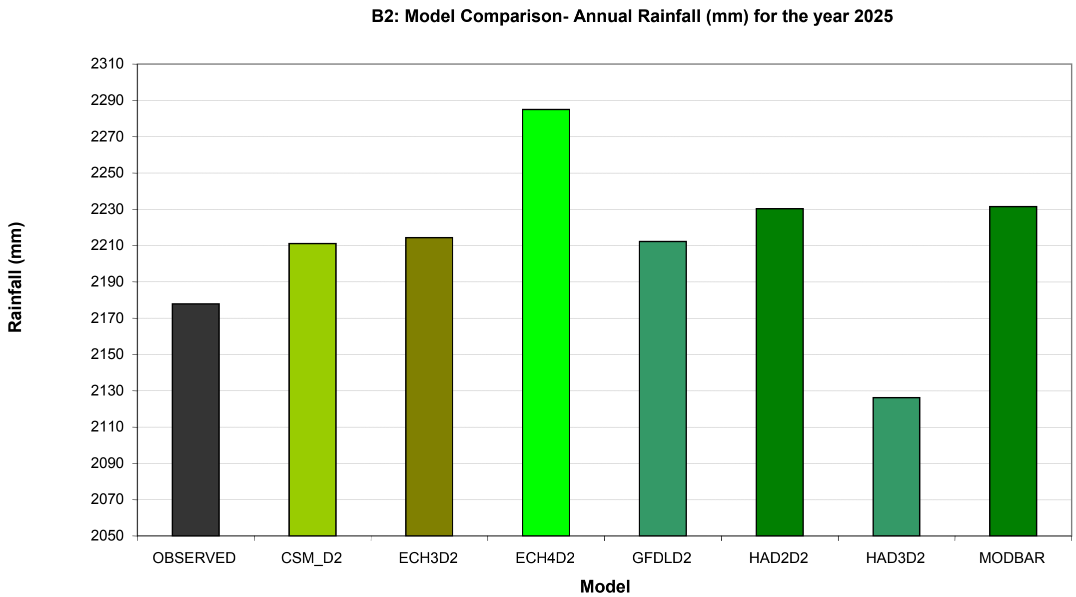

Fig 3.2.5: Observed (1972-1990-Grey color) and model scenarios of annual precipitation values (mm) for the International Airport for the year 2025 for B2 mid-range emission with a mid-range climate sensitivity.

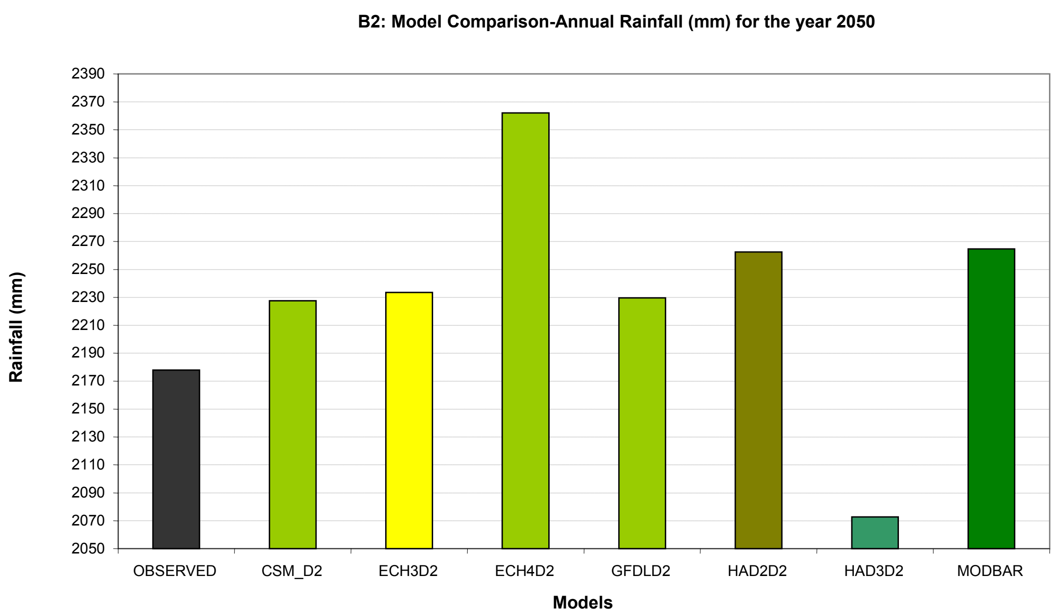

Fig 3.2.6: Observed (1972-1990-Grey color) and model scenarios of annual precipitation values (mm) for the International Airport for the year 2050 for B2 mid-range emission with a mid-range climate sensitivity.

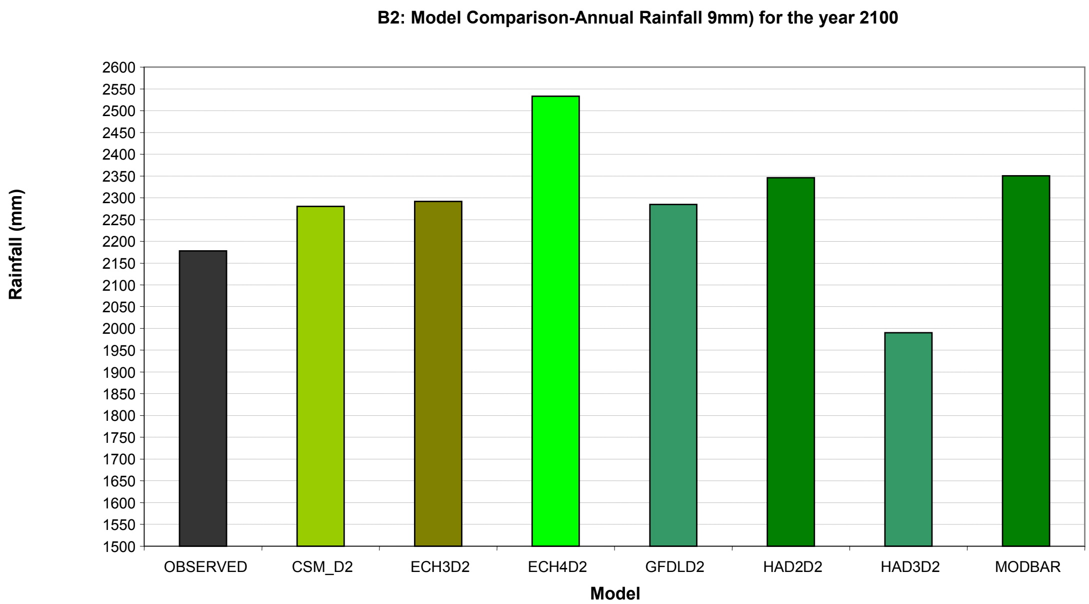

Fig 3.2.7: Observed (1972-1990-Grey color) and model scenarios of annual precipitation values (mm) for the International Airport for the year 2100 for B2 mid-range emission with a mid-range climate sensitivity.

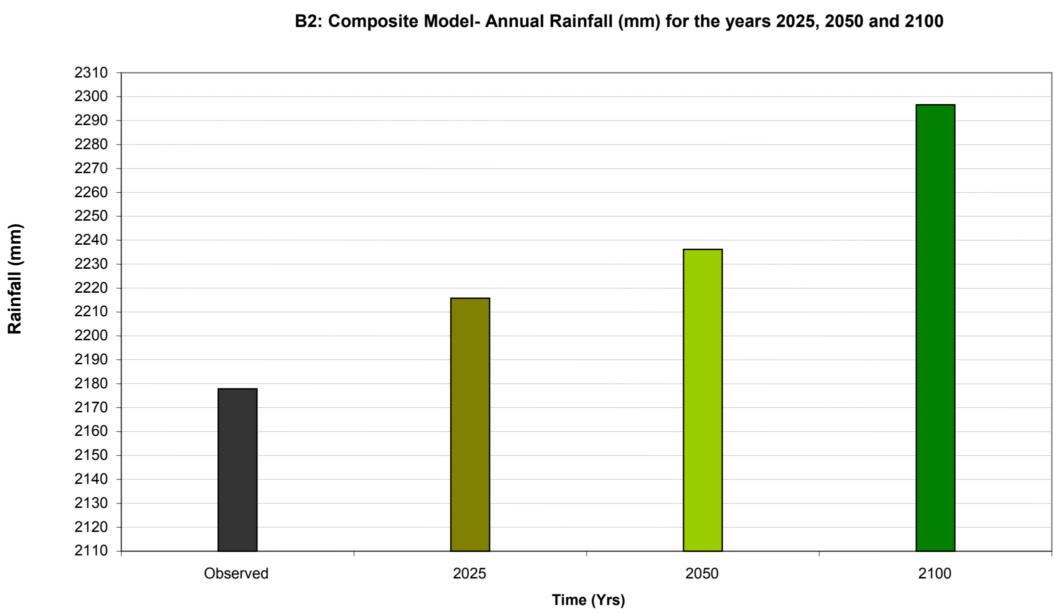

Fig 3.2.8: Observed (1972-1990-Grey color) and composite model scenarios of the annual precipitation values (mm) for the International Airport for the years 2025, 2050 and 2100 for B2 mid-range emission and a mid-range climate sensitivity.

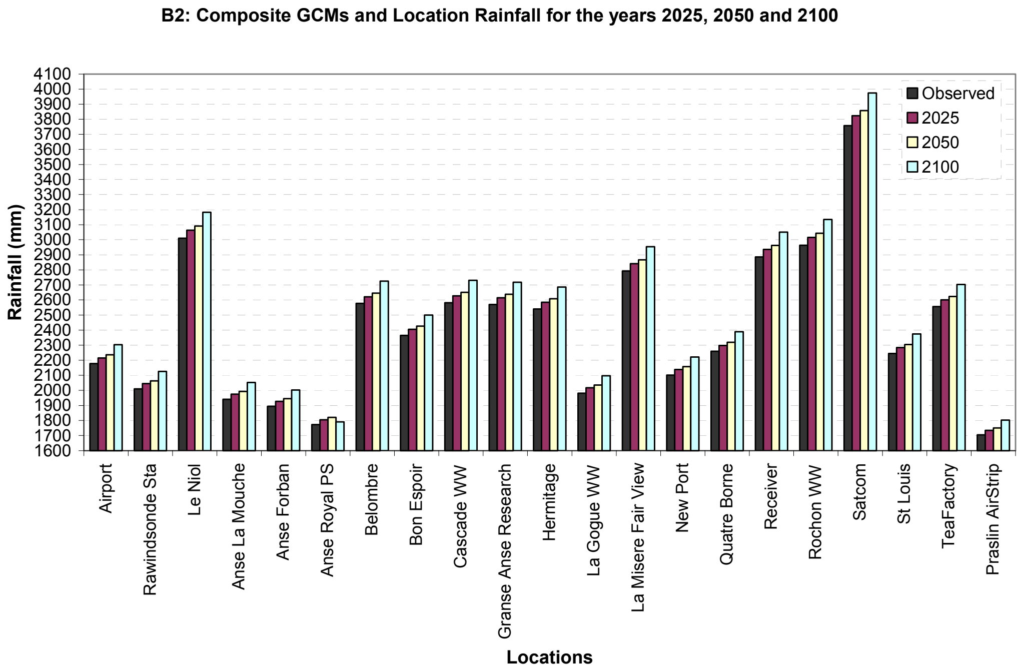

Fig 3.2.9: GCMs annual location rainfall composites (mm) for the years 2025, 2050 and 2100 for B2 mid-range emission and mid-range climate sensitivity

3.2.1 Spatial Temperature Changes

The Standardized -Average GCMs spatial temperature projections for the B2 mid - range emission and mid-range climate sensitivity at 5 degree grid size resolution are shown in figure 3.3 for DJF, MAM, JJA and SON seasons for the projected years. It also includes the annual temperature changes. In summary, the spatial analyses show positive (warmer climate) changes for the DJF, MAM, JJA and SON seasons throughout. In addition, temperature warms up from the year 2025 to the year 2100. However, detailed analyses are carried out by examining the SCENGEN output files.

3.2.2 Extremes of Seasonal Temperature

Table 3.3, shows the detailed temperature statistics for the temperature scenario. In addition, the composite GCM model values are also indicated. The simple downscaling technique is used to adjust to station temperature. The individual model projected change in seasonal temperature for DJF shows warming ranging from +0.5 to +0.6 ^{o}C for the year 2025, +0.9 to +1.3 ^{o}C for the year 2050 and +1.6 to +2.5 ^{o}C for the year 2100. The numbers presented in text are calculated to two decimal places. In the case of MAM, the temperature warming is +0.5 to +0.7 ^{o}C for the year 2025, +1.0 to +1.4^{o} C for the year 2050 and +1.9 to +2.6 ^{o} C for the year 2100. Similarly, the range of temperature warming indicated by individual model for JJA season ranges from +0.5 to +0.8 ^{o}C for the year 2025, +0.8 to +1.6 ^{o}C for the year 2050 and +1.6 to +2.9 ^{o}C for the year 2100. Lastly, the temperature warming for the SON season ranges from +0.5 to +0.7 ^{o}C for the year 2025,+0.9 to +1.3 ^{o}C for 2050 and +1.6 to +2.5 ^{o}C for the year 2100. By considering only the upper range of the individual model projected temperature change, it is observed that MAM, JJA will be warmer by +2.6 and +2.9 ^{o}C by the year 2100. Figures 3.4.1 to 3.4.2 show the observed and the GCMs scenario average maximum and minimum temperature values at the International Airport, Mahe, Seychelles.

3.2.3 Composite of Seasonal Temperature

The DJF, MAM, JJA and SON seasonal GCMs composite of temperature changes for the year 2025 range from +0.5 +0.6 ^{o}C. The warming in temperature for the year 2050 is +1.0, +1.2, +1.1 and +1.2 ^{o}C for the respective seasons, while the year 2100 temperature warming is +2.0, +2.2, +2.1, and +2.0 ^{o}C. The composite magnitude shows increasing warming up to the year 2100, particularly during the MAM, JJA seasons. This implies the projected future climate during the southeast monsoon will be characterized by relatively warmer-like conditions. Figures 3.4.5 and 3.4.6 shows observed and composite GCM scenarios of average maximum and minimum temperature values for the years 2025, 2050 and 2100 at the International Airport, Mahe, Seychelles.

3.2.4 Extreme of Annual Temperature

The extreme annual percentage change in temperature is predicted by the ECH4 GCM. For instance ECH4 GCM projected warming in temperature is +0.7, +1.3, and +2.6 ^{o}C for the years 2025, 2050 and 2100 respectively while the CSM GCM shows lower warming of +0.5, +0.9 and +1.8 ^{o}C for the years 2025, 2050 and 2100 respectively (Table 3.3).

3.2.5 Composite of Annual Temperature

The GCM composite shows warming of +0.6, +1.1 and +2.1 ^{o}C for the years 2025, 2050 and 2100 respectively. Thus, the annual mean temperature will gradually become warmer by the year 2100 (table 3.4).

The next chapter analyses the second possible climate change scenario for the Mahe area by considering the A1 high-range emission with high-range climate sensitivity.

Season	Year		
	2025	**2050**	**2100**
Ann	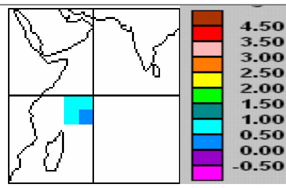	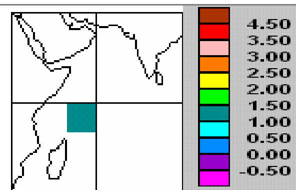	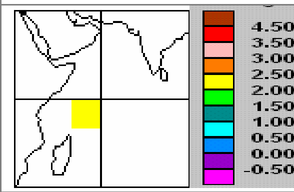
DJF	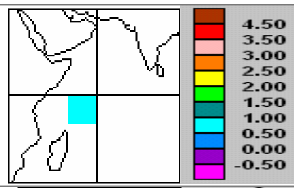	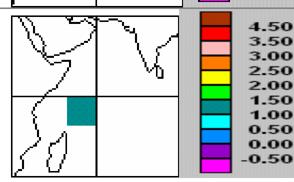	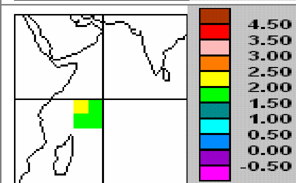
MAM	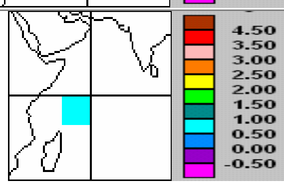	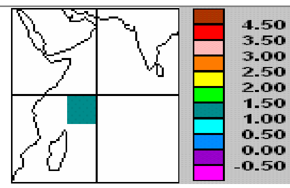	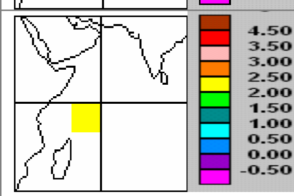
JJA	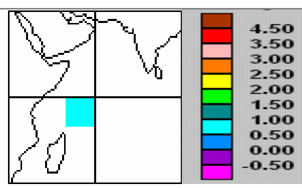	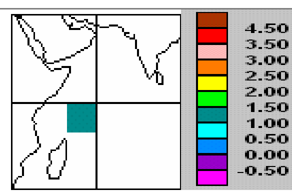	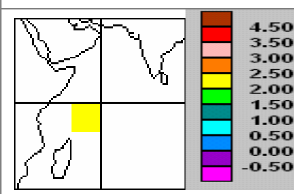
SON	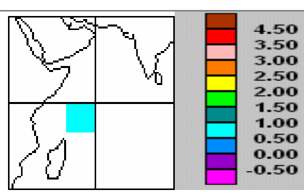	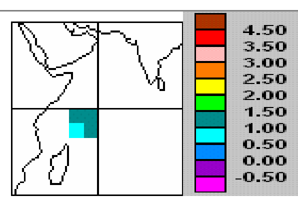	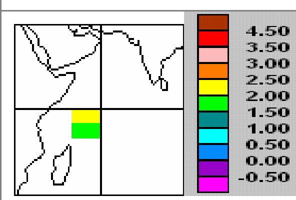
	Global-Mean dT 0.63 (^{o}C)	**Global-Mean dT 1.48** (^{o}C)	**Global-Mean dT 2.76** (^{o}C)

Fig 3.3: Temperature projections (^{o}C) using the B2 mid-range emission and a mid-range climate sensitivity at 5-degree grid size resolution

Year	Model	Change in Temp DJF	Temp DJF	Change in Temp MAM	Temp MAM	Change in Temp JJA	Temp JJA	Change in Temp SON	Temp SON
	Maximum Temperature (^{o}C)								
	Observed		**30.1**		**31**		**28.6**		**29.6**
2025	**CSM_D2**	0.48	30.6	0.53	31.5	0.54	29.1	0.48	30.1
	ECH3D2	0.53	30.6	0.61	31.6	0.62	29.2	0.60	30.2
	ECH4D2	0.63	30.7	0.74	31.7	0.85	29.5	0.73	30.3
	GFDLD2	0.61	30.7	0.64	31.6	0.60	29.2	0.61	30.2
	HAD2D2	0.59	30.7	0.73	31.7	0.60	29.2	0.57	30.2
	HAD3D2	0.54	30.6	0.60	31.6	0.45	29.1	0.49	30.1
	MODBAR	0.56	30.7	0.63	31.6	0.62	29.2	0.57	30.2
	Composite Model	**0.56**	**30.7**	**0.6**	**31.6**	**0.61**	**29.2**	**0.58**	**30.2**
	Minimum Temperature (^{o}C)								
	Observed		24.2		25.1		24.1		24.2
2025	**CSM_D2**	0.48	24.2	0.53	25.1	0.54	24.1	0.48	24.3
	ECH3D2	0.53	24.7	0.61	25.6	0.62	24.6	0.60	24.7
	ECH4D2	0.63	24.7	0.74	25.7	0.85	24.7	0.73	24.8
	GFDLD2	0.61	24.8	0.64	25.8	0.60	25.0	0.61	24.9
	HAD2D2	0.59	24.8	0.73	25.7	0.60	24.7	0.57	24.8
	HAD3D2	0.54	24.8	0.60	25.8	0.45	24.7	0.49	24.8
	MODBAR	0.56	24.7	0.63	25.7	0.62	24.6	0.57	24.7
	Composite Model	**0.56**	**24.8**	**0.64**	**25.7**	**0.61**	**24.7**	**0.58**	**24.8**
	Maximum Temperature (^{o}C)								
	Observed		30.1		31		28.6		29.6
2050	**CSM_D2**	0.89	31.0	0.98	32.0	1.00	29.6	0.87	30.5
	ECH3D2	0.98	31.1	1.12	32.1	1.15	29.7	1.09	30.7
	ECH4D2	1.16	31.3	1.37	32.4	1.56	30.2	1.33	30.9
	GFDLD2	1.13	31.2	1.18	32.2	1.11	29.7	1.11	30.7
	HAD2D2	1.09	31.2	1.35	32.3	1.11	29.7	1.05	30.6
	HAD3D2	0.99	31.1	1.11	32.1	0.84	29.4	0.90	30.5
	MODBAR	1.03	31.1	1.16	32.2	1.14	29.7	1.05	30.7
	Composite Model	***1.04***	**31.1**	**1.18**	**32.2**	**1.13**	**29.7**	**1.06**	**30.7**
	Minimum Temperature (^{o}C)								
2050	**Observed**		24.2		25.1		24.1		24.2
	CSM_D2	0.89	25.1	0.98	26.1	1.00	25.1	0.87	25.1
	ECH3D2	0.98	25.2	1.12	26.2	1.15	25.2	1.09	25.3
	ECH4D2	1.16	25.4	1.37	26.5	1.56	25.7	1.33	25.5
	GFDLD2	1.13	25.3	1.18	26.3	1.11	25.2	1.11	25.3
	HAD2D2	1.09	25.3	1.35	26.4	1.11	25.2	1.05	25.2
	HAD3D2	0.99	25.2	1.11	26.2	0.84	24.9	0.90	25.1
	MODBAR	1.03	25.2	1.16	26.3	1.14	25.2	1.05	25.3
	Composite Model	***1.04***	**25.2**	**1.18**	**26.3**	**1.13**	**25.2**	**1.06**	**25.3**
	Maximum Temperature (^{o}C)								
	Observed		30.1		31		28.6		29.6
2100	**CSM_D2**	1.63	31.7	1.86	32.9	1.88	30.5	1.63	31.2
	ECH3D2	2.04	32.1	2.12	33.1	2.16	30.8	2.04	31.6
	ECH4D2	2.49	32.6	2.58	33.6	2.94	31.5	2.49	32.1

	GFDLD2	2.08	32.2	2.22	33.2	2.08	30.7	2.08	31.7
	HAD2D2	1.96	32.1	2.55	33.5	2.10	30.7	1.96	31.6
	HAD3D2	1.68	31.8	2.10	33.1	1.59	30.2	1.68	31.3
	MODBAR	1.96	32.1	2.20	33.2	2.15	30.7	1.96	31.6
	Composite Model	**1.98**	**32.1**	**2.23**	**33.2**	**2.13**	**30.7**	**1.98**	**31.6**
	Minimum Temperature (^{o} C)								
	Observed		24.2		25.1		24.1		24.2
2100	**CSM_D2**	1.63	25.8	1.86	27.0	1.88	26.0	1.63	25.8
	ECH3D2	2.04	26.2	2.12	27.2	2.16	26.3	2.04	26.2
	ECH4D2	2.49	26.7	2.58	27.7	2.94	27.0	2.49	26.7
	GFDLD2	2.08	26.3	2.22	27.3	2.08	26.2	2.08	26.3
	HAD2D2	1.96	26.2	2.55	27.6	2.10	26.2	1.96	26.2
	HAD3D2	1.68	25.9	2.10	27.2	1.59	25.7	1.68	25.9
	MODBAR	1.96	26.2	2.20	27.3	2.15	26.2	1.96	26.2
	Composite Model	**1.98**	**26.2**	**2.23**	**27.3**	**2.13**	**26.2**	**1.98**	**26.2**

Table 3.3: (a) Observed, (b) change in temperature and (c) seasonal GCMs composite of temperature (^{o} C) for the years 2025, 2050 and 2100 for B2 mid range emission with a mid-range climate sensitivity

Model	Change in Temp 2025 (^{o} C)	Change in Temp 2050 (^{o} C)	Change in Temp 2100 (^{o} C)
CSM_D2	0.51	0.94	1.77
ECH3D2	0.59	1.09	2.05
ECH4D2	0.73	1.35	2.54
GFDLD2	0.61	1.13	2.13
HAD2D2	0.63	1.15	2.17
HAD3D2	0.52	0.95	1.80
MODBAR	0.59	1.09	2.07
Composite	**0.60**	**1.10**	**2.07**

Table 3.4: Annual GCMs temperature (^{o} C) composites for the years 2025, 2050 and 2100 for B2 mid-range emission with a mid-range climate sensitivity

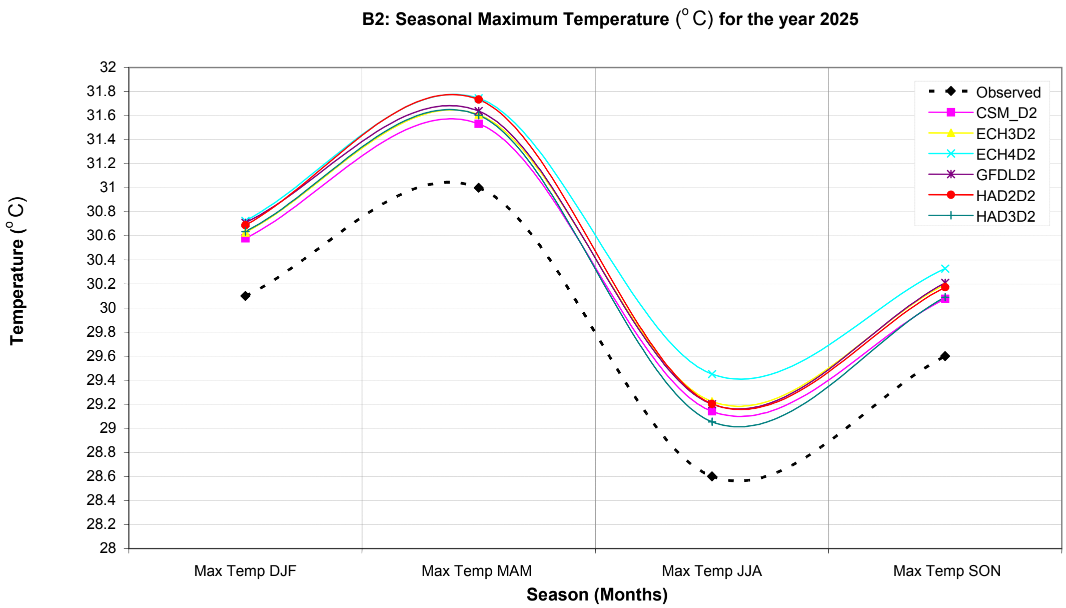

Fig 3.4.1: Observed (1972-90) and scenarios for the average seasonal maximum temperature values(° C) for the International Airport, Mahe, Seychelles for the B2 mid-range emission with a mid-range climate sensitivity for the year 2025

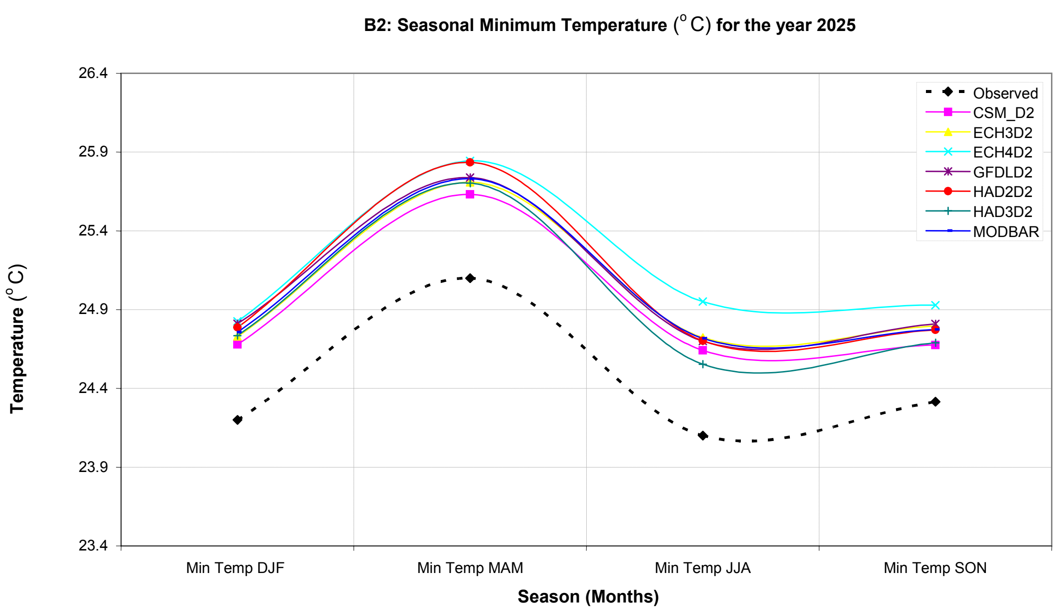

Fig 3.4.2: Observed (1972-90) and scenarios for the average seasonal minimum temperature values (° C) for the International Airport, Mahe, Seychelles for the B2 mid-range emission with a mid-range climate sensitivity for the year 2025

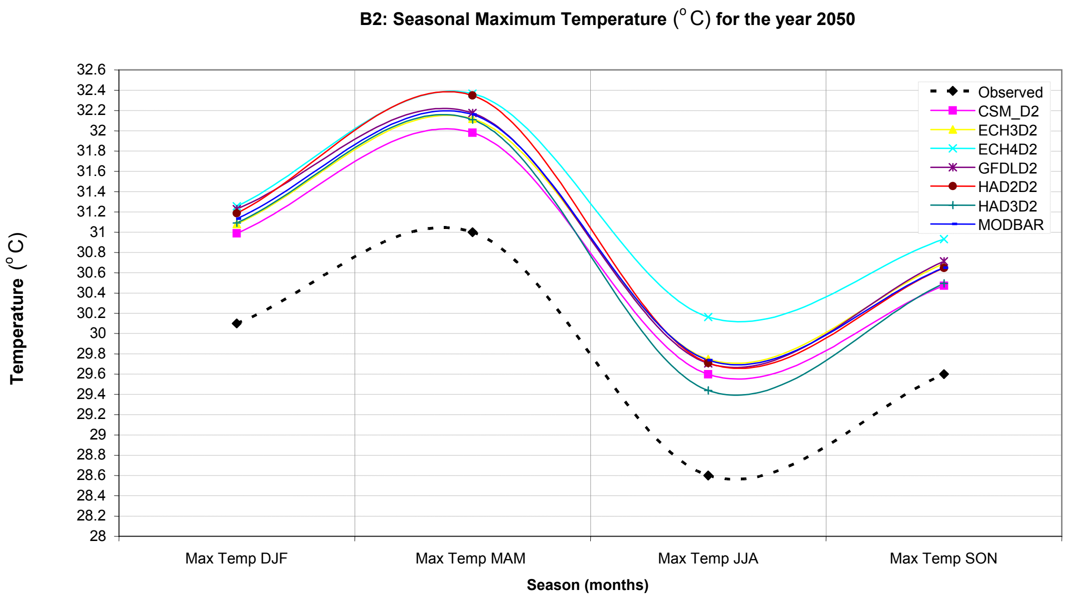

Fig 3.4.3: Observed (1972-90) and scenarios for the average seasonal maximum temperature values(^{o} C) for the International Airport, Mahe, Seychelles for the B2 mid-range emission with a and mid-range climate sensitivity for the year 2050

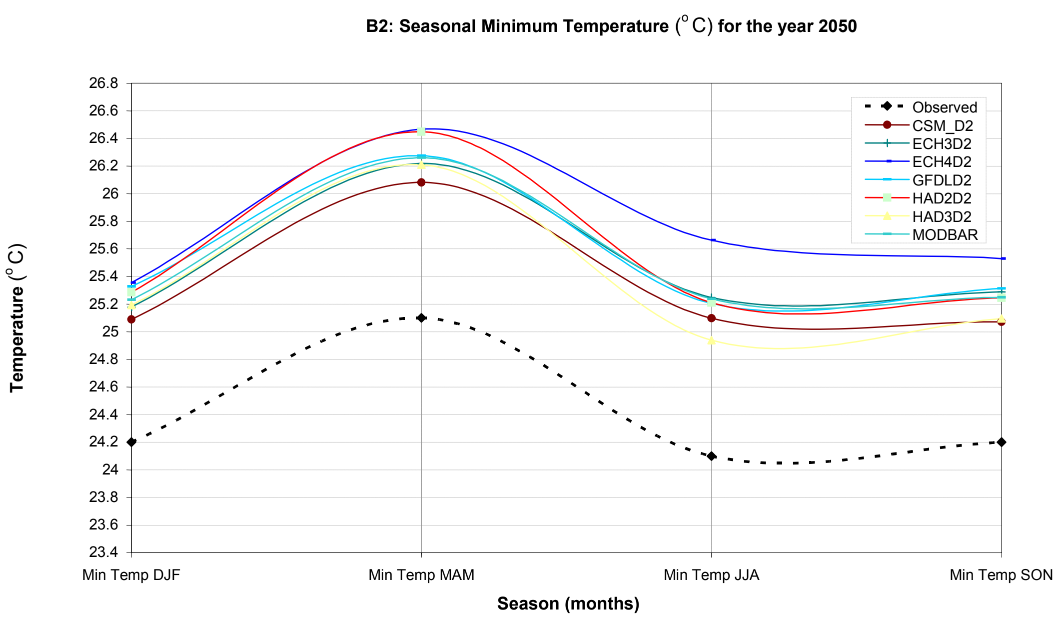

Fig 3.4.4: Observed (1972-90) and scenarios for the average seasonal maximum temperature values(^{o} C) for the International Airport, Mahe, Seychelles for the B2 mid-range emission with a mid-range climate sensitivity for the year 2050

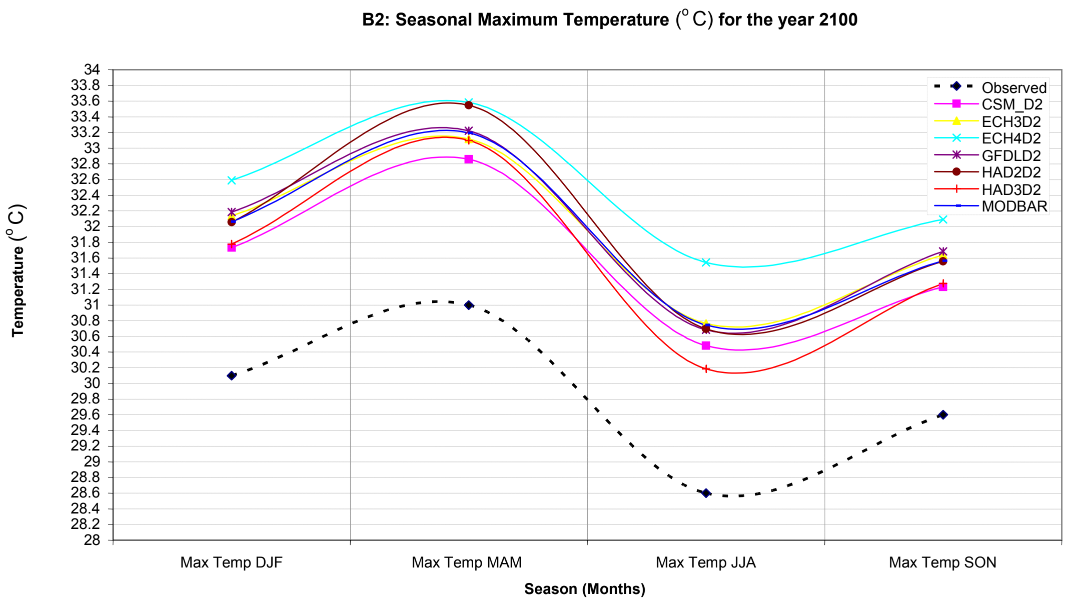

Fig 3.4.5: Observed (1972-90) and scenarios for the average maximum temperature values (° C) for the International Airport, Mahe, Seychelles for the B2 mid-range emission with a mid-range climate sensitivity for the year 2100

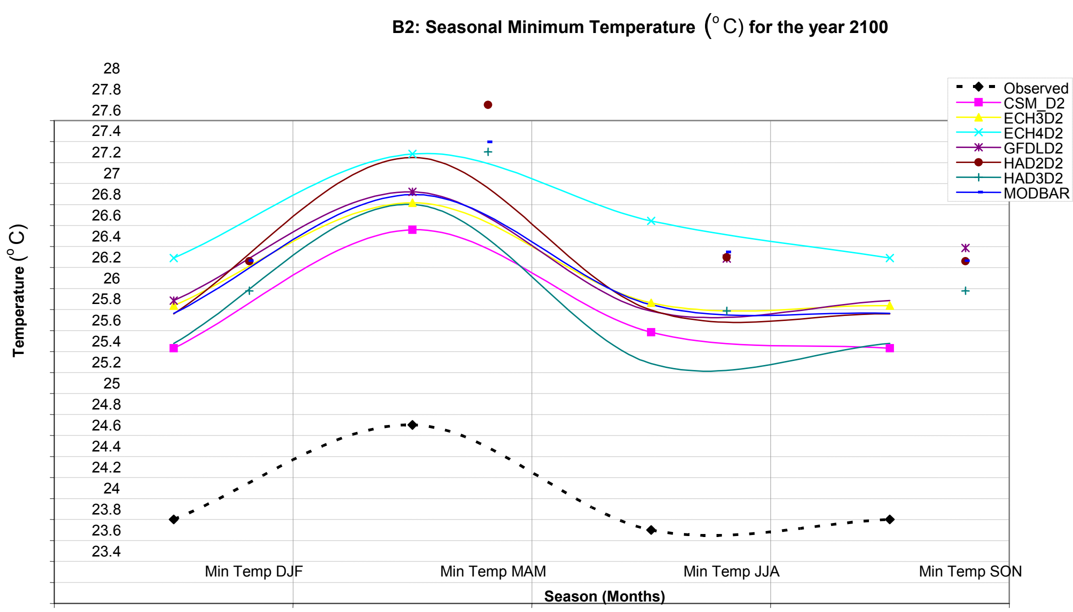

Fig 3.4.6: Observed (1972-90) and scenarios for the average minimum temperature values (° C) for the International Airport, Mahe, Seychelles for the B2 mid-range emission with a mid-range climate sensitivity for the year 2100

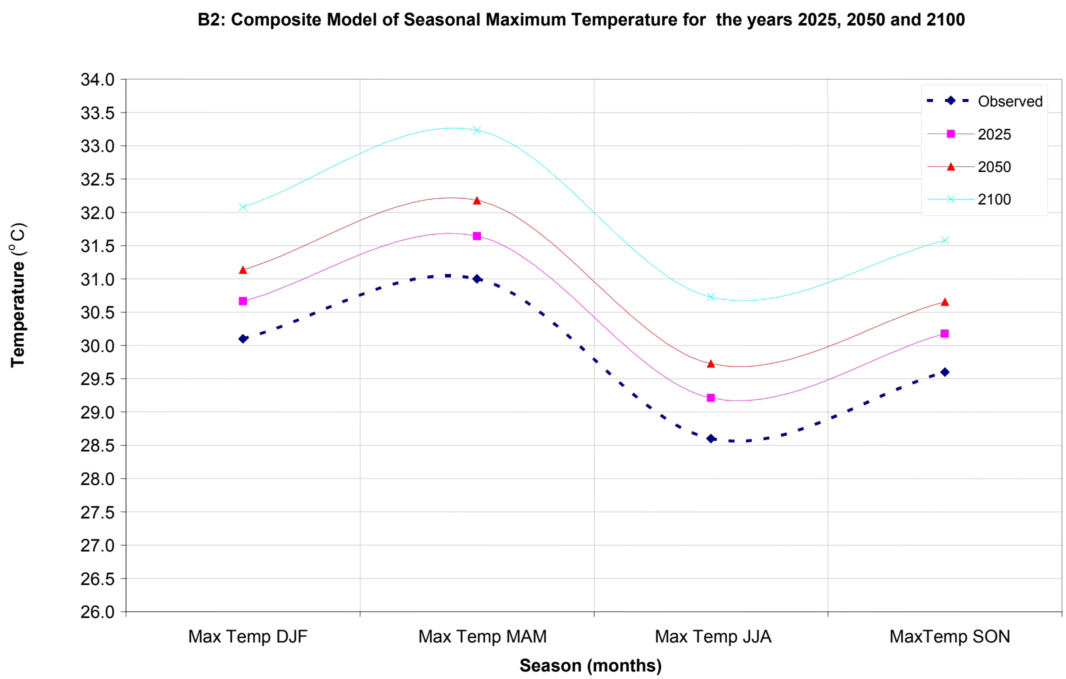

Fig 3.4.7: Observed (1972-90) and composite model scenarios for average maximum temperature values (° C) for the years 2025, 2050 and 2100 at the International Airport, Mahe, Seychelles for the B2 mid-range emission with a mid-range climate sensitivity

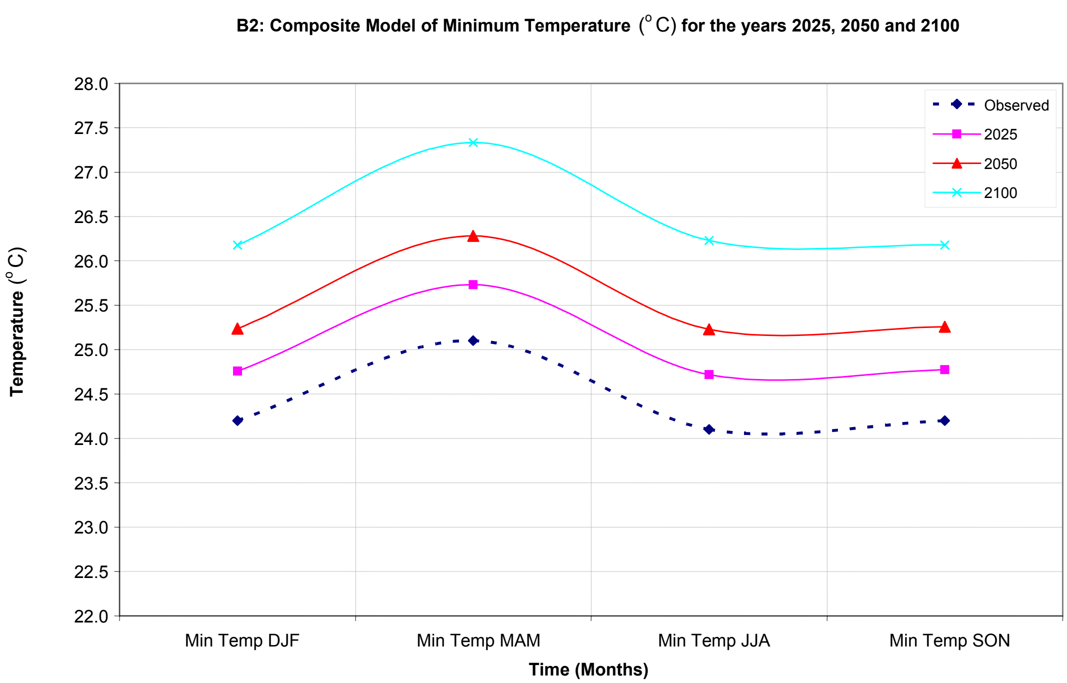

Fig 3.4.8: Observed (1972-90) and composite model scenarios for minimum temperature values (° C) for the years 2025, 2050 and 2100 at the International Airport, Mahe, Seychelles for the B2 mid-range emission with a mid-range climate sensitivity.

Chapter 4

Climate Change for A1 High-Range Emission with a High -Range Climate Sensitivity for the Mahe Area

4.0 Climate Change for A1 High-Range Emission with High-Range Climate Sensitivity for the Mahe Group

4.1.1 Spatial Rainfall Changes

The other global–scale scenario selected is the A1 high emission with a high climate sensitivity, high carbon cycle and high aerosols concentrations. Figure 4.1 below shows the rainfall projections by season and year. Table 4.1 shows the detailed climate scenario statistics.

4.1.2 Extremes of Seasonal Rainfall

The GCM individual projected change in seasonal rainfall for DJF shows a maximum of +6.1% (+19 mm) for the year 2025. The lowest percentage change in rainfall is -3.4 % (-10.6 mm) and a maximum percentage of +8.2 % (+25.4 mm) for the year 2050. The minimum change in rainfall is -6.0 % (-18.6 mm) and +13.1 % (+40.8 mm) for the year 2100.

In the case of the MAM season the change in rainfall is -5.9 % (-9.2 mm) and a maximum of +11.2 % (+17.6 mm) for the year 2025. A minimum change of -9.7 % (-15.2 mm) and a maximum change of +22.7 % (+35.7 mm) is expected for the year 2050. The individual model shows lowest rainfall of +2.7 % (+4.3 mm) and a maximum of +37.7 % (+59.3 mm), for the year 2100. Similarly for the JJA season, the minimum change in rainfall is -12.3 % (-10 mm) while the maximum change is +5.0 % (+4.1 mm) for the year 2025.The minimum change in rainfall is -25.0 % (- 20.3 mm) while the maximum is +7.8 % (+6.3 mm) for the year 2050. The lowest rainfall simulated is -38.3 % (-31.1 mm) and a maximum of +15.8 % (+12.8 %) for the year 2100.

Lastly, the minimum change in rainfall for the SON season is -5.2% (-0.5 mm) while the maximum is +13.0 % (+12.7 mm) for the year 2025. The minimum change in rainfall is -11.2 % (-11.0 mm) whereas the maximum is +14.2 % (+13.9 mm) for the year 2050. The lowest individual model change in rainfall for 2100 is -13.8 % (-13.6 mm) while the maximum change is +26.3 % (+25.8 mm) for the year 2100. Figures

4.2.1 to 4.2.3 show the GCMs projected seasonal rainfall for the years 2025, 2050 and 2100.

4.1.3 Composite of Seasonal Rainfall

The predicted composite anomaly in rainfall for the DJF season when compared to the baseline mean of 311 mm is +11.2 mm, +10.5 mm and +16 mm respectively for the years 2025, 2050 and 2100 (Table 4.1.1). Similarly, for the MAM season, the predicted rainfall anomaly from the mean of 157.9 mm is +3.6, +9.7 and +23.8 mm. The actual average rainfall anomaly for JJA season when compared to the current mean of 81.1 mm is +3.0, -7.0 and -9.2 mm respectively for the years 2025, 2050 and 2100. The SON season projected rainfall anomaly from the mean of 98.3 mm is +5.7, +4.6 and +12.2 mm respectively for the same target years. Figure 4.2.4 shows the GCMs seasonal composite mean of precipitation for the Seychelles International Airport.

4.1.4 Extremes of Annual Rainfall

The ECH4 model predicts the maximum annual change in rainfall of +6.4% (140 mm), +9.7% (+211.7 mm), +17.2 % (+375mm) for the years 2025, 2050 and 2100 respectively while HAD3 model predicts the lowest change in rainfall of -2.0 % (-43 mm) for the year 2025 and -9.1% (-198 mm) for the year 2100 respectively (Table 4.1.2). However, the CSM model simulates the lowest change in rainfall of +2.3 % (+50mm) for 2100. Figures 4.2.5 to 4.2.7 show individual GCMs maximum and minimum annual changes in precipitation.

4.1.5 Composite of Annual Rainfall

The GCMs composite of annual rainfall is +2.8 %, +4.6 %, and +5.8 % for the years 2025, 2050 and 2100 respectively (Table 4.1.2). Figure 4.2.8 shows the observed (1972-1990-Grey color) and composite GCM model scenarios of the annual precipitation values for the International Airport Mahe, Seychelles. The predicted increase with reference to the 1972-1990 periods annual mean rainfall of 2177.9 mm is +60.4, +99.2, and +125.3 mm for the years 2025, 2050 and 2100 respectively.

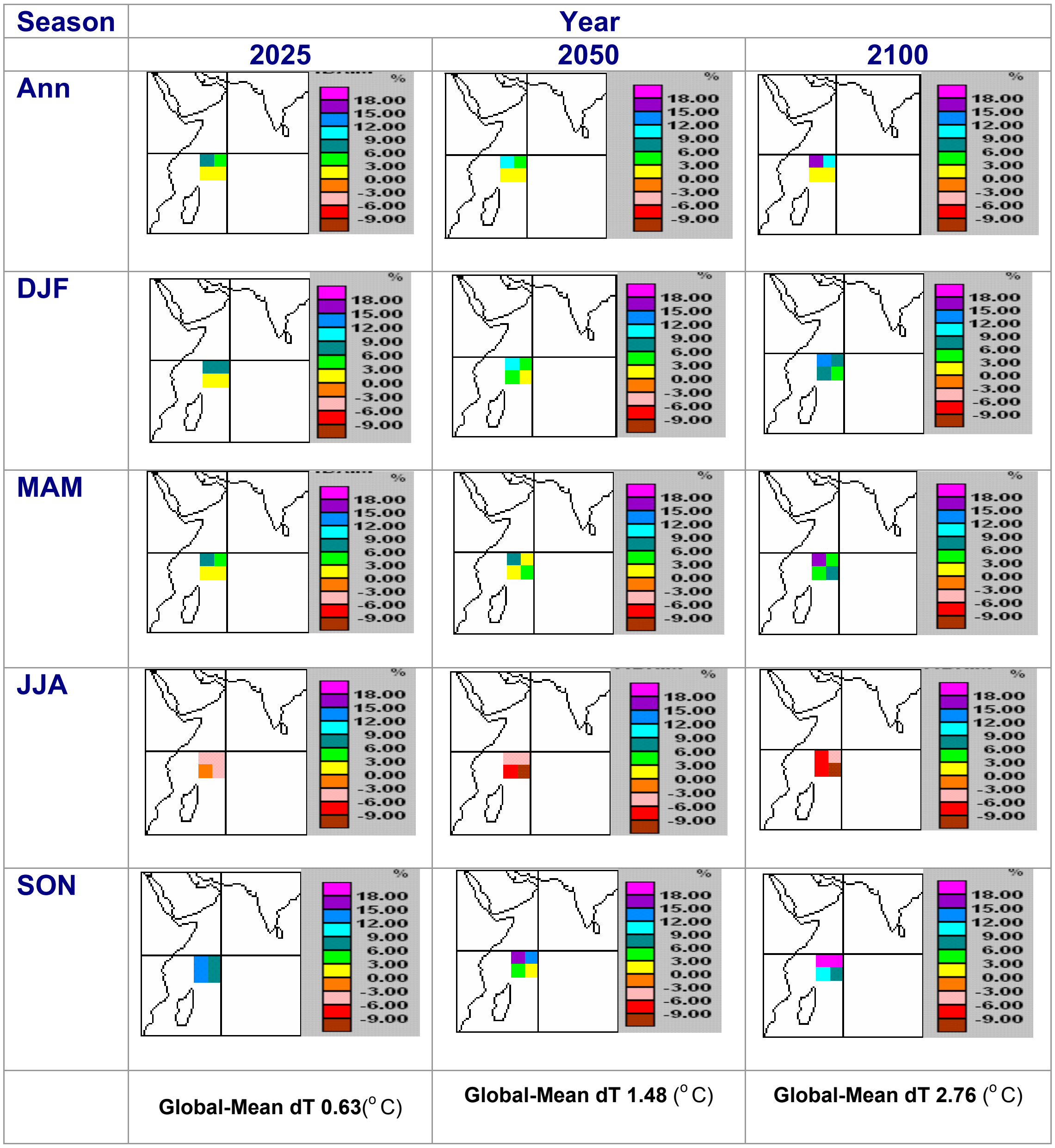

Fig 4.1: Standardized -Average GCMs (CSM, ECH3, ECH4, GFD, HAD2, HAD3, and MODBAR) rainfall projections for A1 high-range emission with high-range climate sensitivity at 5-degree grid size resolution.

Year	GCM Model	Season											
		DJF			MAM			JJA			SON		
		% Change in Rf	Predicted Rf (mm)	Change in Rf (mm)	% Change in Rf	Predicted Rf (mm)	Change in Rf (mm)	% Change in Rf	Predicted Rf (mm)	Change in Rf (mm)	% Change in Rf	Predicted Rf (mm)	Change in Rf (mm)
	Base Rf		**311.0**			**157.3**			**81.13**			**98.3**	
2025	**CSM_D2**	5.3	327.6	16.6	3.7	163.1	5.9	-2.1	79.4	-1.7	-0.4	98.3	-0.4
	ECH3D2	0.0	311.1	0.0	0.0	157.3	0.0	4.2	84.5	3.4	12.4	97.9	12.2
	ECH4D2	2.5	318.9	7.9	11.2	174.8	17.6	5.0	85.2	4.1	13.0	110.4	12.7
	GFDLD2	4.4	324.8	13.8	2.3	160.9	3.6	-8.5	74.2	-6.9	9.5	111.0	9.4
	HAD2D2	6.1	330.0	19.0	5.7	166.3	9.0	-9.2	73.7	-7.4	9.5	107.6	9.4
	HAD3D2	2.1	317.4	6.4	-5.9	148.0	-9.2	-12.3	71.2	-10.0	1.9	107.6	1.9
	MODBAR	4.6	325.3	14.3	1.7	159.9	2.7	-2.8	78.9	-2.2	10.0	100.2	9.9
	Composite Model	**3.6**	**322.2**	**11.1**	**2.7**	**161.5**	**4.2**	**-3.67**	**78.1**	**0.0**	**8.0**	**104.7**	**7.9**
2050	**CSM_D2**	6.7	331.9	20.8	8.5	170.7	13.4	-5.7	76.5	-4.7	-11.2	87.2	-11.0
	ECH3D2	-3.4	300.4	-10.6	1.5	159.6	2.3	6.2	86.2	5.0	13.1	111.1	12.9
	ECH4D2	1.4	315.3	4.2	22.7	192.9	35.7	7.8	87.5	6.3	14.2	112.2	13.9
	GFDLD2	5.0	326.6	15.6	5.8	166.4	9.1	-17.9	66.6	-14.5	7.7	105.8	7.5
	HAD2D2	8.2	336.4	25.4	12.3	176.7	19.4	-19.1	65.6	-15.5	7.7	105.8	7.5
	HAD3D2	0.5	312.5	1.5	-9.7	142.1	-15.2	-25.0	60.8	-20.3	-6.8	91.6	-6.6
	MODBAR	5.3	327.4	16.4	4.7	164.6	7.4	-7.0	75.5	-5.6	8.6	106.7	8.5
	Composite Model	**3.4**	**321.5**	**10.5**	**6.6**	**167.6**	**10.3**	**-8.7**	**74.1**	**0.0**	**4.8**	**102.9**	**4.7**
2100	**CSM_D2**	10.7	344.3	33.3	14.4	179.8	22.6	-6.6	75.8	-5.3	-13.8	84.7	-13.6
	ECH3D2	-6.0	292.5	-18.6	2.7	161.5	4.3	13.1	91.8	10.7	26.3	124.1	25.8
	ECH4D2	1.9	317.0	5.9	37.7	216.5	59.3	15.8	93.9	12.8	28.1	125.9	27.6
	GFDLD2	7.9	335.6	24.6	9.9	172.8	15.5	-26.6	59.6	-21.6	17.3	115.3	17.0
	HAD2D2	13.1	351.8	40.8	20.7	189.7	32.5	-28.6	57.9	-23.2	17.3	115.3	17.0
	HAD3D2	0.5	312.5	1.4	15.6	181.9	24.6	-38.3	50.0	-31.1	-6.5	91.9	-6.4
	MODBAR	8.3	337.0	26.0	8.0	169.9	12.6	-8.6	74.2	-7.0	18.9	116.8	18.6
	Composite Model	**5.2**	**327.2**	**16.2**	**15.6**	**181.7**	**24.5**	**-11.4**	**71.9**	**-9.2**	**12.5**	**110.5**	**12.3**

Table 4.1.1: Observed, percentage change in rainfall (%), predicted seasonal rainfall (mm) and change in rainfall (mm) for the years 2025, 2050 and 2100 for A1 high-range emission with a high-range climate sensitivity

Year	Model	Change in Rf (%)	Change in Rf (mm)	Projected Annual Rf (mm)
1972-1990	OBSERVED			2177.9
2025	CSM_D2	2.5	54.9	2232.8
	ECH3D2	2.7	58.7	2236.6
	ECH4D2	6.4	140.1	2318.0
	GFDLD2	2.6	56.3	2234.2
	HAD2D2	3.5	77.1	2255.0
	HAD3D2	-2.0	-43.0	2134.9
	MODBAR	3.6	78.5	2256.4
	Composite Model	**2.8**	**60.4**	**2238.3**
2050	CSM_D2	2.3	50.0	2227.9
	ECH3D2	2.6	57.2	2235.1
	ECH4D2	9.7	211.7	2389.6
	GFDLD2	2.4	52.6	2230.5
	HAD2D2	4.2	92.0	2269.9
	HAD3D2	6.2	136.0	2313.9
	MODBAR	4.3	94.6	2272.5
	Composite Model	**4.6**	**99.2**	**2277.1**
2100	CSM_D2	5.0	108.3	2286.2
	ECH3D2	5.5	120.2	2298.1
	ECH4D2	17.2	375.1	2553.0
	GFDLD2	5.2	112.6	2290.5
	HAD2D2	8.2	177.7	2355.6
	HAD3D2	-9.1	-198.5	1979.4
	MODBAR	8.4	182.0	2359.9
	Composite Model	**5.8**	**125.3**	**2303.2**

Table 4.2: Percentage change in rainfall (%), change in rainfall (mm) and annual model rainfall (mm) for the years 2025, 2050, and 2100 for A1 high-range emission with a high-range climate sensitivity

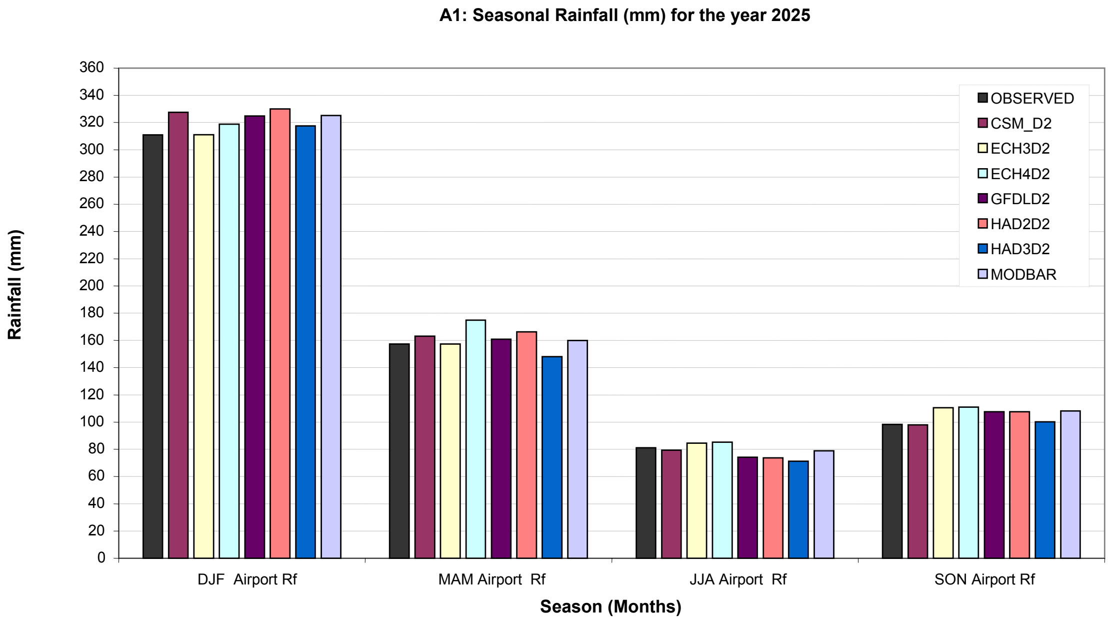

Fig 4.2.1: Observed (1972-1990 –Grey color) and scenarios of seasonal precipitation values (mm) for the International Airport, for A1 high-range emission with a high – range climate sensitivity for the year 2025

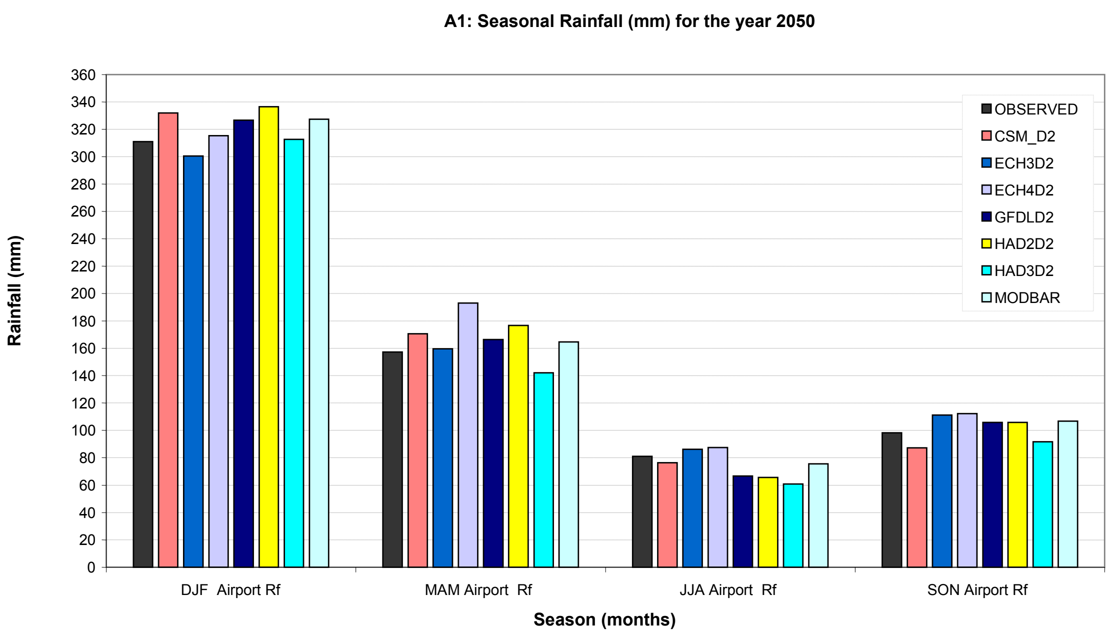

Fig 4.2.2: Observed (1972-1990 –Grey color) and scenarios of seasonal precipitation values (mm) for the International Airport, for A1 high-range emission with a high-range climate sensitivity for the year 2050

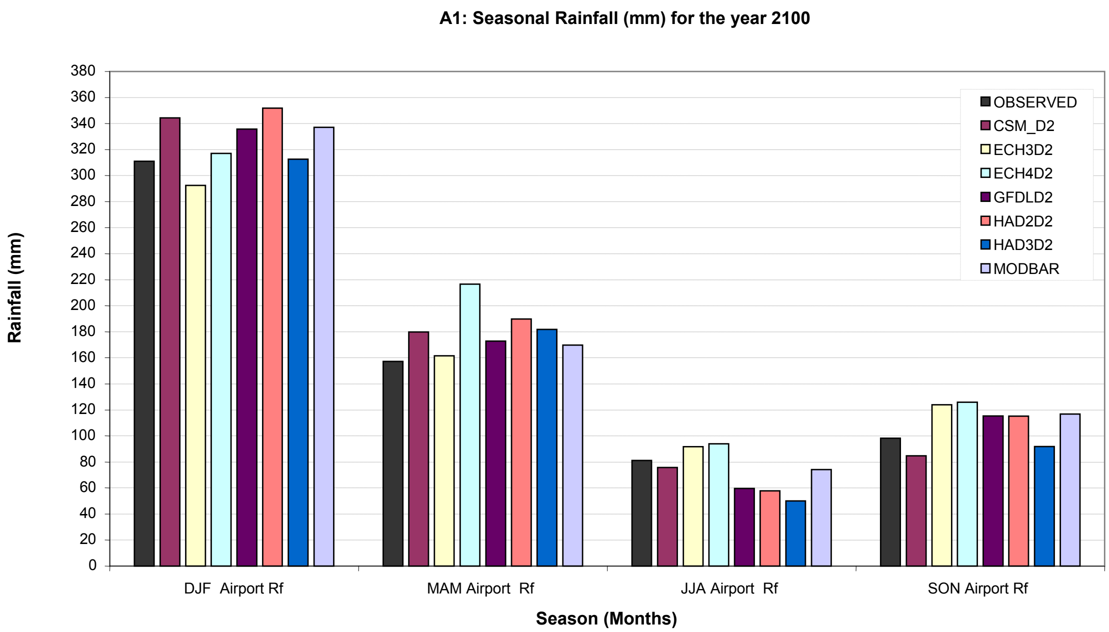

Fig 4.2.3: Observed (1972-1990 –Grey color) and scenarios of seasonal precipitation values (mm) for the International Airport, for A1 high-range emission with a high – range climate sensitivity for the year 2100

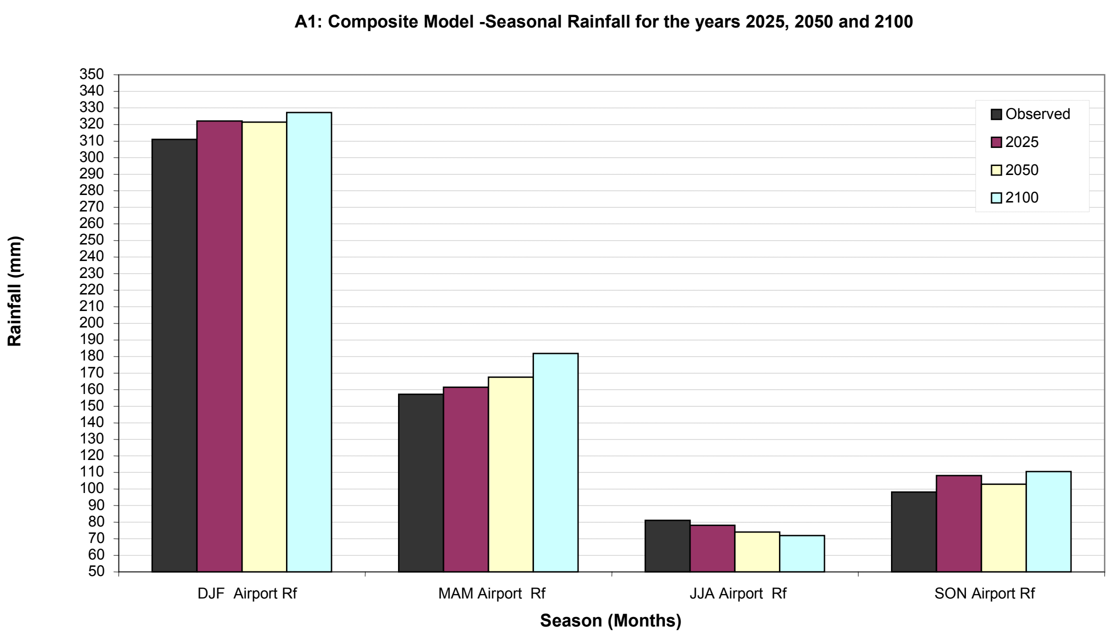

Fig 4.2.4: Observed (1972-1990-Grey color) and composite model scenarios of seasonal precipitation values (mm) for the International Airport for the years 2025, 2050 and 2100 for A1 high-range emission with a high-range climate sensitivity.

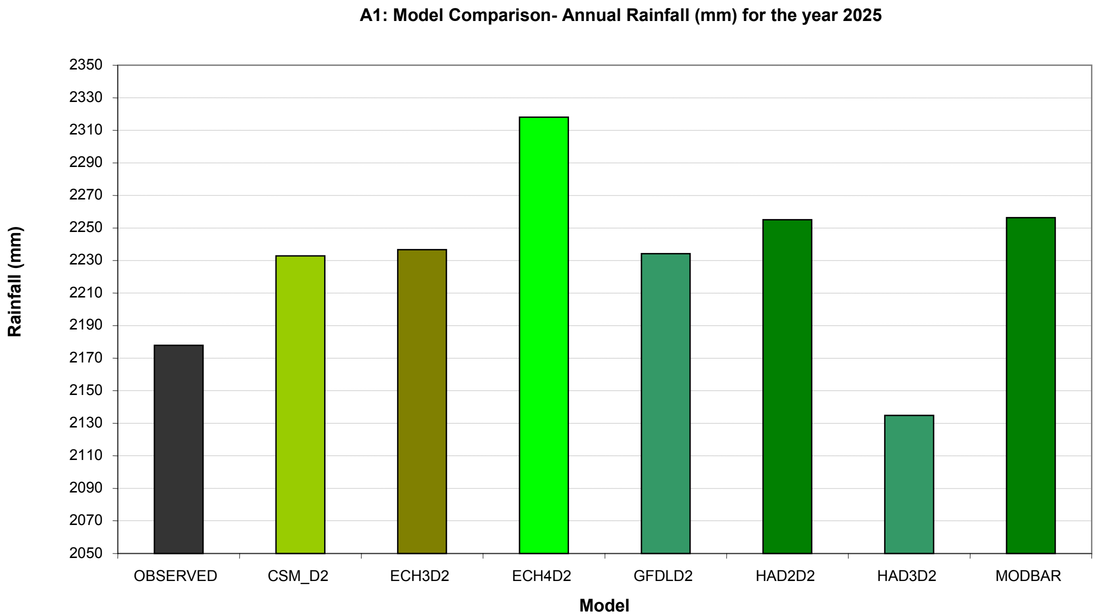

Fig 4.2.5: Observed (1972-1990-Grey color) and model scenarios of annual precipitation values (mm) for the International Airport for the year 2025 for A1 high – range emission with a high-range climate sensitivity.

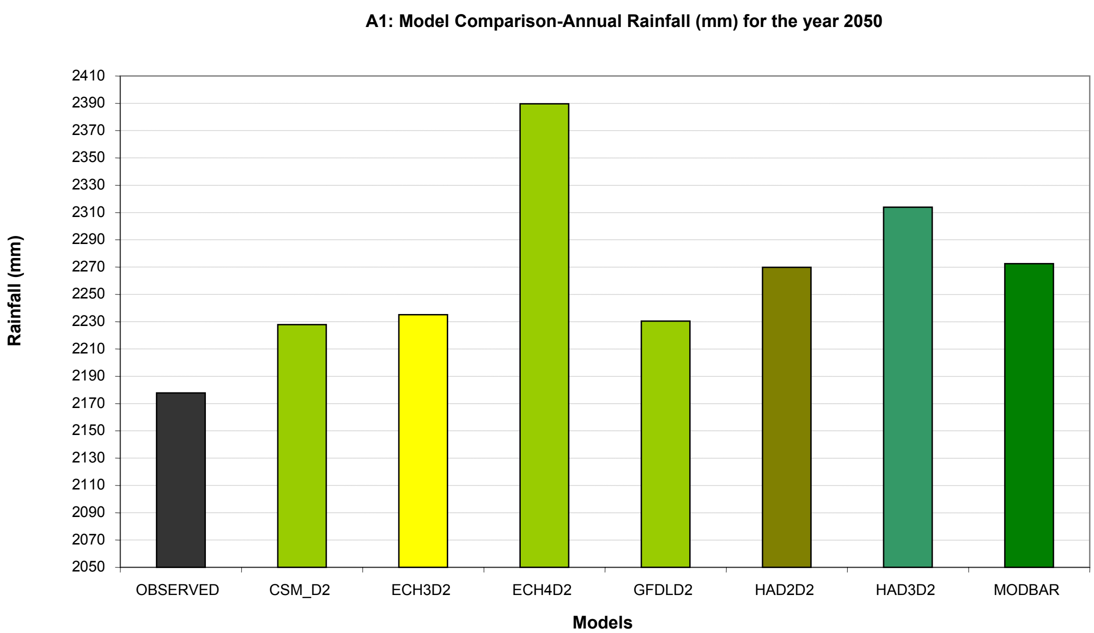

Fig 4.2.6: Observed (1972-1990-Grey color) and model scenarios of annual precipitation values (mm) for the International Airport for the year 2050 for A1 high – range emission with a high-range climate sensitivity.

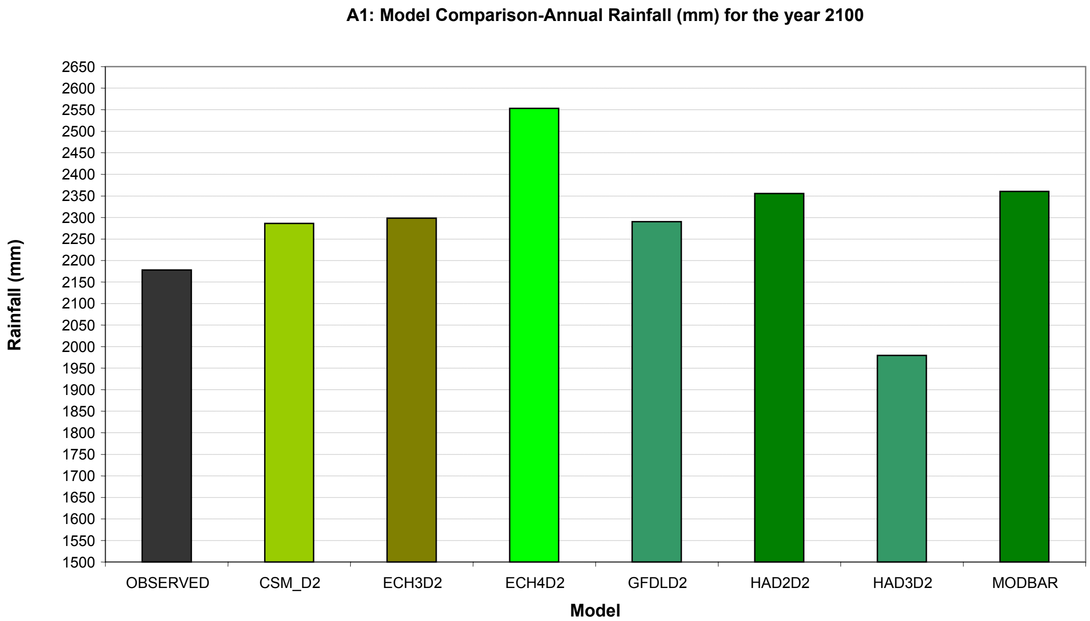

Fig 4.2.7: Observed (1972-1990-Grey color) and model scenarios of annual precipitation values (mm) for the International Airport for the year 2100 for A1 high-range emission with a high-range climate sensitivity.

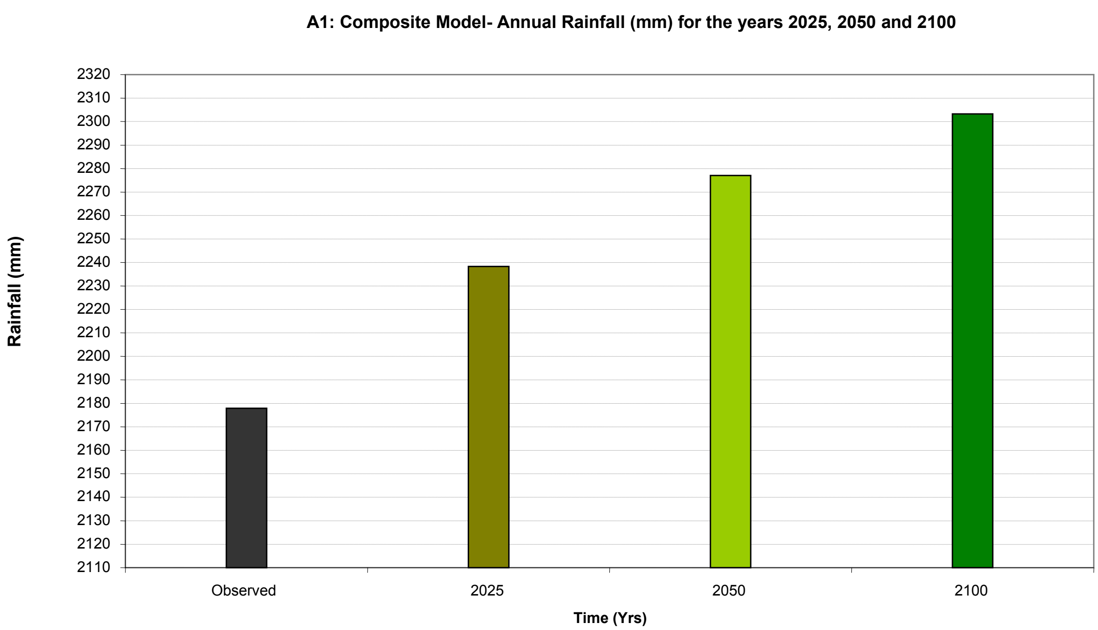

Fig 4.2.8: Observed (1972-1990-Grey color) and composite model scenarios of the annual precipitation values (mm) for the International Airport for the years 2025, 2050 and 2100 for A1 high-range emission with a high-range climate sensitivity.

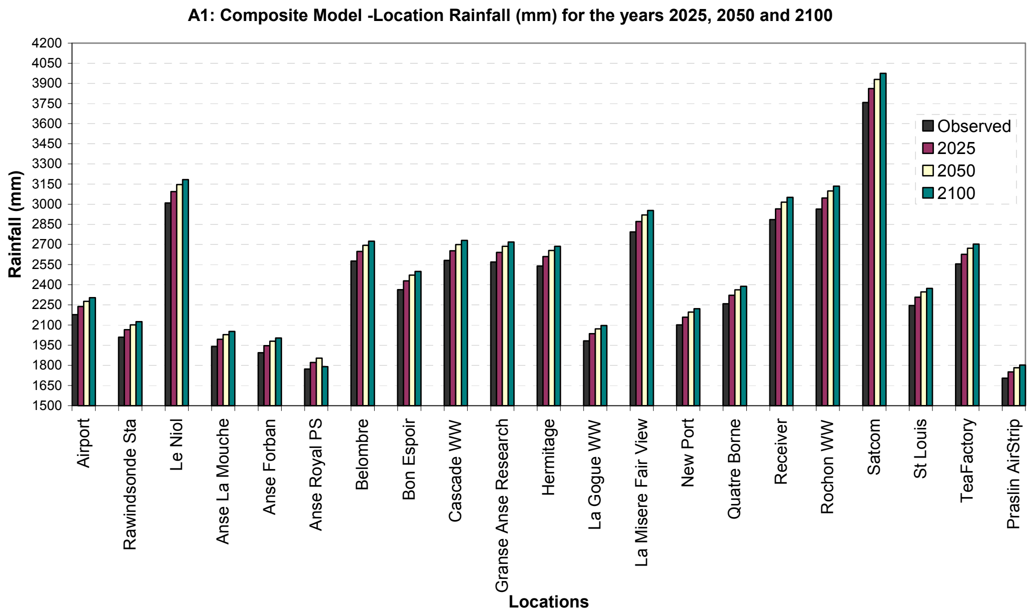

Fig 4.2.9: GCMs annual location rainfall (mm) composite for the years 2025, 2050 and 2100 for A1 high-range emission with high- range climate sensitivity

4.2.1 Spatial Temperature Changes

For brevity, the spatial change in temperature for the A1 high emission with high climate sensitivity from SCENGEN is not shown here. Thus, only the simple downscaling for maximum and minimum temperatures is shown for the International Airport, Mahe, Seychelles.

4.2.2 Extremes of Seasonal Temperature

Table 4.3, shows the detailed temperature statistics for the A1 high-range emission with a high-range climate sensitivity scenario. The individual model projected change in seasonal temperature for the DJF season shows warming from +0.4 to +0.6 ^{o}C for the year 2025, +1.0 to +1.3 ^{o}C for the year 2050 and +1.8 to +2.3 ^{o}C for the year 2100. In the case of the MAM season, the temperature warming is +0.5 to +0.7 ^{o}C for the year 2025, +1.2 to +1.6 ^{o}C for the year 2050 and +1.9 to +2.7 ^{o}C for the year 2100. Similarly for the JJA season, the temperature warming ranges from +0.3 to +0.8 ^{o}C for the year 2025, +0.9 to +1.8 ^{o}C for the year 2050 and +1.7 to +3.1 ^{o}C for the year 2100. Lastly, the SON season temperature warming ranges from +0.4 to +0.7 ^{o}C for the year 2025, +0.9 to +1.5 ^{o}C for the year 2050 and 1.7 to 2.6 ^{o}C for the year 2100. Thus the MAM, JJA seasons will be become relatively increasingly warmer at the end of the century. Figures 4.3.1 to 4.3.6 show the observed (1972-90) and the GCMs scenarios average maximum and minimum temperature values at the International Airport, Mahe, Seychelles.

4.2.3 Composite of Seasonal Temperature

The composite of temperature shows warming of +0.5, +0.6, +0.5 and +0.5 ^{o}C respectively for the DJF, MAM, JJA, and SON seasons (Table 4.3). The year 2050 temperature changes for these respective months are +1.2, +1.3, +1.3 and +1.2 ^{o}C. The temperature warming for the year 2100 for the same respective months are +2.1, +2.4, +2.2, and +2.1 ^{o}C.

The GCMs composite of the A1 high-range emission with a high-range climate sensitivity also shows increasing warming, particularly during the MAM and JJA seasons. Figure 4.3.7 shows the observed (1972-90) and GCM composites of average maximum and minimum temperature values for the years 2025, 2050 and 2100 at the International Airport, Mahe, Seychelles.

4.2.4 Extreme of Annual Temperature

The annual maximum change in temperature is predicted by the ECH4 model (Table not shown). For instance ECH4 shows warming from +0.7, +1.3, and +2.7 ^{o}C for the years 2025, 2050 and 2100 respectively while the CSM shows lower temperature change of +0.6, +0.9 and +1.8 ^{o}C for the years 2025, 2050 and 2100 respectively.

4.2.5 Composite of Annual Temperature

The composite of annual temperature shows warming of +0.5, +1.3 and +2.2 ^{o}C respectively. Thus, the annual mean temperature will become warmer by the year 2100.

Year	Model	Change in DJF Temp	Change in Temp DJF	Change in MAM Temp	Change in Temp MAM	Change in JJA Temp	Change in Temp JJA	Change in SON Temp	Change in Temp SON
	Maximum Temperature (°C)								
	Observed		**30.1**		**31**		**28.6**		**29.6**
2025	**CSM_D2**	0.40	30.5	0.46	31.5	0.43	29.0	0.37	30.0
	ECH3D2	0.45	30.6	0.55	31.5	0.52	29.1	0.51	30.1
	ECH4D2	0.57	30.7	0.70	31.7	0.78	29.4	0.66	30.3
	GFDLD2	0.55	30.6	0.58	31.6	0.49	29.1	0.52	30.1
	HAD2D2	0.52	30.6	0.69	31.7	0.50	29.1	0.48	30.1
	HAD3D2	0.46	30.6	0.54	31.5	0.33	28.9	0.39	30.0
	MODBAR	0.49	30.6	0.57	31.6	0.52	29.1	0.48	30.1
	Composite Model	**0.49**	**30.6**	**0.58**	**31.6**	**0.51**	**29.1**	**0.49**	**30.1**
	Minimum Temperature (°C)								
	Observed		24.2		25.1		24.1		24.2
2025	**CSM_D2**	0.40	24.6	0.46	25.6	0.43	24.5	0.37	24.6
	ECH3D2	0.45	24.7	0.55	25.6	0.52	24.6	0.51	24.7
	ECH4D2	0.57	24.8	0.70	25.8	0.78	24.9	0.66	24.9
	GFDLD2	0.55	24.7	0.58	25.7	0.49	24.6	0.52	24.7
	HAD2D2	0.52	24.7	0.69	25.8	0.50	24.6	0.48	24.7
	HAD3D2	0.46	24.7	0.54	25.6	0.33	24.4	0.39	24.6
	MODBAR	0.49	24.7	0.57	25.7	0.52	24.6	0.48	24.7
	Composite Model	**0.49**	**24.7**	**0.58**	**25.7**	**0.51**	**24.6**	**0.49**	**24.7**
	Maximum Temperature (°C)								
	Observed		30.1		31		28.6		29.6
2050	**CSM_D2**	1.00	31.1	1.16	32.2	1.16	29.8	0.94	30.5
	ECH3D2	1.22	31.3	1.31	32.3	1.37	30.0	1.28	30.9
	ECH4D2	1.30	31.4	1.51	32.5	1.78	30.4	1.47	31.1
	GFDLD2	1.26	31.4	1.34	32.3	1.40	30.0	1.22	30.8
	HAD2D2	1.29	31.4	1.55	32.6	1.27	29.9	1.17	30.8
	HAD3D2	1.13	31.2	1.28	32.3	0.93	29.5	0.87	30.5
	MODBAR	1.18	31.3	1.29	32.3	1.33	29.9	1.16	30.8
	Composite Model	**1.20**	**31.3**	**1.35**	**32.3**	**1.32**	**29.9**	**1.16**	**30.8**
	Minimum Temperature (°C)								
	Observed		24.2		25.1		24.1		24.2
2050	**CSM_D2**	1.00	25.2	1.16	26.3	1.16	25.3	0.94	25.1
	ECH3D2	1.22	25.4	1.31	26.4	1.37	25.5	1.28	25.5
	ECH4D2	1.30	25.5	1.51	26.6	1.78	25.9	1.47	25.7
	GFDLD2	1.26	25.5	1.34	26.4	1.40	25.5	1.22	25.4
	HAD2D2	1.29	25.5	1.55	26.7	1.27	25.4	1.17	25.4
	HAD3D2	1.13	25.3	1.28	26.4	0.93	25.0	0.87	25.1
	MODBAR	1.18	25.4	1.29	26.4	1.33	25.4	1.16	25.4
	Composite Model		**25.4**	**1.35**	**26.4**	**1.32**	**25.4**	**1.16**	**25.4**
	Maximum Temperature (°C)								
2100	**CSM_D2**	1.80	31.9	1.97	33.0	1.99	30.6	1.72	31.3
	ECH3D2	1.98	32.1	2.24	33.2	2.29	30.9	2.15	31.8
	ECH4D2	2.32	32.4	2.73	33.7	3.11	31.7	2.63	32.2
	GFDLD2	2.27	32.4	2.35	33.3	2.20	30.8	2.20	31.8

	HAD2D2	2.19	32.3	2.69	33.7	2.21	30.8	2.07	31.7
	HAD3D2	2.00	32.1	2.22	33.2	1.67	30.3	1.77	31.4
	MODBAR	2.08	32.2	2.32	33.3	2.27	30.9	2.08	31.7
	Composite Model	**2.09**	**32.2**	**2.36**	**33.4**	**2.25**	**30.8**	**2.09**	**31.7**
	Minimum Temperature (°C)								
2100	**CSM_D2**	1.80	26.0	1.97	27.1	1.99	26.1	1.72	25.9
	ECH3D2	1.98	26.2	2.24	27.3	2.29	26.4	2.15	26.4
	ECH4D2	2.32	26.5	2.73	27.8	3.11	27.2	2.63	26.8
	GFDLD2	2.27	26.5	2.35	27.4	2.20	26.3	2.20	26.4
	HAD2D2	2.19	26.4	2.69	27.8	2.21	26.3	2.07	26.3
	HAD3D2	2.00	26.2	2.22	27.3	1.67	25.8	1.77	26.0
	MODBAR	2.08	26.3	2.32	27.4	2.27	26.4	2.08	26.3
	Composite Model	**2.09**	**26.3**	**2.36**	**27.5**	**2.25**	**26.3**	**2.09**	**26.3**

Table 4.3: Observed, change in temperature and seasonal GCMs composite of temperature (°C) for the years 2025, 2050 and 2100 for A1 high-range emission with a high-range climate sensitivity

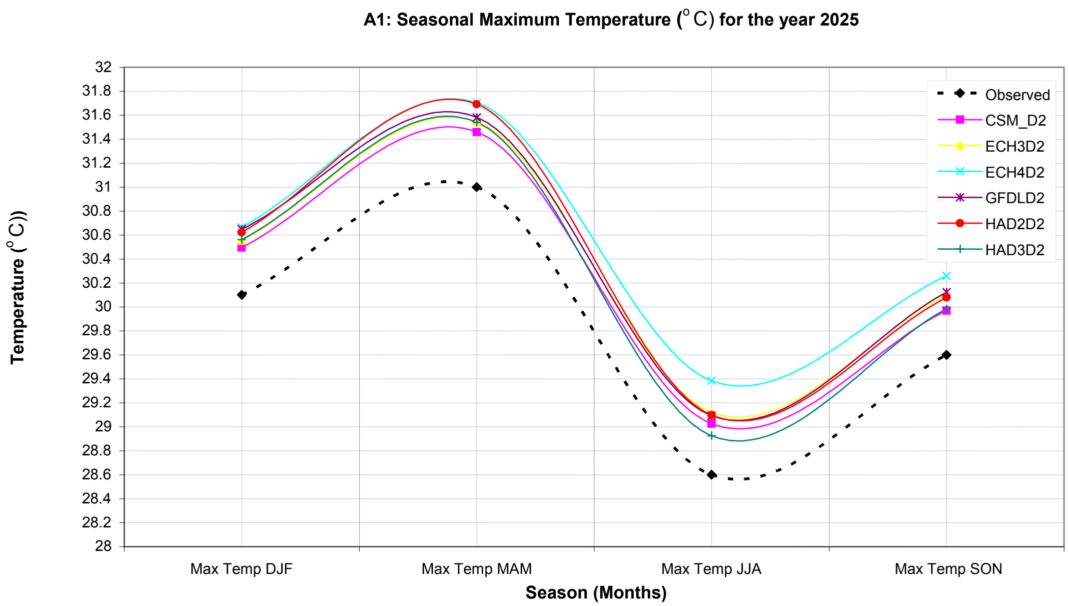

Fig 4.3.1: Observed (1972-90) and scenarios for the average seasonal maximum temperature values (°C) for the International Airport, Mahe, Seychelles for the A1 high-range emission with a high-range climate sensitivity for the year 2025

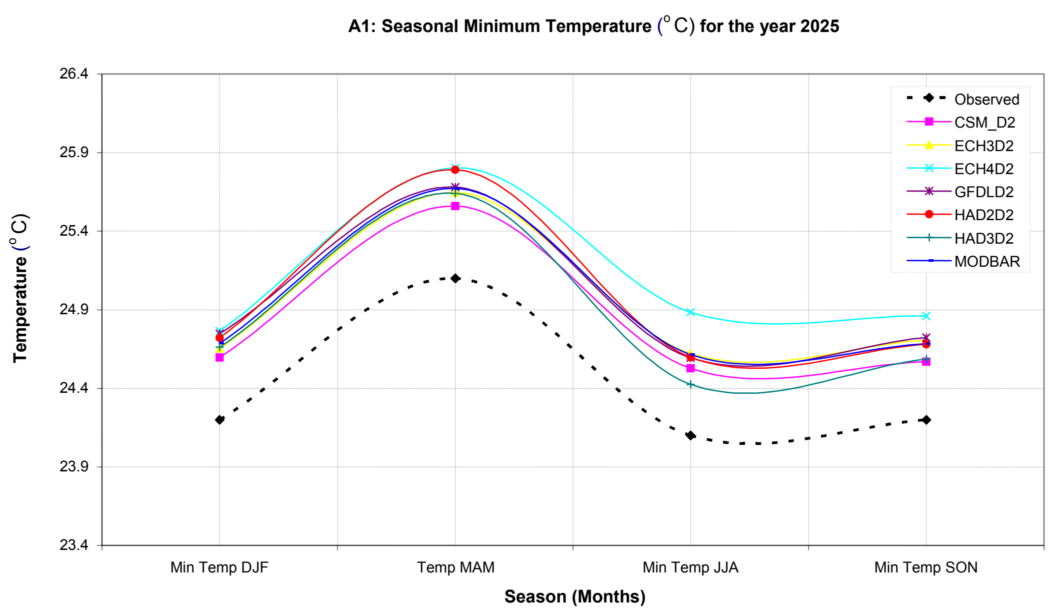

Fig 4.3.2: Observed (1972-90) and scenarios for the average seasonal minimum temperature values (°C) for the International Airport, Mahe, Seychelles for the A1 high-range emission with a high-range climate sensitivity for the year 2025

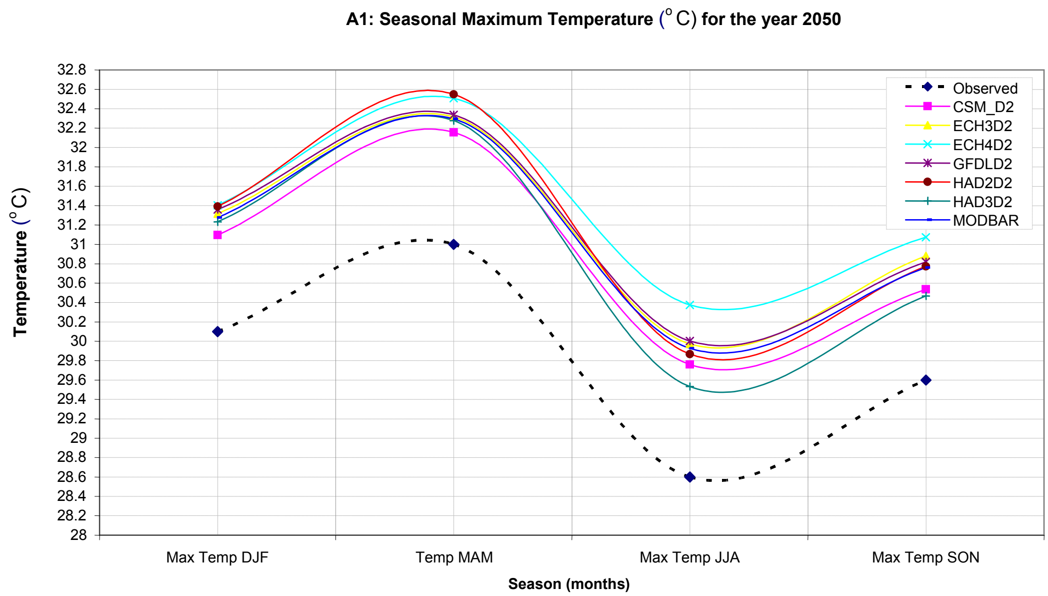

Fig 4.3.3: Observed (1972-90) and scenarios for the average seasonal maximum temperature values (° C) for the International Airport, Mahe, Seychelles for the A1 high-range emission with a high-range climate sensitivity for the year 2050

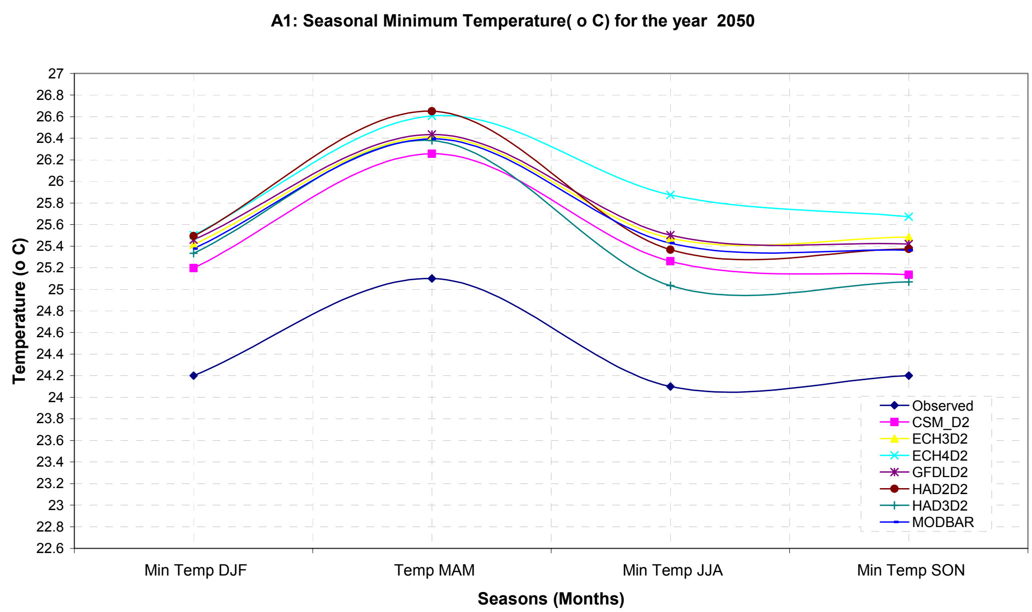

Fig 4.3.4: Observed (1972-90) and scenarios for the average seasonal minimum temperature values (° C) for the International Airport, Mahe, Seychelles for the A1 high–range emission with a high-range climate sensitivity for the year 2050

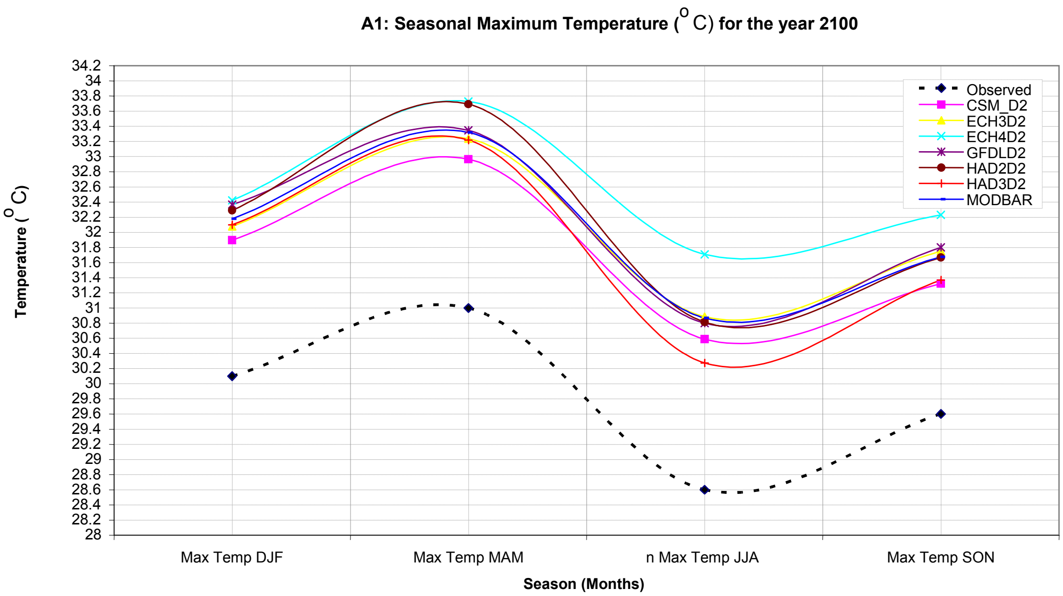

Fig 4.3.5: Observed (1972-90) and scenarios for the average seasonal maximum temperature values (° C) for the International Airport, Mahe, Seychelles for the A1 high-range emission with a high-range climate sensitivity for the year 2100

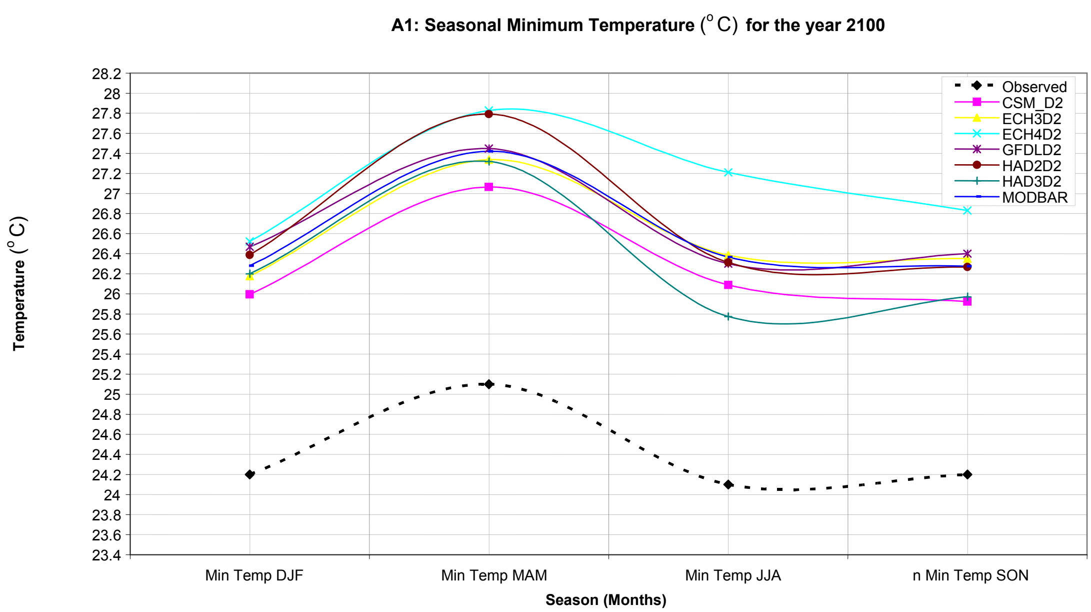

Fig 4.3.6: Observed (1972-90) and scenarios for the average seasonal minimum temperature values (° C) for the International Airport, Mahe, Seychelles for the A1 high-range emission with a high-range climate sensitivity for the year 2100

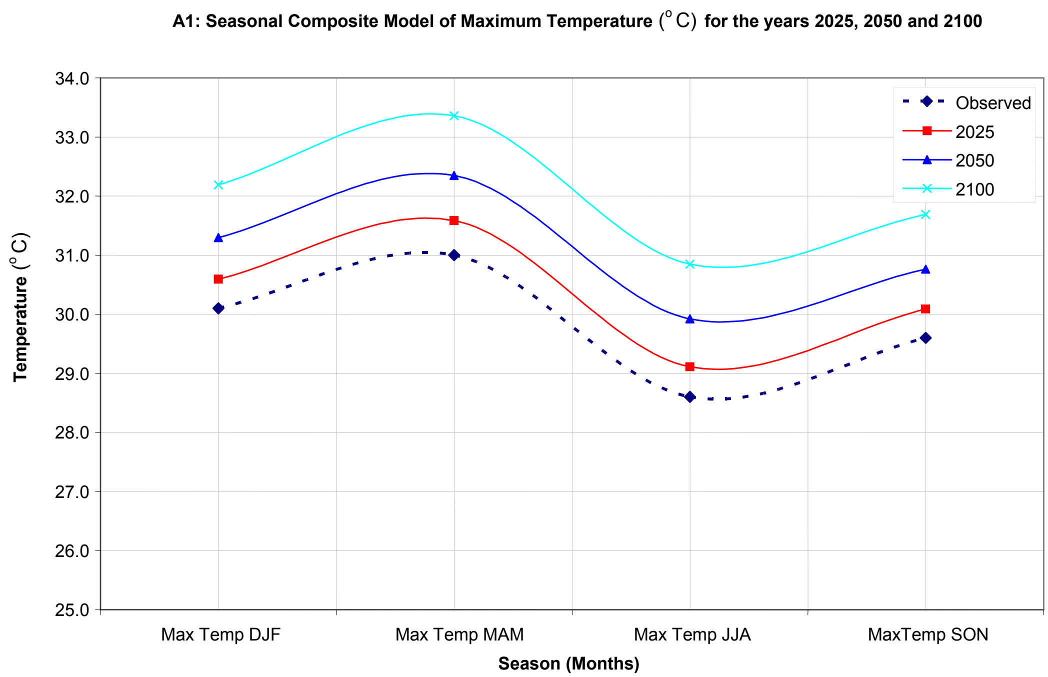

Fig 4.3.7: Observed (1972-90) and GCMs composite seasonal maximum temperature values (° C) for the International Airport, Mahe, Seychelles for the A1 high-range emission with a high-range climate sensitivity for the years 2025, 2050 and 2100

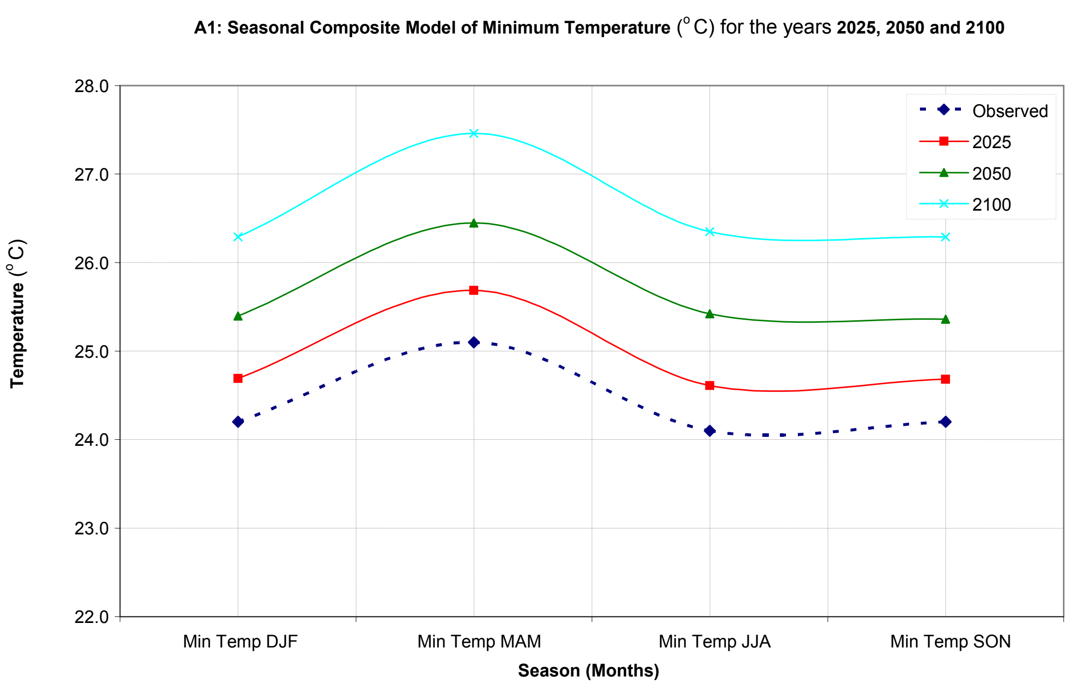

Fig 4.3.8: Observed (1972-90) and GCMs composite seasonal minimum temperature values (° C) for the International Airport, Mahe, Seychelles for the A1 high-range emission with a high-range climate sensitivity for the years 2025, 2050 and 2100

Chapter 5

Comparison between Climate Scenarios

5.0 Comparison between Climate Scenarios

In this section, the B2 mid-range emission with mid-range climate sensitivity and the A1 high-range emission and high climate sensitivity for rainfall climate scenarios are compared.

5.1.1 Extreme Seasonal Rainfall

The individual models output show that maximum and minimum percentage change in rainfall for the DJF season is quite similar for both climate scenarios, but the AH scenario projects a slightly dryer DJF season (-9.4 %) compared to the BM scenario (-5.3 %) (Table 5.1). In the case of the MAM season, the AH scenario shows a wetter climate (+71.6%) compared to the BM scenario with 62.8%. The BM scenario shows a wetter type of climate (+39.8 %) compared to the AH scenario (+25.6 %) for the JJA season, however both scenarios tend to be in close agreement in terms of projecting a dryer climate during the southeast monsoon. The AH scenario shows a slightly wetter SON season compared to the BM scenario, but both scenarios agree closely in terms of simulating the minimum rainfall for the SON season.

5.1.2 Seasonal Rainfall Composite

Table 5.2 shows the GCMs seasonal rainfall composite. The BM and AH scenarios composite are fairly consistent in predicting the DJF season rainfall, however, it is clear that the AH climate scenario projects a wetter climate for the MAM and SON seasons and a dryer climate for the JJA season compared to the BM climate scenario. Figure 5.1 shows the general projected seasonal and annual trends with respect to the two climate scenarios.

5.2.1 Extreme Annual Rainfall

The GCMs extreme projected change in annual rainfall is shown in Table 5.3 below. The AH scenario shows maximum predicted rainfall, while the BM scenario shows dryer annual rainfall for the year 2050. The AH scenario simulates more extreme rainfall (-9.1% to 17.2%) for the year 2100 compared to the BM scenario.

5.2.2 Annual Rainfall Composite

The rainfall composite shows that AH scenario projects a slightly wetter climate compared to the BM scenario (Table 5.4, Fig 5.2). Thus, the A1 high-range emission with a high climate sensitivity scenario (AH) also shows extreme rainfall changes compared to the B2 mid-range emission with mid-range climate sensitivity (BM).

Overall, the AH scenario tends to project a wetter climate for the MAM, and SON seasons while the BM scenario predicts a relatively dryer and wetter climate for the MAM and JJA seasons respectively. Both scenarios are fairly consistent in projecting the rainfall in the DJF season.

The next chapter analyses climate scenario for Aldabra area using the B2 mid-range emission with mid-range climate sensitivity

Year	BM DJF % Change	AH DJF % Change	BM MAM % Change	AH MAM % Change	BM JJA % Change	AH JJA % Change	BM SON % Change	AH SON % Change
2025	0.6 to 5.9	0 to 6.1	-5.4 to 9.4	-5.9 to 11.2	-12.7 to 2.3	-12.3 to 5.0	-5.2 to 6.4	-5.2 to 12.7
2050	-0.3 to 9.3	-3.4 to 8.2	-9.2 to 17.7	-9.7 to 22.7	-7.7 to 22.7	-2.5 to 7.8	-10.4 to 10.7	-11.2 to 14.2
2100	-5.6 to 12.4	-6.0 to 13.1	-14.8 to 35.7	2.7 to 37.7	-36.3 to 14.9	-38.3 to 12.8	-13.1 to 26.6	-13.8 to 26.3
Total	-5.3 to 27.6	-9.4 to 27.4	-29.4 to 62.8	-12.9 to 71.6	-56.7 to 39.8	-53.1 to 25.6	-28.7 to 43.7	-30.3 to 53.2

Table 5.1: GCMs projected extreme percentage change (%) in seasonal rainfall for the AH and BM climate scenarios

Year	BM DJF % Change	AH DJF % Change	BM MAM % Change	AH MAM % Change	BM JJA % Change	AH JJA % Change	BM SON % Change	AH SON % Change
2025	3.7	3.6	2.0	2.7	-3.3	-3.7	3.8	8.0
2050	5.3	3.4	4.3	6.6	7.3	-8.7	2.4	4.8
2100	4.9	5.2	10.5	15.6	-10.8	-14.4	11.8	12.5
Total	13.9	12.2	16.8	24.9	-6.8	-26.8	18.0	25.3

Table 5.2: GCMs projected composite percentage change (%) in seasonal rainfall with AH and BM climate scenarios.

Year	BM % Change in Rainfall	AH % change in Rainfall
2025	-2.0 to 6.4	-2.0 to 6.4
2050	-4.8 to 8.5	2.3 to 9.7
2100	-8.6 to 16.3	-9.1 to 17.2

Table 5.3: GCMs projected extreme percentage change (%) in annual rainfall with AH and BM climate scenarios

Year	BM % change in Rainfall	AH % change in Rainfall
2025	2.8	2.8
2050	2.7	4.6
2100	5.4	5.8

Table 5.4: GCMs projected composite percentage change (%) in annual rainfall with AH and BM climate scenarios

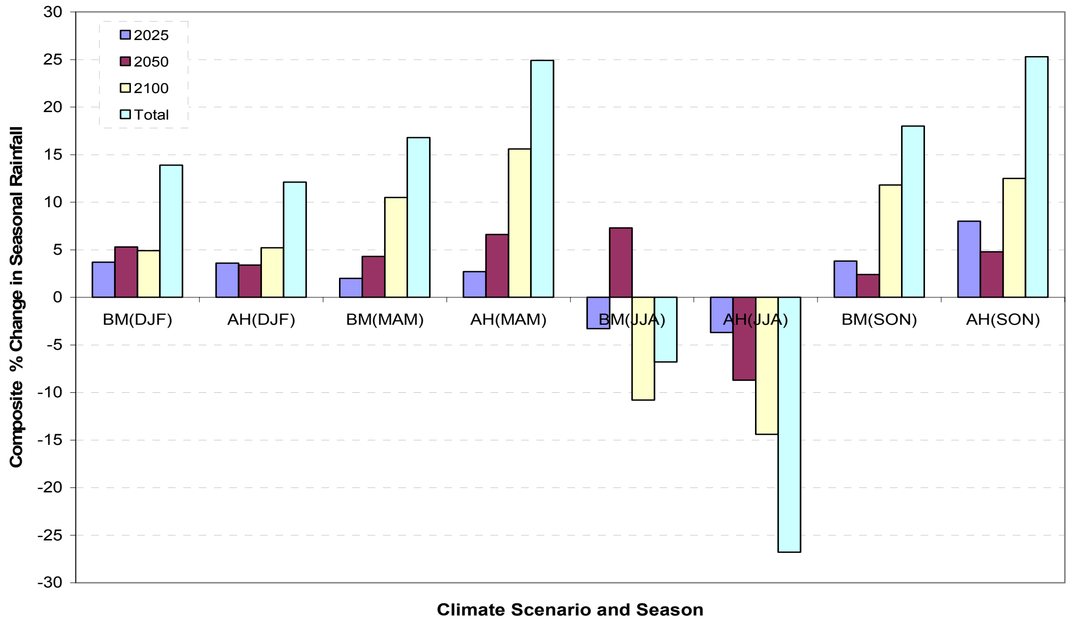

Fig 5.1: GCMs projected composite percentage change (%) in seasonal rainfall with AH and BM climate scenarios.

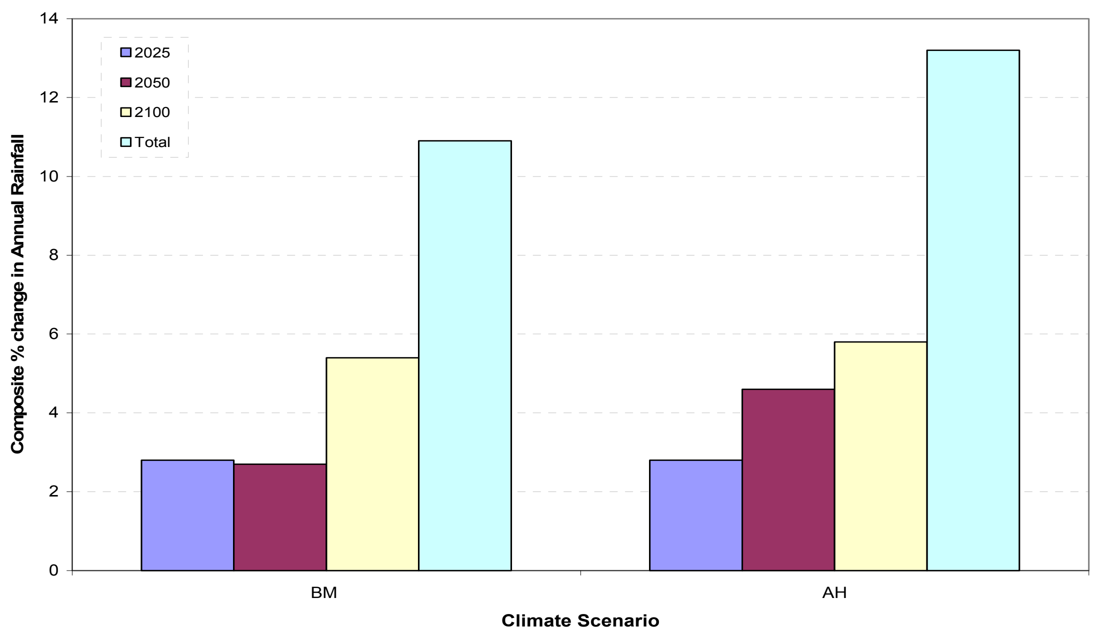

Fig 5.2: GCMs projected composite percentage change (%) in annual rainfall with AH and BM climate scenarios

.

Chapter 6

Climate Changes for Aldabra Group- B2 Mid-Range Emission with Mid-Range Climate Sensitivity

6.0 Climate Changes for Aldabra Group- B2 Mid-Range Emission with Mid-Range Climate Sensitivity (BM)

6.1.1 Spatial Rainfall Changes

The GCMs spatial percentage change in rainfall in the case of the BM scenario for Aldabra area are shown in Figure 6.1 for the DJF and the JJA seasons only. It also includes the annual percentage precipitation changes. In principle, one can apply the percentage change to any rainfall data located within the defined boundary (Fig 1b). However, in this section, only the percentage change in rainfall is analyzed.

The spatial graphical output shows positive, wetter-like climate changes for the DJF season while much anticipated negative, dryer –like climate for the JJA season. The percentage change in annual rainfall is not significant. The wet and the drying spatial changes seems to suggest dryer and wetter conditions by the year 2100.The SCENGEN output files are therefore analyzed for further details. Table 6.1, shows the detailed statistics for the Aldabra climate scenario for the DJF and the JJA seasons and the annual percent change in rainfall.

6.1.2 Extremes of Seasonal rainfall

The individual GCM projected change in seasonal rainfall for the DJF season show a minimum of -0.3 % and a maximum change of +7.2 % in rainfall for the year 2025. The lowest change in predicted rainfall is -1.1% while the maximum change is +12.6 % for the year 2050 and -6.2 %, +19.5 % for the year 2100.On the other hand, the GCMs individual projections for the JJA season shows consistent negative change in rainfall from -1.9 % to -17.4 % for the year 2025, -1.9 % to -30.1 % for the year 2050 and 8.1 %, to -44.6 % for the year 2100. Figures 6.1.1 to 6.1.3 show the GCMs rainfall projections for years 2025, 2050 and 2100.

6.1.3 Composite of Seasonal and Annual Change in Rainfall

The composite rainfall changes for the year 2025 are +3.1 % and -10.5 % for the DJF and the JJA seasons respectively. The year 2050 composite rainfall changes for these respective months are +5.1 %, and -17.6 % while the year 2100 composite rainfall changes are 5.5 %, and -21.1 %.Thus, the GCMs composite shows slightly wetter climate for the DJF season and significantly dryer climate up to -21.1 % for the Aldabra area by the year 2100 compared to the 1972-1990 period.

In contrast, the GCMs composite change in annual rainfall for the years 2025, 2050 and 2100 is -1.6, -2.5 and -2.5 % respectively. The annual rainfall is projected to decrease slightly by the year 2100, but it is projected that there could be a major decrease in rainfall during the southeast monsoon (JJA). Figure 6.1.4 shows the GCMs composite for the DJF and JJA seasonal and annual precipitation values for the Aldabra area for the years 2025, 2050 and 2100.

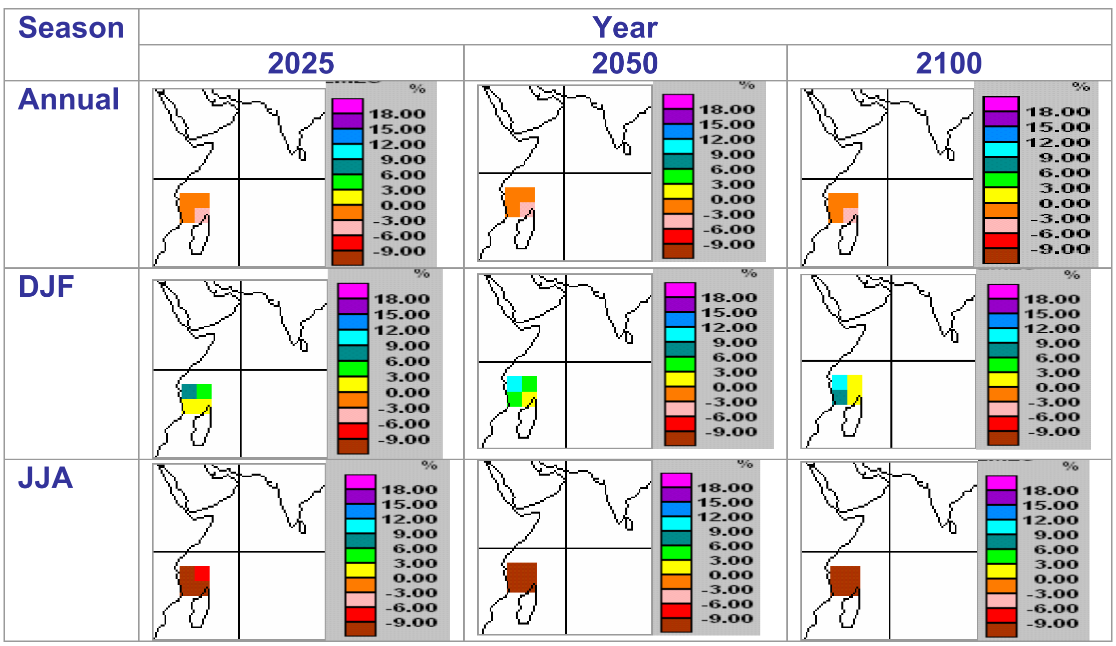

Fig 6.1: Rainfall projections as percentage change (%) for the B2 mid-range emission with a mid-range climate sensitivity at 5 degree grid size resolution for climatic region 2 (Aldabra area, Seychelles)

Year	GCM Model	DJF (% change)	JJA (% change)	Annual (% change)
2025	CSM_D2	5.125	-1.982	2.557
	ECH3D2	-0.32	-7.455	-1.773
	ECH4D2	2.091	-15.405	-4.02
	GFDLD2	0.568	-4.456	0.474
	HAD2D2	7.204	-17.403	-2.006
	HAD3D2	3.991	-16.532	-3.959
	MODBAR	3.11	-10.539	-1.454
	COMPOSITE MODEL	3.1	-10.5	-1.6
2050	CSM_D2	8.815	-1.991	4.835
	ECH3D2	-1.111	-11.965	-3.058
	ECH4D2	3.284	-26.458	-7.153
	GFDLD2	0.508	-6.5	1.038
	HAD2D2	12.604	-30.099	-3.482
	HAD3D2	6.748	-28.51	-7.043
	MODBAR	5.142	-17.587	-2.477
	COMPOSITE MODEL	5.1	-17.6	-2.5
2100	CSM_D2	12.381	8.113	11.267
	ECH3D2	-6.24	-10.599	-3.541
	ECH4D2	2.005	-37.786	-11.223
	GFDLD2	-3.204	-0.345	4.143
	HAD2D2	19.488	-44.618	-4.336
	HAD3D2	8.504	-41.637	-11.016
	MODBAR	5.489	-21.146	-2.451
	COMPOSITE MODEL	5.5	-21.1	-2.5

Table 6.1: Percentage change (%) in mean seasonal, annual and composite model rainfall for the years 2025, 2050 and 2100 for the B2 mid-range emission with a mid range climate sensitivity (Aldabra area, Seychelles)

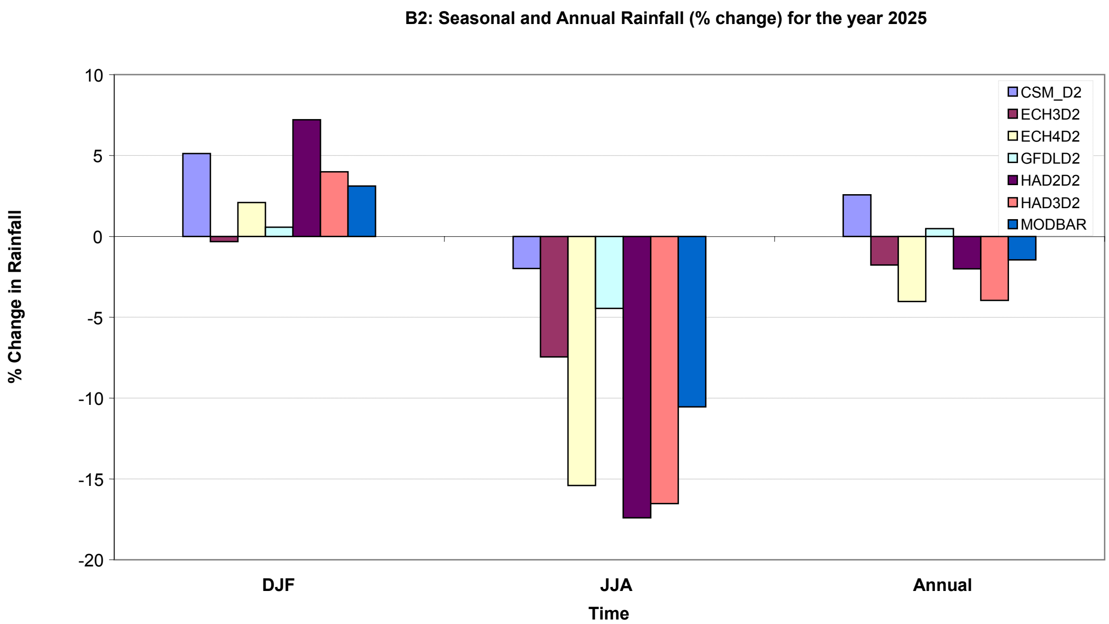

Fig 6.1.1: Seasonal and annual percentage change (%) in rainfall for the year 2025 (Aldabra area, Seychelles)

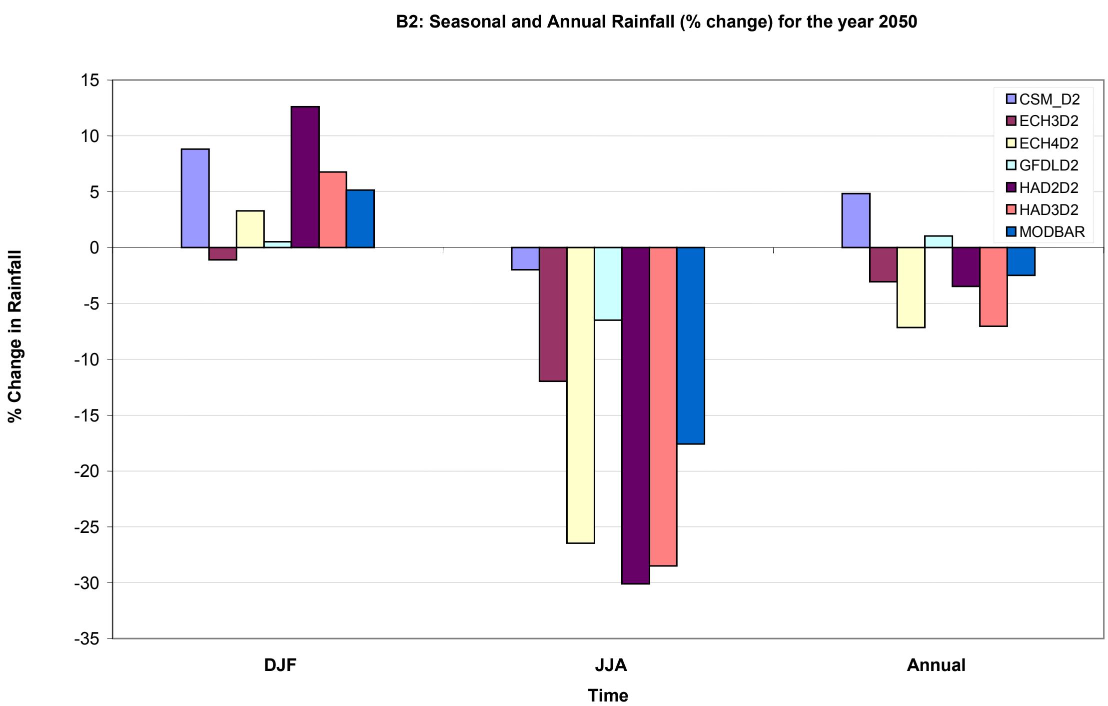

Fig 6.1.2: Seasonal and annual percentage change (%) in rainfall for the year 2050 (Aldabra area, Seychelles)

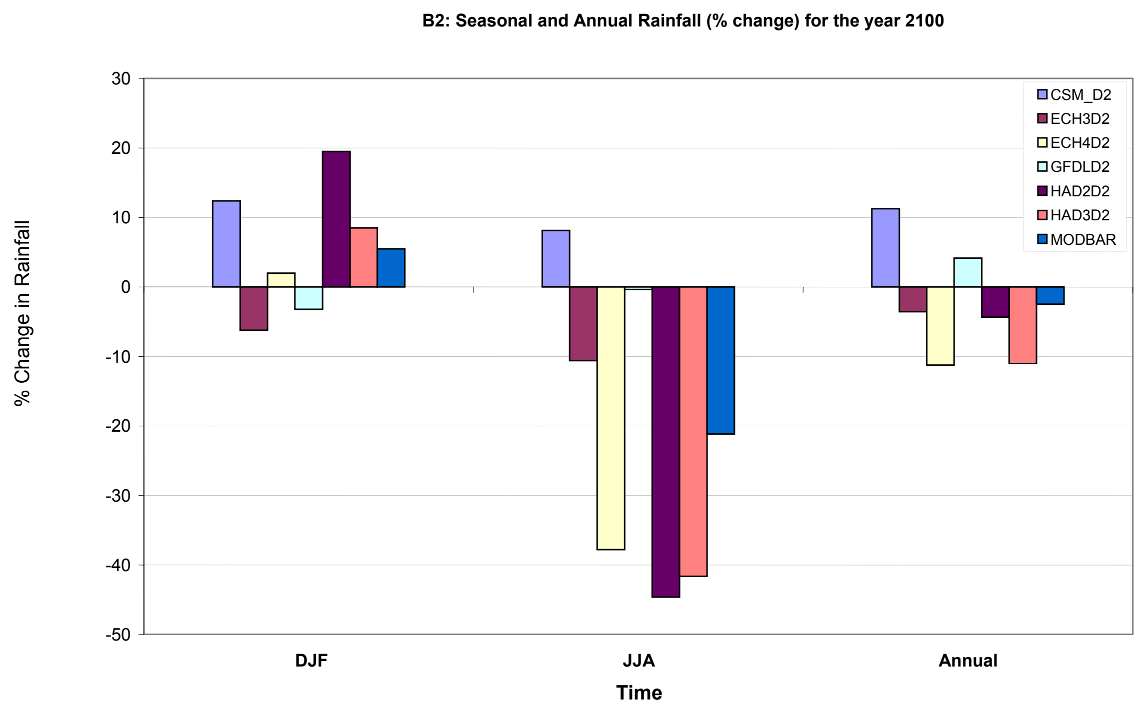

Fig 6.1.3: Seasonal and annual percentage change (%) in rainfall for the year 2100 (Aldabra area, Seychelles)

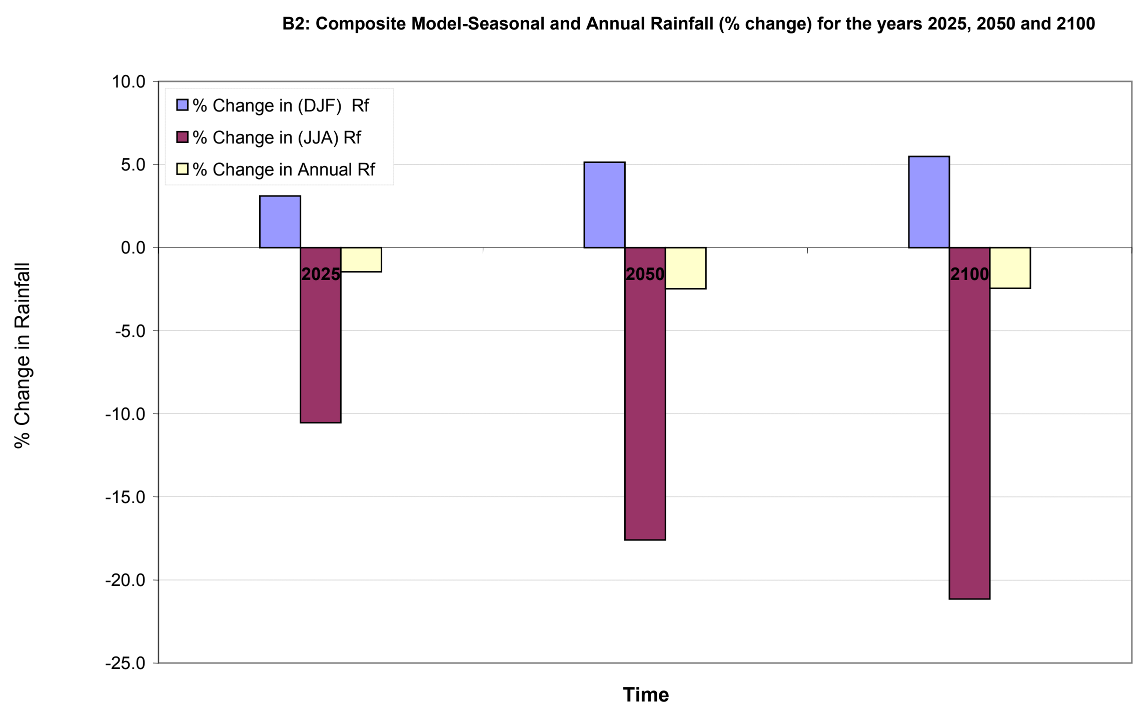

Fig 6.1.4: Composite Model of seasonal and annual percentage change (%) in rainfall for the years 2025, 2050 and 2100 (Aldabra area, Seychelles)

6.2 Spatial Temperature Changes

The spatial temperature is shown Figure 6.2.1. There is an indication of seasonal and annual warming for the years 2025, 2050 and 2100. Further detailed analyses are carried out using the SCENGEN output files.

6.2.1 Extreme change in temperature

The GCMs projected change in seasonal temperature shows warming ranging from +0.5 to +0.6 ^{o}C for the year 2025, +0.8 to +1.1 ^{o}C for the year 2050 and +1.6 to +2.1 ^{o}C for the DJF season. The warming range from +0.5 to +0.8 ^{o}C for the year 2025, +0.8 to +1.5 ^{o}C for 2050 and +1.5 to +2.9 ^{o}C for the year 2100 (Table 6.2). Figures 6.2.2 to 6.2.4 show the GCM seasonal change in temperature for the Aldabra area.

The GCMs projections for the annual temperature (Table 6.2 and Figures 6.2.2 to 6.2.4) show temperature ranging from +0.4 to +0.7 ^{o}C for the year 2025, +0.9 to +1.4 ^{o}C for the year 2050 and +2.0 to +2.9 ^{o}C for the year 2100. Thus, individual GCM shows warming of +0.8, +1.7 and +3.5 ^{o}C for the JJA season for the years 2025, 2050 and 2100 respectively. The annual temperature projection by GCM shows maximum warming of +0.6, +1.2, and +2.6 ^{o}C respectively in the years 2025, 2050 and 2100.

6.2.2 Composite of Seasonal and Annual Change in Temperature

The composite of temperature changes for the year 2025 are +0.5, and +0.7 ^{o}C for the DJF and JJA seasons respectively (Fig 6.2.5). The year 2050 temperature changes for these respective months are +1.0 and +1.2 ^{o}C. The individual model respective seasonal temperature change for the year 2100 is +1.9 and +2.2 ^{o}C. Therefore, the GCMs composite shows a warmer type of climate, especially for the JJA season. Figure 6.2.5 shows the GCMs change in the DJF, JJA seasons and annual temperature values for the Aldabra area, for the years 2025, 2050 and 2100.

To test the consistency of the results obtained above, the P50, business as usual emission is set as the policy scenario. The result by individual model shows maximum warming of +0.8, +1.7 and +3.5 ^{o}C for the JJA season respectively for the years 2025, 2050 and 2100. Similarly, the annual temperature projection for the years 2025, 2050 and 2100 shows +0.6, +1.2 and +2.6 °C warming respectively. The GCMs rainfall projections for the JJA season are also fairly consistent with the BM scenario, but characterized by dryer climate. The lowest predicted change in rainfall is -33.7 % for the year 2050 and -53.7 % for the Aldabra area in the year 2100.

The next chapter explores GCM –statistical analyses of regional climate change.

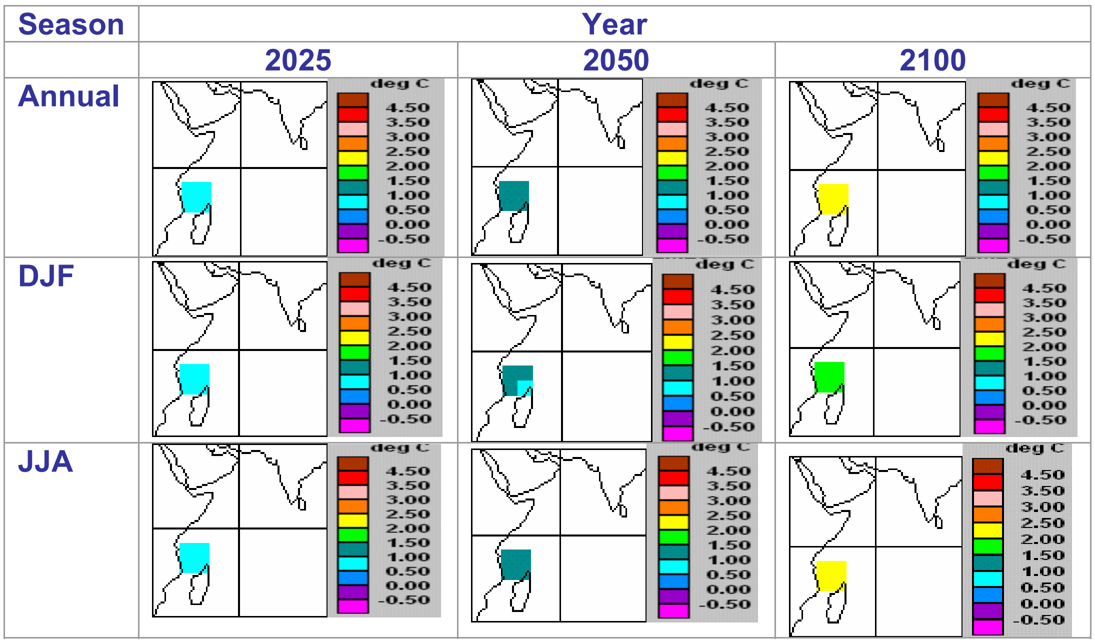

Fig 6.2.1: Temperature (°C) projections for the B2 mid-range emission with a mid-range climate sensitivity at 5 degree grid size resolution for Aldabra area, Seychelles.

Year	GCM Model	(DJF) (^{o}C)	(JJA) (^{o}C)	Annual (^{o}C)
2025	**CSM_D2**	0.449	0.566	0.496
	ECH3D2	0.541	0.716	0.612
	ECH4D2	0.603	0.849	0.699
	GFDLD2	0.546	0.716	0.593
	HAD2D2	0.595	0.632	0.627
	HAD3D2	0.508	0.451	0.469
	MODBAR	0.54	0.655	0.583
	COMPOSITE MODEL	**0.5**	**0.7**	**0.6**
2050	**CSM_D2**	0.832	1.02	0.907
	ECH3D2	1.001	1.292	1.118
	ECH4D2	1.114	1.534	1.278
	GFDLD2	1.01	1.292	1.085
	HAD2D2	1.099	1.139	1.146
	HAD3D2	0.94	0.809	0.858
	MODBAR	0.999	1.181	1.065
	COMPOSITE MODEL	**1.0**	**1.2**	**1.1**
2100	**CSM_D2**	1.613	1.911	1.739
	ECH3D2	1.929	2.422	2.135
	ECH4D2	2.142	2.876	2.434
	GFDLD2	1.947	2.422	2.072
	HAD2D2	2.113	2.135	2.187
	HAD3D2	1.814	1.515	1.648
	MODBAR	1.926	2.214	2.036
	COMPOSITE MODEL	**1.9**	**2.2**	**2.0**

Table 6.2: Change in mean seasonal, annual and composite model mean temperature (^{o}C) for the years 2025, 2050 and 2100 for the B2 mid-range emission with a mid-range climate sensitivity (Aldabra area, Seychelles)

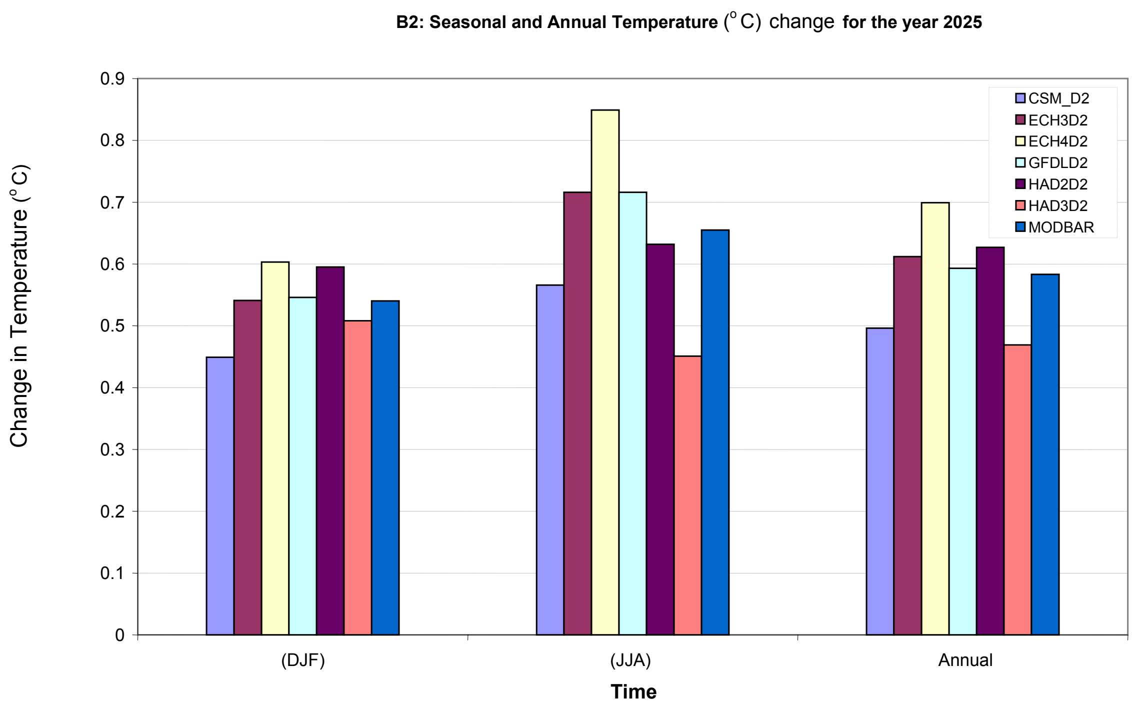

Fig 6.2.2: Change in seasonal and annual mean temperatures (^{o}C) for the year 2025 (Aldabra area, Seychelles)

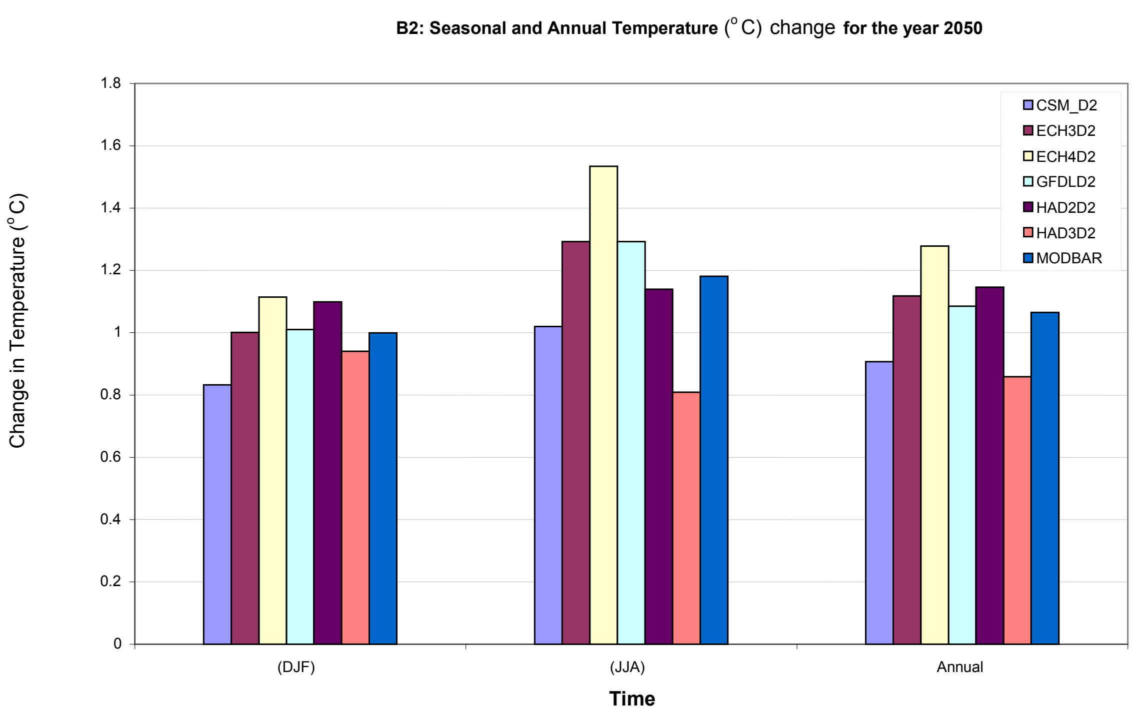

Fig 6.2 .3: Change in seasonal and annual mean temperatures (^{o}C) for the year 2050 (Aldabra area, Seychelles)

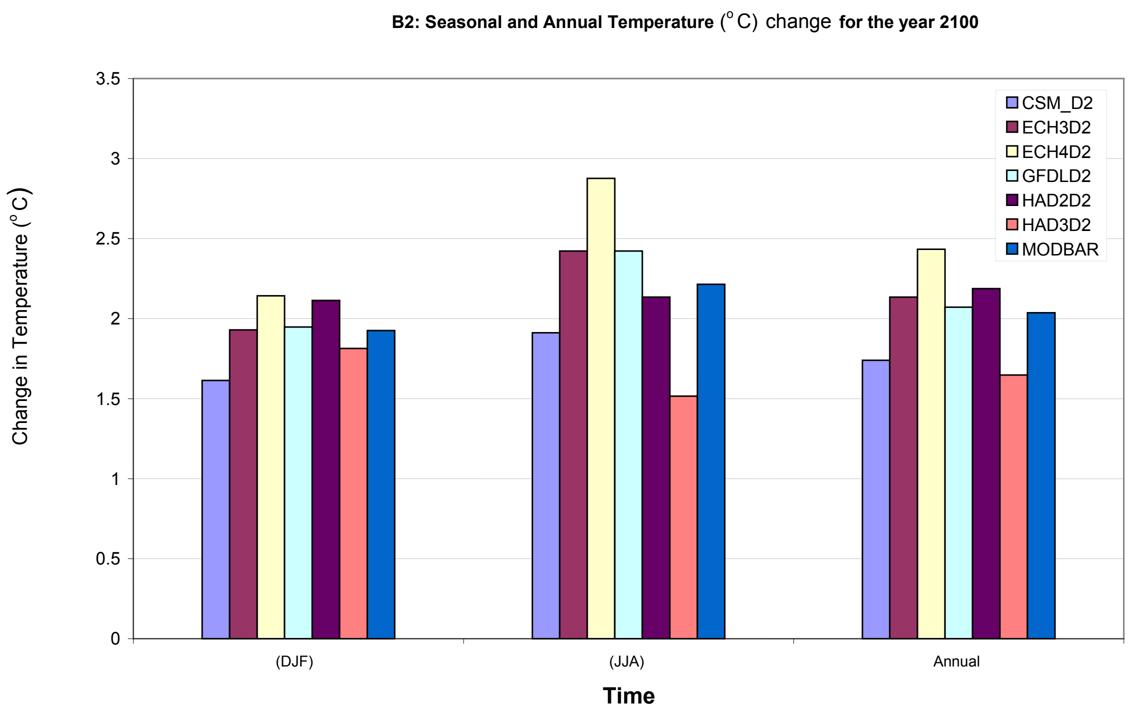

Fig 6.2.4: Change in seasonal and annual mean temperatures (°C) for the year 2100 (Aldabra area, Seychelles)

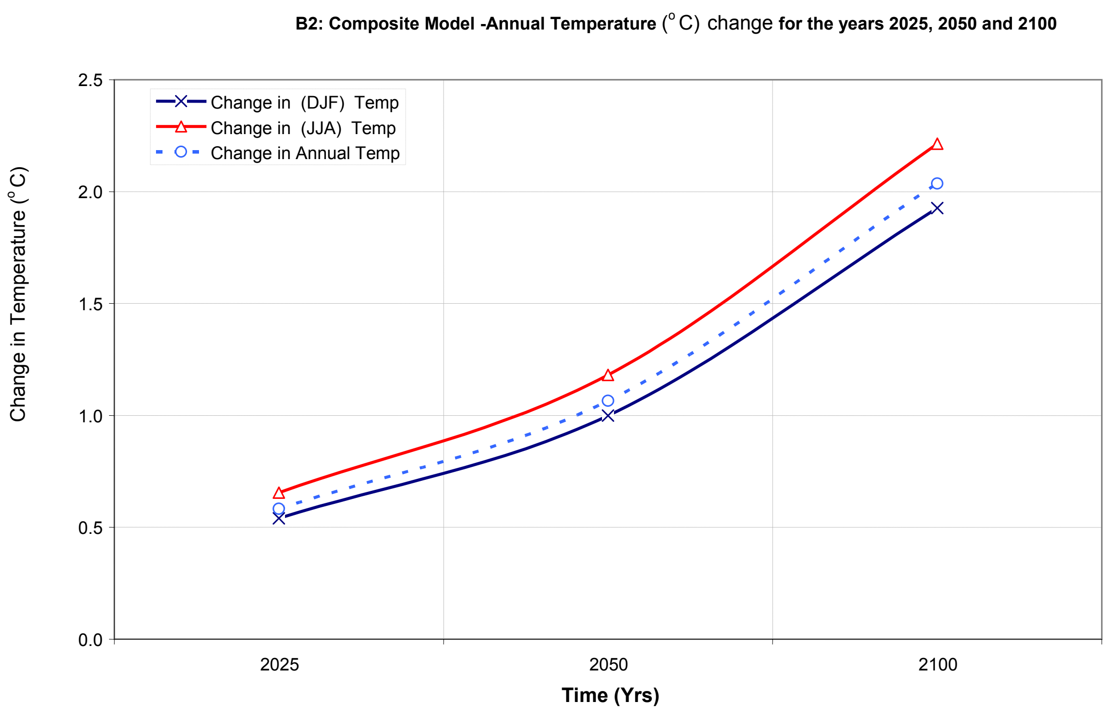

Fig 6.2.5: Composite model of seasonal and annual change in mean temperature (°C) for the years 2025, 2050 and 2100 (Aldabra area, Seychelles)

Chapter 7

General Circulation Model (GCM) and Statistical Regional Climate Change

7.0 GCM and Statistical Regional Climate Change

In this section, the GCM-Guided Perturbation Method (GPM) for regional climate change scenarios developed by Hewitson, University of Cape Town and the Regional Climate-Change Projection from Multi-Model Ensembles (RCPM) developed by the National Center for Atmospheric Research (NCAR) and the University Corporation for Atmospheric Research (UCAR) are investigated as other possible results for integration in the assessment.

7.1 GCM-Guided Perturbation Method (GPM) for Regional Climate Change

7.1.1 Rainfall changes

GPM is not a GCM downscaled methodology, but it does represent a regional scale perturbation in accord with the GCM first order response to greenhouse gas forcing. Consequently, this allows one to undertake an assessment of fundamental regional sensitivities to climate change, in a manner that is not arbitrary, but guided by GCMs. The climate scenario selected is for the A2 and B2 emission scenario. The GCMS are also slightly different. The time resolution is at a monthly time scale. Only the results for the year 2100 are presented here. The overall objective is to explore differences in the climate trends. Figure 7.1 shows the A2 GCMs monthly rainfall for the year 2100. The NACR-CSM GCM-Guided Perturbation Method (GPM) shows peak rainfall anomaly from November to February for the A2 scenario (Fig 7.1), but for the B2 emission (Fig 7.2), the NACR-CSM model output is significantly different to the rather constant rainfall anomaly of between 20-40 mm for all the months. In contrast, the NACR-PCM shows peak positive rainfall anomaly in February but gradually decreases towards December. In the case of the B2 emission scenario the trend apparently reverses with peak rainfall in December. Overall, the NACR-PCM and NCAR-CSM GCM-Guided Perturbation Method (GPM) show large positive anomaly in rainfall; indicating wetter-like climate for most of the months especially during the rainy season. The dry season is projected to be slightly wetter than normal. Apart from the NACR-PCM and the NCAR-CSM, all the GCM-GPM tend to project very small rainfall departures from the mean rainfall. The rainfall anomaly for both the A2 and B2 scenarios between the NCAR-PSM and the NACR-CSM GCM-Guided Perturbation Method (GPM) are found to have large deviations in predicted rainfall compared to the other four models. It is also suspicious to observe that there is no predicted decrease in rainfall for all the months. The GCM-GPM method portrays the complete absence of droughts with future green house induced climate changes.

7.1.2 Temperature changes

On further examination, the projected maximum and minimum temperature reveals that the southeast monsoon (JJA) would become warmer than the northwest monsoon (DJF), with the exception of the NACR-CSM GCM-Guided Perturbation Method (GPM) output. The NACR-CSM GCM-Guided Perturbation Method is not available for the B2 emission scenario. This simply implies a total shift in the seasonal temperature patterns. However, it is unclear why the normal rainfall peaks do not shift to be in phase with the projected seasonal thermodynamic shift. Thus, only the output from the NACR-CSM can be considered meaningful.

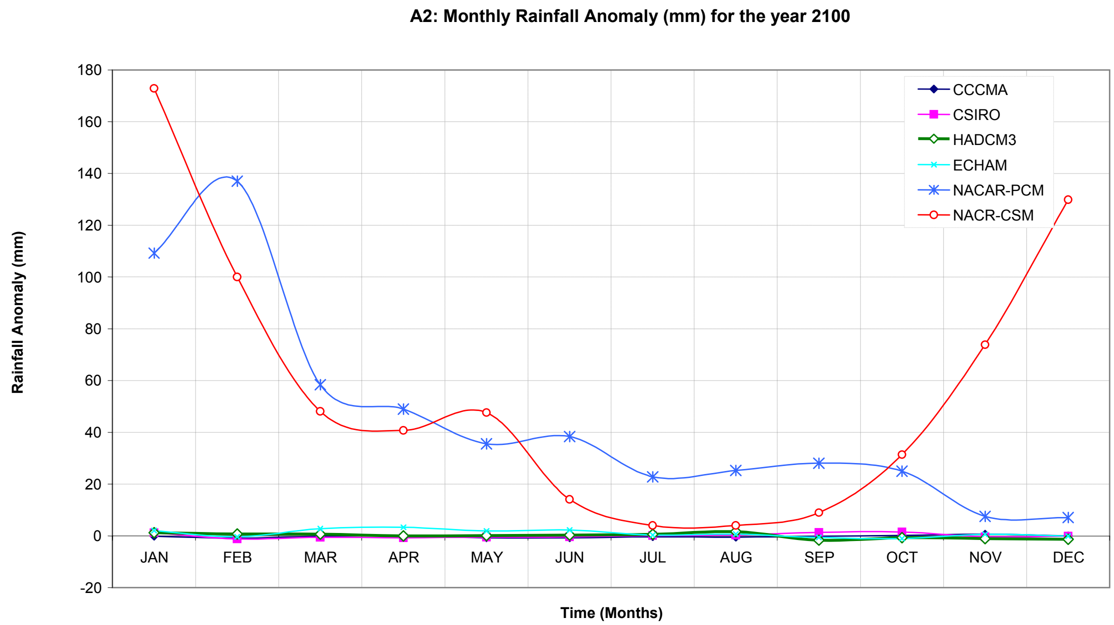

Fig 7.1: A2 GCMs monthly rainfall anomaly (mm) for the year 2100

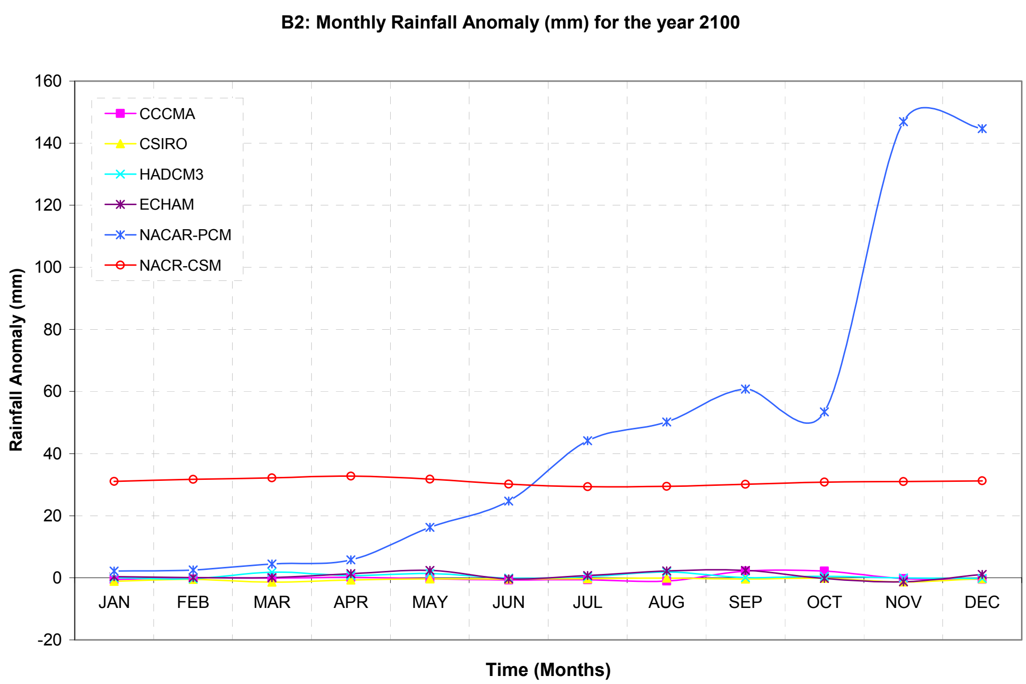

Fig 7.1.2: B2 GCMs monthly rainfall anomaly (mm) for the year 2100

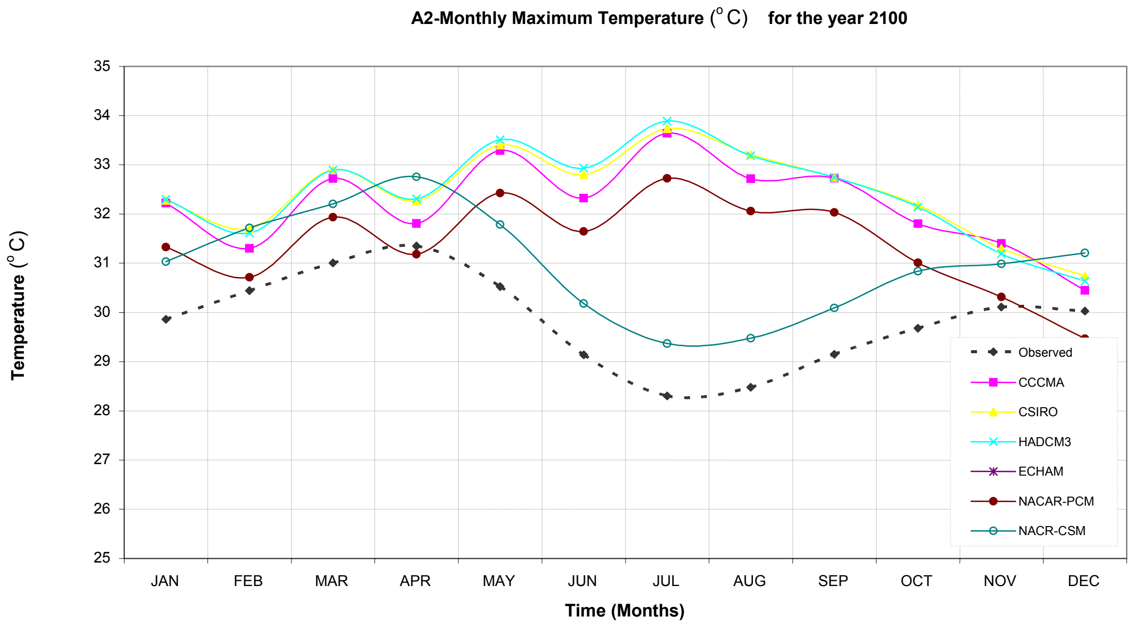

Fig 7.2.1: A2 GCMs monthly maximum temperature (°C) anomaly for the year 2100

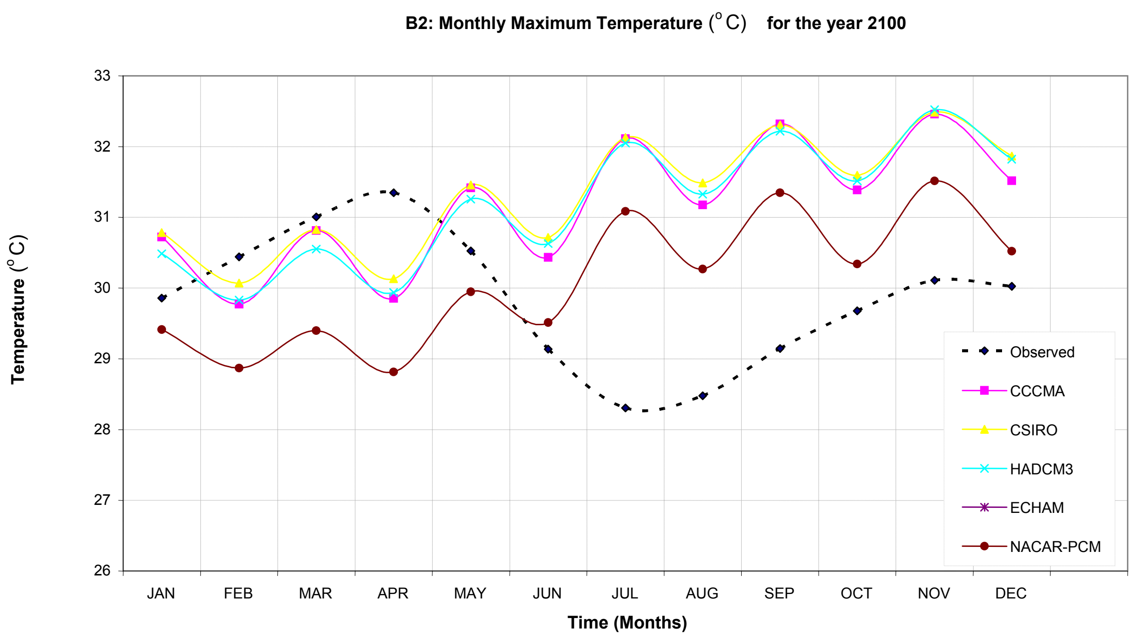

Fig 7.2.2: B2 GCMs monthly maximum temperature anomaly (°C) for the year 2100

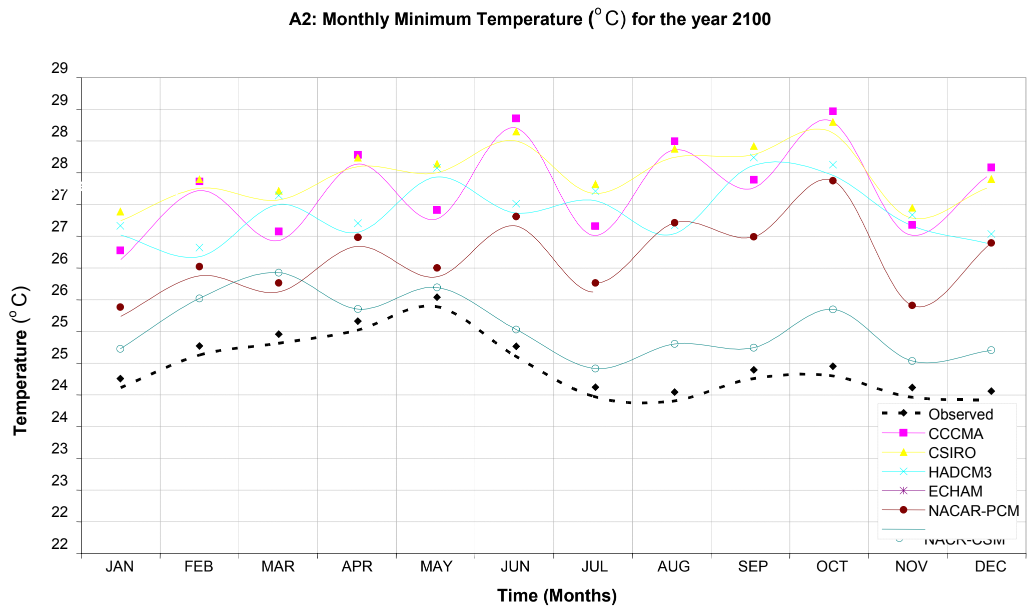

Fig 7.2.3: A2 GCMs monthly minimum temperature anomaly (°C) for the year 2100

7.2 Regional Climate-Change Projection from Multi-Model Ensembles (RCPM)

7.2.1 Rainfall changes

Regional Climate-Change Projection from Multi-Model Ensembles (RCPM) is a statistical analysis of the projections made by different climate models. The Bayesian statistical model is used to synthesize the information in an ensemble of global climate models (GCMs) into a probability density function (PDF) of change in temperature or precipitation for a given geographic region. The PDF describes the likelihood that an unknown variable will take on a value found within a particular range as described in chapter 1.

Figure 7.3.1 shows the DJF season PDF curve for the year 2030. It is fairly well distributed but slightly positively skewed with a peak probability of 0.45 (45%) and an increase in precipitation ranging up to +0.8 mm per day. This suggests slightly wetter climate for the year 2030. The probability of a decrease in precipitation rates from -1 to -2 mm per day is less than 0.2(20%). On the other hand, the probability of an increase in precipitation rate exceeding +1 mm per day is less than 0.3(30%).

The JJA season PDF curve has a peak probability of 0.55(55%) for an increase in rainfall up to +0.5 mm per day (Fig 7.3.2). A slightly wetter climate pattern is projected for the year 2030; however, the PDF is also characterized by a secondary maxima with probabilities ranging from 0.18 (18%) to 0.10 (18%) for a decrease in precipitation rate ranging from -1.0 to -1.5 mm per day.

Figure 7.3.3 shows the DJF season PDF for the year 2050. It is also fairly well distributed but skewed slightly to the right with a peak probability of close to 0.5 (50 %) for increased rainfall rates up to +0.7 mm per day. The probability of a decrease in precipitation rate exceeding -1 mm per day is less than 0.1(10%). On the other hand, the probability of increasing precipitation rate exceeding +1 mm per day is less than 0.3 (30%).

The PDF curve for the JJA season shows a peak probability of 0.58 (58%) slightly centered between -0.2 and 0.2 mm per day (Fig. 7.3.4). Thus, the JJA season precipitation change in rainfall is rather not clear.

Figure 7.3.5 shows the DJF season PDF curve for the year 2090. There is a clear shift in the probability distribution towards the positive side. There is a peak probability of 0.48 (48%) for increase precipitation rate up to +1.0 mm per day. The probability of increasing precipitation rate exceeding +1.0 mm is lower than 0.4 (40%). On the other hand, the probability of a decrease in precipitation rate of -1.0 mm is less than 0.15(15%).

In the case of the JJA season, the PDF curve has a peak probability of 0.55(55%) for a decrease of up to -0.2mm per day (Fig. 7.3.6). There is a tendency for dryer conditions at much lower probabilities. The PDF area on the left or negative side of the curve is larger than that on the right. This implies the JJA season is projected to become drier by the year 2090, but with low probabilities.

Figures 7.4.1 to 7.4.2 show that the peak of the PDF curve is well shifted to the right with a high probability of 0.8 (80%) for an increase in rainfall exceeding +0.5 mm per day from the years 2030 to 2100. For instance, the probability for an increase in precipitation of 1mm per day is 50 % while for a decrease of -1mm it is close to zero. Therefore, it is very likely that the climate will be wetter by the year 2100.

7.2.2 Temperature changes

Probability density functions are normalized so the area under the curve integrates to 1. It is only meaningful to speak of probabilities for a range of possible values (e.g. 60% probability of warming *between 2 and 4* ^{o}C*)* rather than for a single value. Thus, the DJF season of 2030 shows a 50% probability of warming between +0.5 and +1.2 ^{o}C while the JJA season (Fig. 7.5.2) PDF curve shows an 80% probability of warming between +0.6 and +1.2 ^{o}C. In the case of the year 2050, the DJF and JJA seasons PDF curves show an 80% probability of warming between +1.1 to +1.7 ^{o}C (Fig. 7.5.3 and 7.5.4). The DJF season (Fig. 7.5.5) and the JJA season (Fig 7.5.6) PDF curves for the year 2090 show 80 % probability warming between 2.2 and 2.7 ^{o}C.

The annual PDF curves show a 60% probability warming between +0.5 and +1.3 ^{o}C, +1.0 to +1.7 ^{o}C, and +2.0 to +2.7 ^{o}C for the years 2030, 2050 and 2090 respectively (Fig. 7.5.7 to 7.5.9).

The subsequent chapter is an important chapter focusing on uncertainties in constructing climate change scenarios

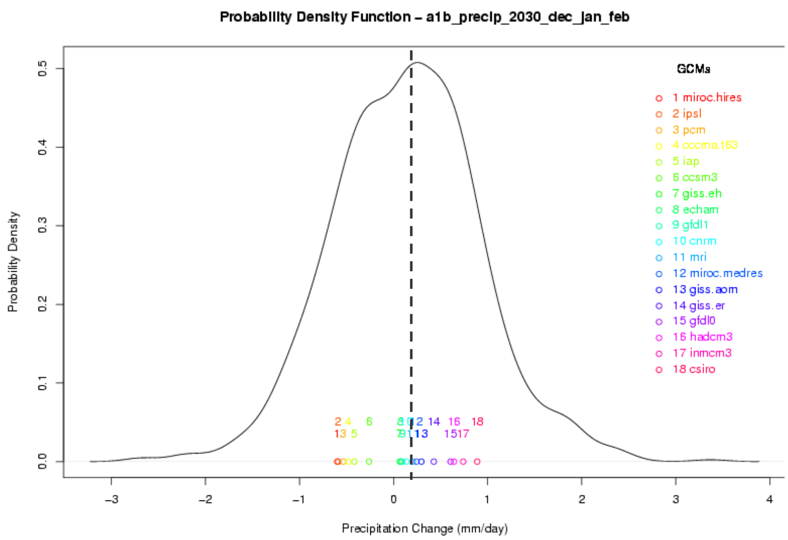

Fig 7.3.1 Probability density functions of precipitation change (mm per day) for the DJF season for the year 2030

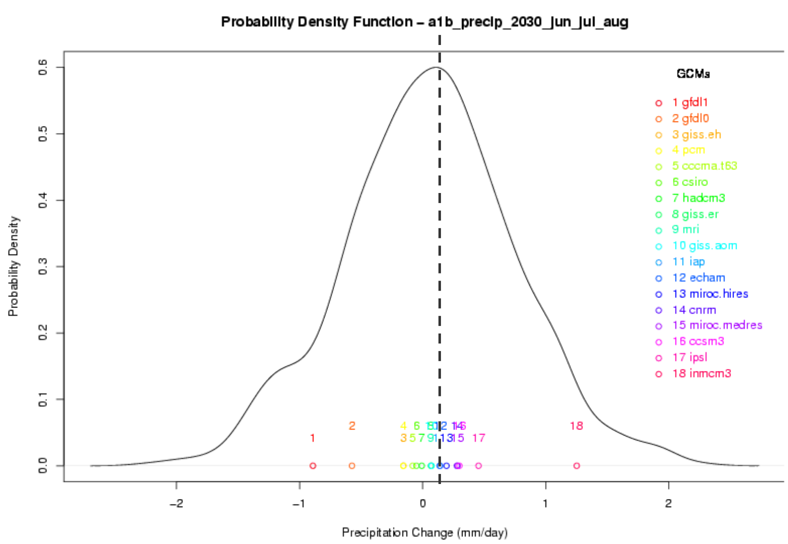

Fig 7.3.2 Probability density functions of precipitation change (mm per day) for the JJA season for the year 2030

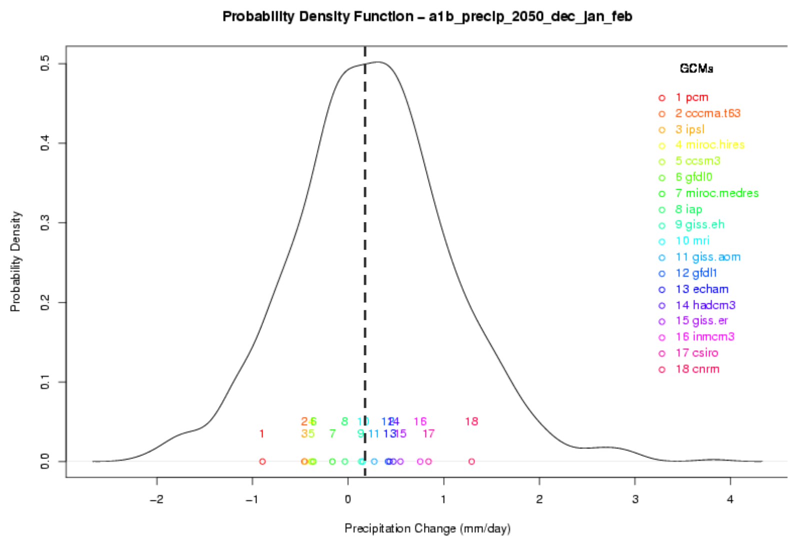

Fig 7.3.3 Probability density functions of precipitation change (mm per day) for the DJF season for the year 2050

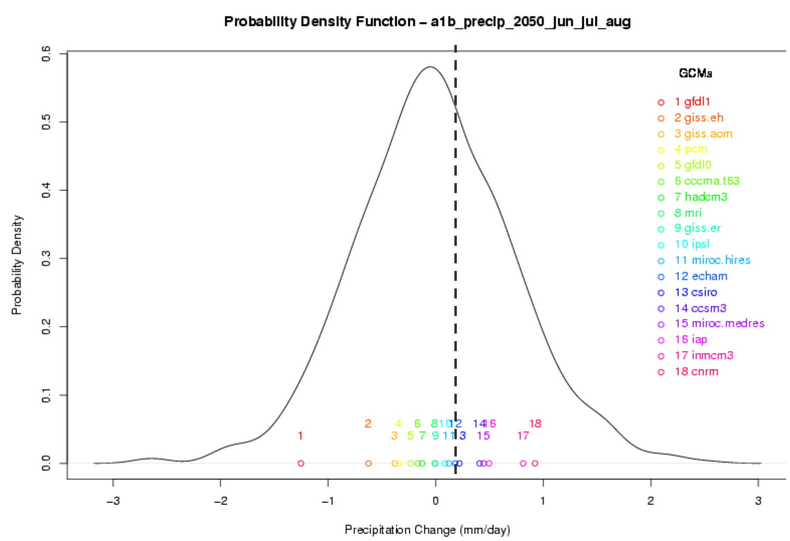

Fig 7.3.4: Probability density functions of precipitation change (mm per day) for the JJA season of the year 2050

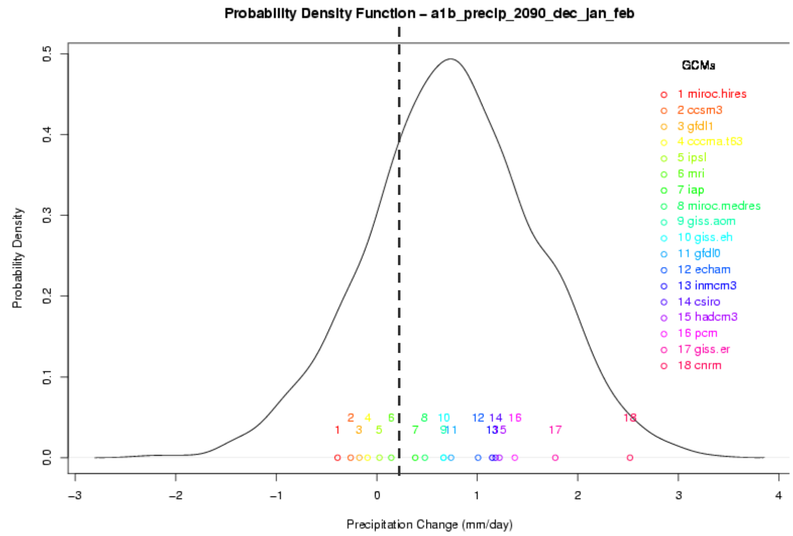

Fig 7.3.5: Probability density functions of precipitation change (mm per day) for the DJF season for the year 2090

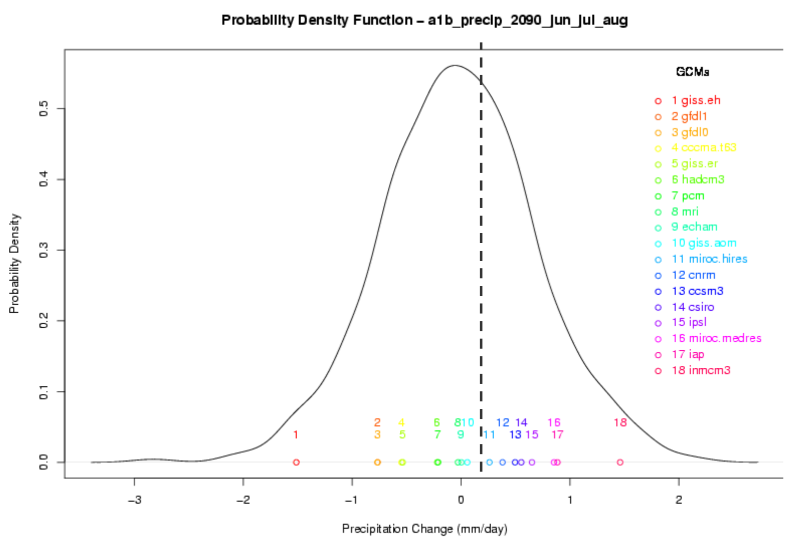

Fig 7.3.6 Probability density functions of precipitation change (mm per day) for the JJA season for the year 2090

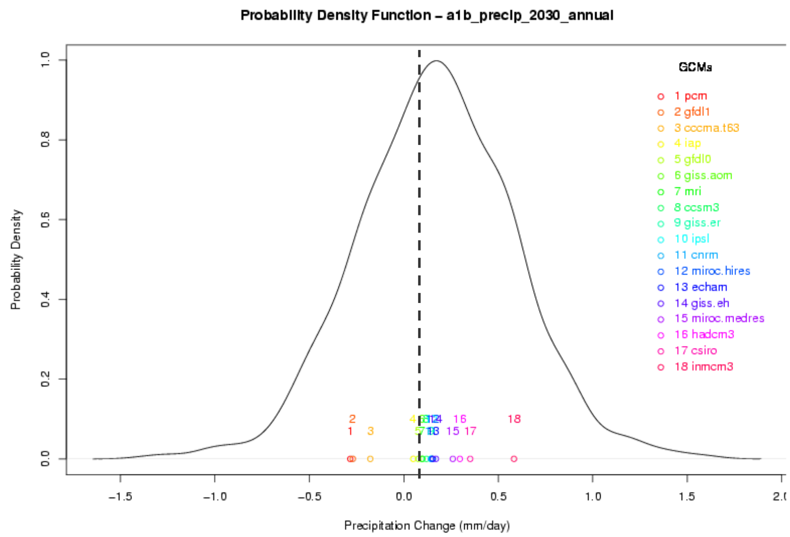

Fig 7.4.1 Probability density functions of annual precipitation change (mm per day) for the year 2030

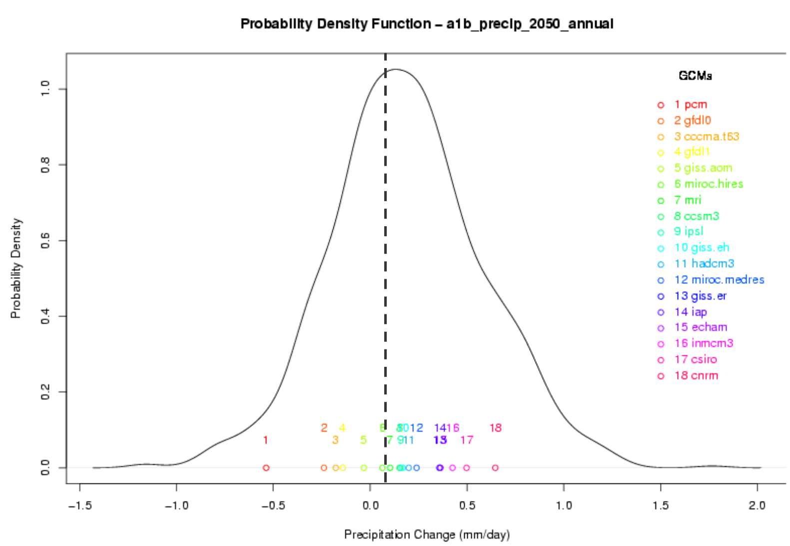

Fig 7.4.2 Probability density functions of annual precipitation change (mm per day) for the year 2050

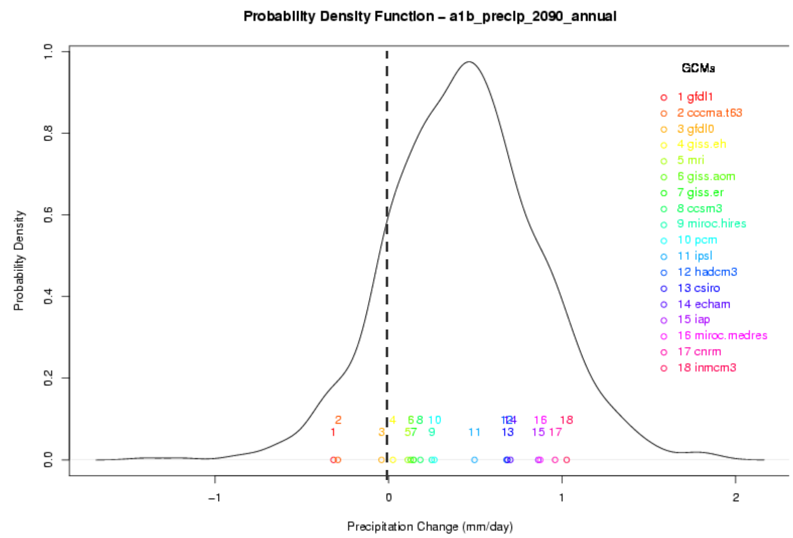

Fig 7.4.3 Probability density functions of annual precipitation change (mm per day) for the year 2090

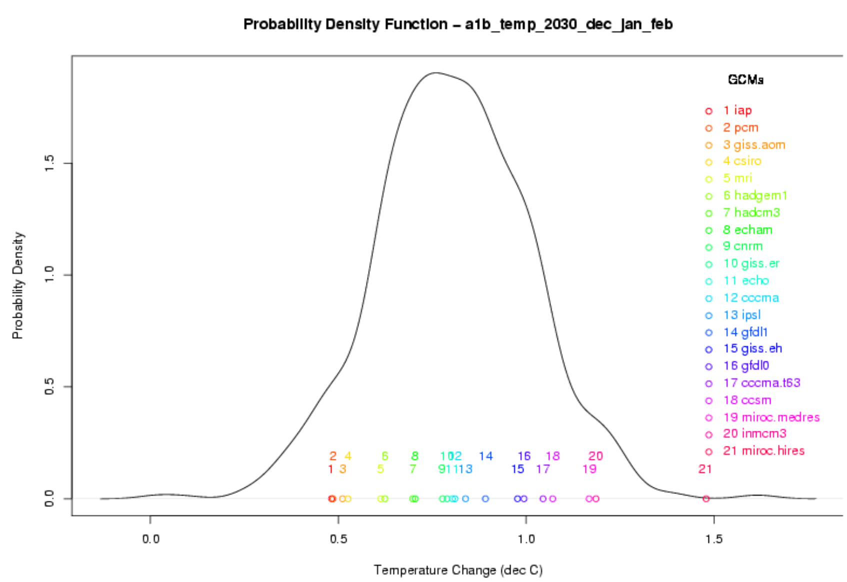

Fig 7.5.1: Probability density functions of the DJF season temperature change (^{o} C) for the year 2030

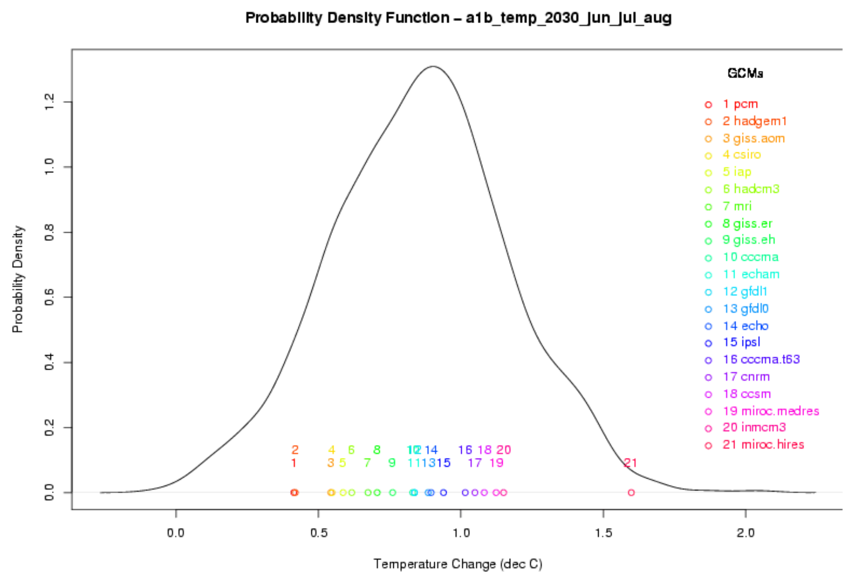

Fig 7.5.2: Probability density functions of the JJA season temperature change (^{o}C) for the year 2030

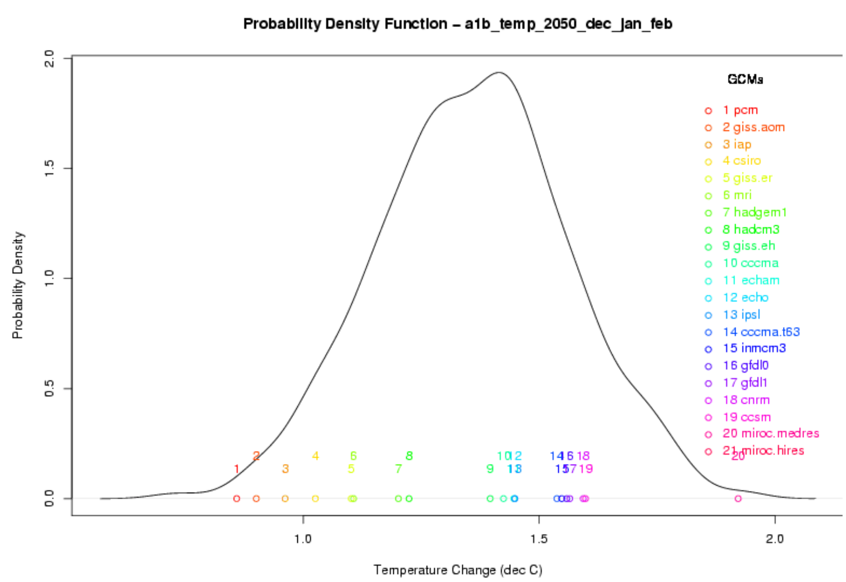

Fig 7.5.3: Probability density functions of the DJF season temperature change (^{o}C) for the year 2050

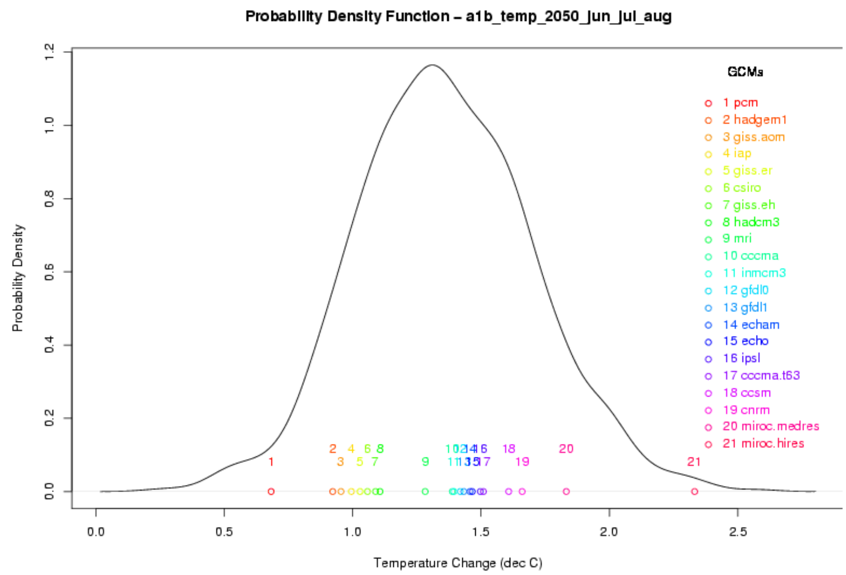

Fig 7.5.4: Probability density functions of the JJA season temperature change (^{o} C) for the year 2050

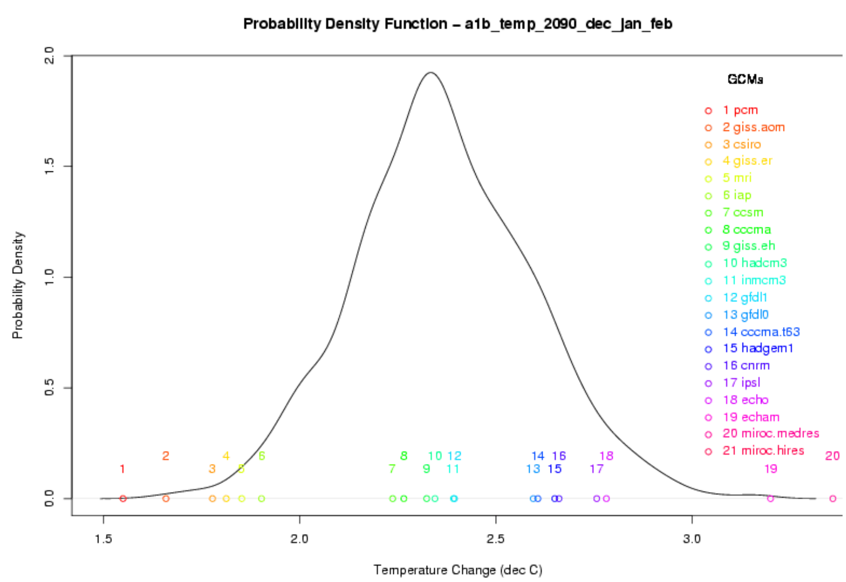

Fig 7.5.5: Probability density functions of the DJF season temperature change (^{o} C) for the year 2090

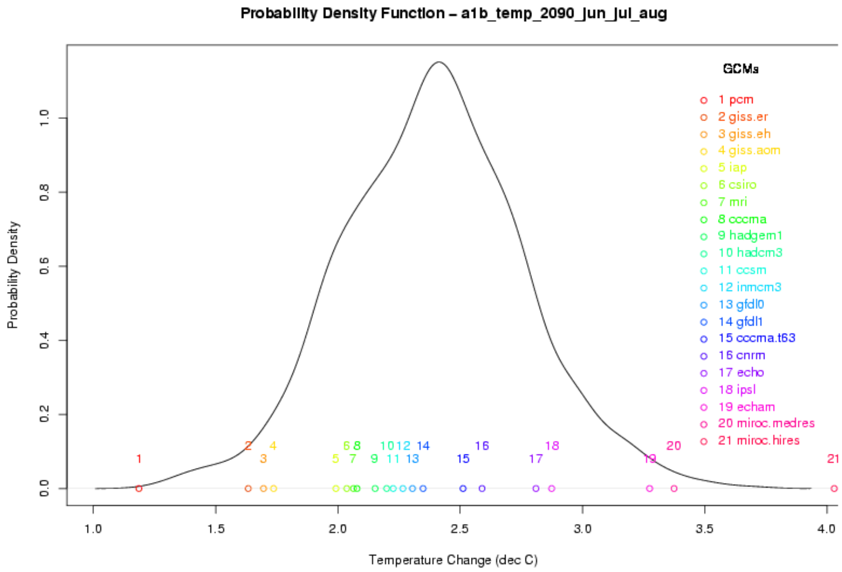

Fig 7.5.6: Probability density functions of the JJA season temperature change (^{o}C) for the year 2090

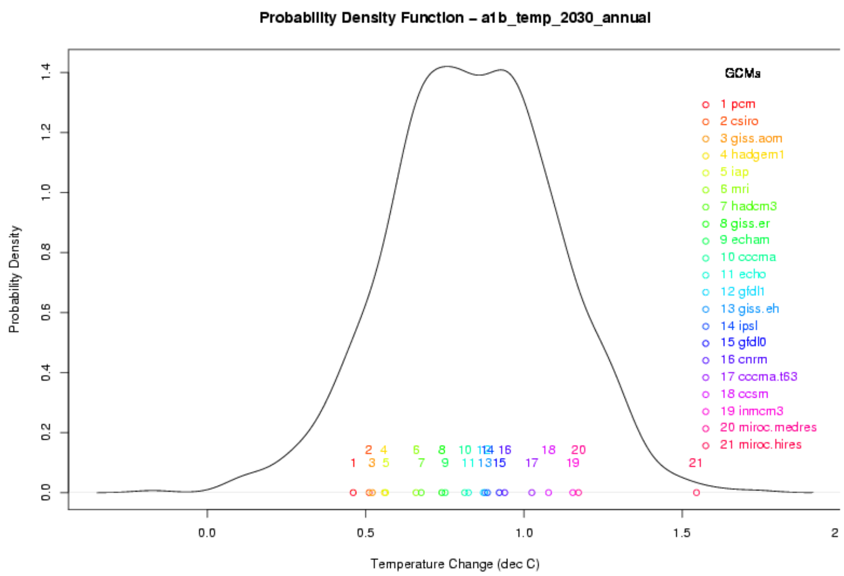

Fig 7.5.7: Probability density functions of the annual temperature change (^{o}C) for the year 2030

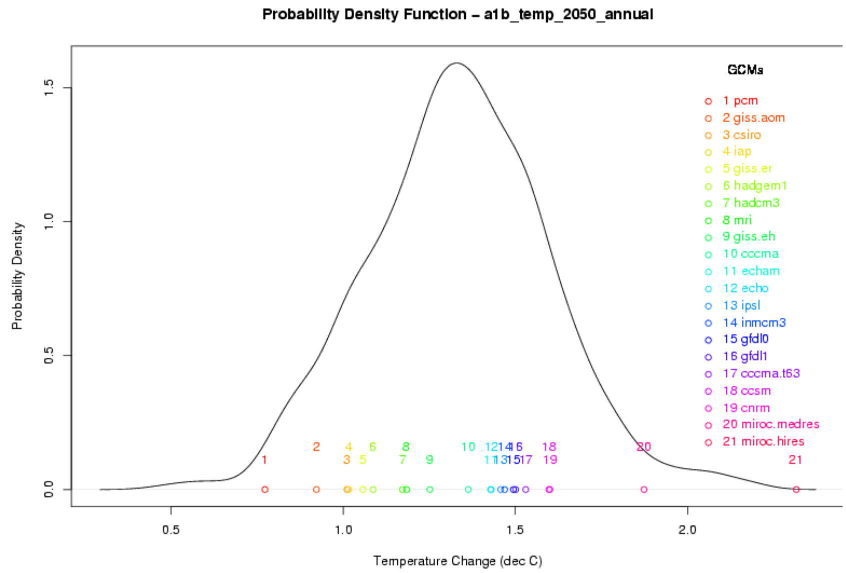

Fig 7.5.8: Probability density functions of annual temperature change (^{o}C) for the year 2050

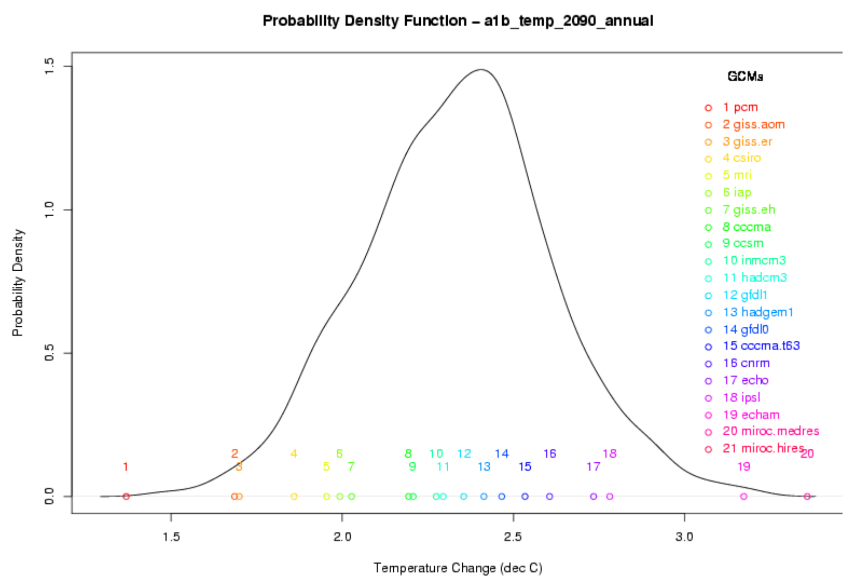

Fig 7.5.9: Probability density functions of annual temperature change (^{o}C) for the year 2090

Chapter 8

Scenario Uncertainties

8.0 Scenario Uncertainties

As indicated in the previous chapters, one is able to make a number of decisions concerning the emission scenarios, the model parameters, and the spatial pattern of climate change used in the construction of the climate change scenarios. These decisions will govern the magnitude, the spatial pattern and the range of climate changes represented in the output scenarios. These options involve some of the current uncertainties in climate change science and its prediction. The uncertainties driving the scenarios in MAGICC /SCENGEN are the emission scenarios, the carbon cycle, the aerosols radiative forcing, the climate sensitivity and the regional climate change. However, in this section, emphasis is on uncertainties in regional climate change patterns and uncertainties related to the GCM selection. It is recalled that in chapters 2, 3 and 4 comparisons of different model results were shown for the changes in the area patterns for seasonal and annual precipitation and temperature. Thus, the assessment has already accounted largely for model differences in simulating changes in area patterns. It is very important to critically look at scenario uncertainties. Very often many fail to address and understand this scientific component. The cost of failing to address climate scenario uncertainties obscures our capacities to understand and respond correctly to the process. It is therefore simply incorrect to claim that the climate will be dryer, wetter, warmer or colder without addressing scenario uncertainties. It is noted that one of the major successes of the IPCC Fourth Assessment Report (FAR) is its advancement in understanding climate uncertainties. Probabilistic likelihood methods were used widely in FAR to convey the uncertainty levels for the benefit of policy and decision makers. Therefore, an assessment of the likelihood levels is explored. Another issue is the variability and the divergence of climate models. As an example, policy makers are often perplexed by the large differences between individual model climate-change results at the regional level. Information like this can help to define adaptation strategies that are robust to such uncertainties.

Thus, the following investigations are carried out to address some of the issues in a simple but comprehensive manner:

1. To investigate changes in variability;
2. To quantify uncertainties in terms of inter-model differences;
3. To asses climate change and give probabilistic outputs.

8.1.1 Change in variability for the Mahe Area

In this section the changes in variability (expressed in SCENGEN in terms of percentage changes in inter-annual standard deviation) in the selected grid box is investigated. This is done by averaging all models to create a composite mean (Fig 8.1.1). In summary, the percentage change in rainfall variability is -2.5 % to +2.5 % on an annual basis, -2.5% to +10 % for the DJF season and 0 to -10 % for the JJA season for the year 2025. The changes in rainfall variability are -5% to 10% annually, -5 % to -15% in the DJF season and 0 to -15 % in the JJA season for the year 2050. For the year 2100, the changes in variability are -15 % to 10 % annually, -15% to +25% for the DJF season and 0 to -15% for the JJA season.

In simple terms, most of the cells within the selected grid box show that, on average, changes in variability are rather small with a magnitude of less than 15% and tend to have the same trends as found in the earlier chapters. This does not mean that individual models all show small changes in variability (a fact that one can verify by selecting individual models). Rather, the low variability changes arise from the fact that different models give quite different results for the patterns of change in annual precipitation variability, and the individual extremes tend to cancel out. Only the DJF season of the year 2100 shows significant changes in variability which amount to 25 %. Thus, the relatively large variability of 25% suggests that models tend to converge or agree with slightly higher confidence compared to the rest for an increase in rainfall for the DJF season for the year 2100.

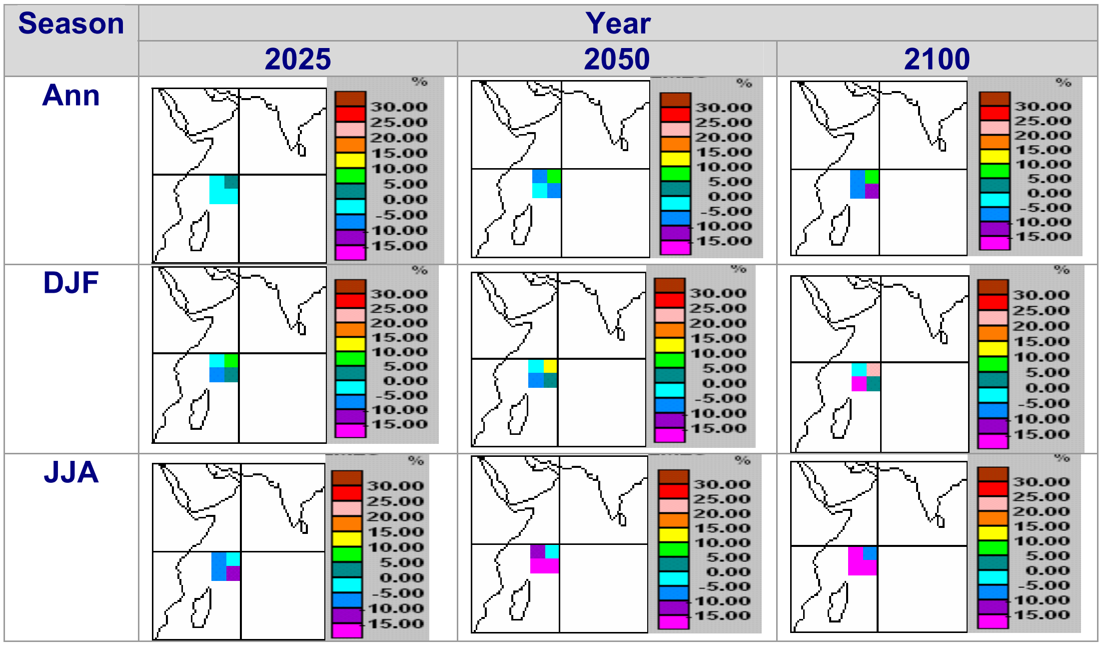

Fig 8.1.1: Change in spatial rainfall variability by season and year for the projected years 2025, 2050 and 2100 for the Mahe area

The model-to-model pattern correlations for normalized variability change fields for the selected models (variable and season) are analyzed, but not shown here. It provides a quantitative verification of change variability. In the case of the precipitation-change fields it is found that models do have some disagreements.

The seasonal comparison of model-to-model pattern correlations shows that the ECH4 and the HAD3 tend to disagree with the other models. In this case negative cross- correlations ranges between –7 and -86 %, but with mean negative value less than 50 %. HAD2 climate model pattern is negatively correlated with the other models, including the HAD3 at an annual time scale.

It is recalled from Tables 3.1 and 3.2 in chapters 2 and 3 that ECH3 model consistently predicted the lowest percentage change in rainfall (+0.6 %, -0.3% and +5.6 %) while HAD2 consistently predicted the maximum change in rainfall(+5.9 %, +9.3 % and +12.4 %) for the DJF season of the years 2025, 2050 and 2100 respectively. On the other hand, for the JJA season, HAD3 model frequently predicted the lowest change in rainfall (-12.7%, -7.7% and -36.3 %) while ECH4 model predicted mostly the maximum change in rainfall (+2.3% and +14.9%) for the years 2025 and 2100 respectively. On an annual basis, the ECH4 model predicted peak rainfall while HAD3 projected lowest rainfall percentages. Thus, it is apparent that the ECH4 model tends to predict maximum rainfall changes while HAD3D predicts the lowest change in rainfall.

8.1.2 Model Error for the Mahe area

The next step is to demonstrate model validation which involves comparing model baseline with observed data. In the example below, model errors in simulating present-day patterns of precipitation relative to the observed climate, for the seven models are further assessed. Table 8.1.1 shows the pattern correlations, the spatial root-mean-square error, and the spatial-mean error for all the selected models for the Mahe area. It is found that ECH3 and ECH4 have the lowest root-mean-square error (RMSE) and mean difference in simulating current climate patterns with observed climate at an annual scale. ECH3 also turns out to be more skillful in predicting present DJF season rainfall, but the MODBAR and the CSM followed by ECH4 models tend to have least error in simulating the JJA seasonal rainfall. This simple assessment provides a benchmark of the initial model performance with respect to various time scales i.e one model can perform better during the southeast monsoon(dry season) and less so in the northwest monsoon(rainy season) etc.

	Annual			DJF			JJA		
Models	**R**	**RMSE**	**Mean Diff**	**R**	**RMSE**	**Mean Diff**	**R**	**RMSE**	**Mean Diff**
CSM_TR	0.81	4.309	-4.273	0.933	10.931	-10.902	0.871	0.672	0.02
ECH3TR	0.367	1.134	0.607	-0.322	2.065	-0.065	0.62	1.189	0.817
ECH4TR	0.624	1.382	-0.845	0.666	2.926	-2.273	0.693	1.043	0.585
GFDLTR	0.228	1.512	1.07	-0.117	2.521	1.125	0.971	1.242	1.005
HAD2TR	0.968	2.074	-2.005	0.801	2.152	-1.892	0.533	-2.495	2.132
HAD3TR	-0.036	1.654	-1.158	-0.244	3.986	-3.277	0.509	1.378	1.013
MODBAR	0.645	1.338	-1.1	0.534	3.239	-2.881	0.952	0.645	0.218

Table 8.1.1: Model validation pattern correlations (R), the spatial root-mean-square error (RMSE), and the spatial-mean error (Mean Diff) for the selected models for the Mahe area.

8.1.3 Probability of Increase in Precipitation for the Mahe area

The probability of an increase in precipitation is determined by comparing the model-mean change with the inter-model standard deviation. The output map (Fig 8.1.2) is displayed below. Normally, regions with $P \geq 0.95$ indicate a high probability of an increase in precipitation. This normally occurs at the mid to high latitudes of both hemispheres. Regions with $P \leq 0.05$ indicate a high probability of a precipitation decrease. These regions are restricted mainly to the subtropical highs, where precipitation is already low. The probability of an increase in rainfall ranges from 0.5 to 0.8 (50-80%) on an annual basis and 0.6 to 0.7(60-70%) for the DJF season. Thus, it is likely that the rainfall in the DJF season and the annual rainfall will increase. The probability of change in rainfall for the JJA season varies from 0.2 to 0.4 (20-40%) (Fig.8.1.2). A statistician might claim that the only significant results are when $P \geq 0.95$ or $P \leq 0.05$. From a practical point of view, however, these probabilistic results are much more valuable. What this means is that a precipitation decrease is from three to four times more likely than a precipitation increase, based on all 7 models in the SCENGEN data base. Thus, a decrease in rainfall is more likely over the Mahe area for the JJA season and unlikely to increase in the JJA season.

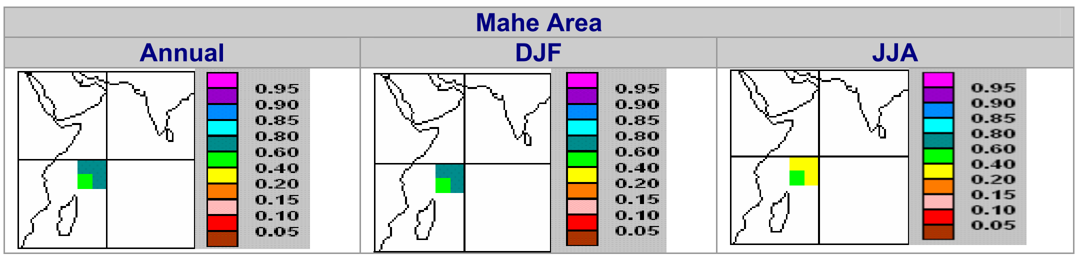

Fig 8.1.2: Probability of an increase in precipitation for the DJF, JJA seasons and annually for the Mahe area

8.2.0 Aldabra

It was found in chapter 6 that rainfall changes over the Aldabra area were very significant especially during the southeast monsoon (JJA). Individual models performance as simulated by HAD2 shows up to -17.4%, -30.1 % and -44.6 percentage decrease in rainfall as highlighted again here in Table 8.2 and Fig 8.2.0 for the JJA season only. The HAD3, ECH4 and BODBAR models also predict decreasing magnitudes in rainfall. The extreme decrease in rainfall over Aldabra is of great concern and interest as it highlights one of the key questions of the assessment which is to explore and where possible, quantify the vulnerability of various systems and sectors to climate variability and climate change. It is apparent that these identified critical thresholds of regional climate change are perhaps beyond what the Aldabra area ecosystems or sectors may be able to endure leading to un-sustainability of the ecosystems and a possible eventual collapse. It is therefore justifiable to asses and quantify the ‘worse’ case dry season scenario as projected by the models for the Aldabra area.

Models	Year		
	2025 % Change	2050 % Change	2100 % Change
CSM_D2	-1.982	-1.991	8.113
ECH3D2	-7.455	-11.965	-10.599
ECH4D2	-15.405	-26.458	-37.786
GFDLD2	-4.456	-6.5	-0.345
HAD2D2	-17.403	-30.099	-44.618
HAD3D2	-16.532	-28.51	-41.637
MODBAR	-10.539	-17.587	-21.146
COMPOSITE MODEL	-10.5	-17.6	-21.1

Table 8.2.1: GCM model output for percentage change (%) in the JJA season rainfall for the Aldabra area in the year 2100

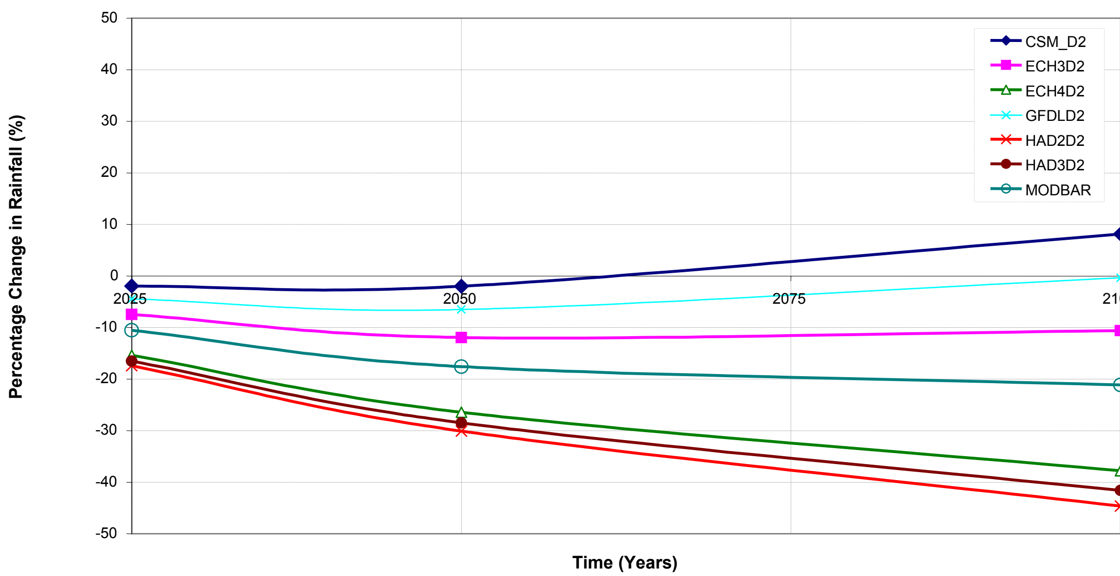

Fig 8.2.0: JJA seasonal percentage change (%) rainfall projections for the Aldabra area

8.2.1 Change in Rainfall variability for Aldabra Area

Figure 8.2.1 shows spatial rainfall variability for the Aldabra area. In brief, the percentage changes in variability show -4 % to +4 % change in variability on an annual basis, -3.5% to +4 % for the DJF season and -2 to -10 % for the JJA season for the year 2025. The changes in rainfall variability are -1% to -5% annually, -5% to +5 % for the DJF season and -5 % to -15 % for the JJA season for the year 2050. For the year 2100, the changes in variability are -2% to -10 % annually, -10% to +12 % for the DJF season and -8% to -32 % for the JJA season.

Most of the cells within the Aldabra selected area show that, on average, changes in variability are rather small with a magnitude of less than 15% with the exception of the JJA season of the year 2100 when the projected rainfall variability is -32%. The low variability changes arise from the fact that different models give quite different results for the patterns of change in annual precipitation variability, and the individual extremes tend to cancel out. The rather large variability of -32% suggests that that models tends to agree for a significant decrease in rainfall for the JJA season of the year 2100.

8.2.2 Model Error for Aldabra area

As discussed earlier, model error involves assessing present-day patterns of precipitation relative to the observed climate. Table 8.2.1 shows the pattern correlations, the spatial root-mean-square error, and the spatial-mean error for all the selected models for the Aldabra area. It is found that MODBAR has the lowest model error (RSME, mean difference) followed by HAD2, GFD, and ECH4 etc at an annual time scale. The best model with the least model error in simulating the DJF season climate is the HAD2, followed by MODBAR, ECH3, and ECH4 etc. The ECH4 turns out to have the lowest model error, followed by HAD3, MODBAR in simulating the JJA season climate patterns. Therefore, since there is compulsion in the fact that the JJA season will be significantly drier, then ECH4, HAD3, and MODBAR, are the general circulation models to emphasize. However, it should be noted that future model stability is not guaranteed.

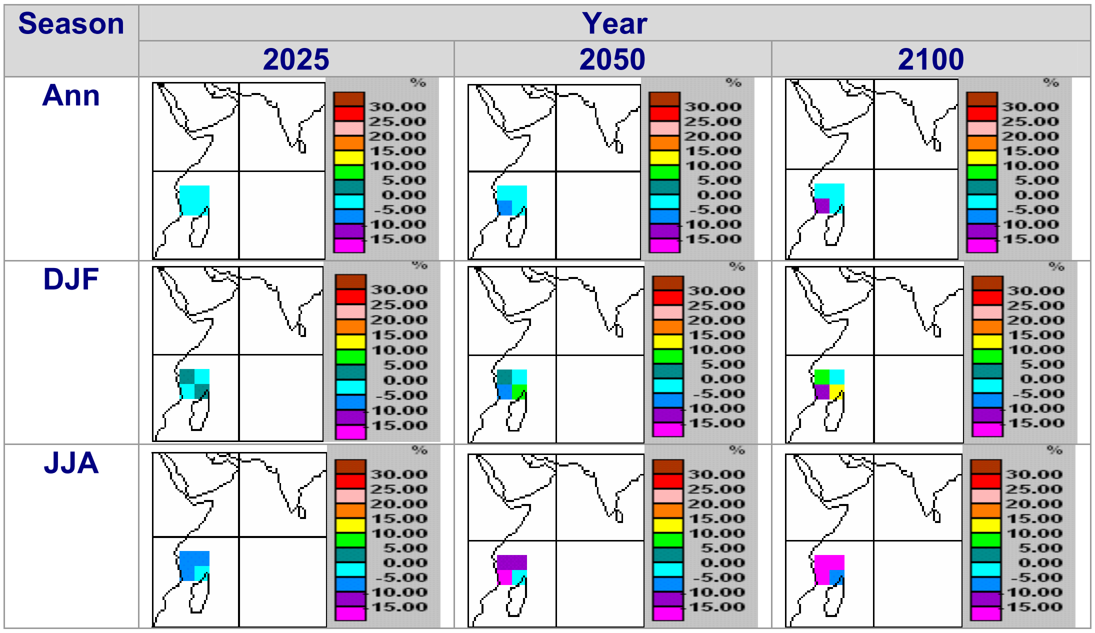

Fig 8.2.1 Change in spatial rainfall variability by season, year and projected years 2025, 2050 and 2100 for the Aldabra area

	Annual			DJF			JJA		
Models	**R**	**RMSE**	**Mean Diff**	**R**	**RMSE**	**Mean Diff**	**R**	**RMSE**	**Mean Diff**
CSM_TR	0.335	1.399	-1.158	0.527	3.578	-2.897	-0.151	0.96	-0.895
ECH3TR	0.583	1.206	-0.853	0.886	1.624	-1.385	0.31	1.547	-1.43
ECH4TR	0.402	0.882	0.767	0.771	2.496	2.135	-0.069	0.442	-0.37
GFDLTR	-0.394	0.874	0.672	0.939	2.887	2.403	0.46	1.121	-1.025
HAD2TR	0.613	0.556	-0.397	0.975	0.98	0.89	0.476	1.396	-1.29
HAD3TR	-0.795	1.012	-0.427	0.338	1.732	0.15	-0.675	0.745	-0.405
MODBAR	0.505	0.468	-0.232	0.881	1.032	0.216	0.41	0.924	-0.902

Table 8.2.1: Model validation pattern correlations (R), the spatial root-mean-square error (RMSE), and the spatial-mean error (Mean Diff) for all the selected models for the Aldabra area.

8.2.3 Probability of Increase in Precipitation

The probability of an annual increase in rainfall is lower than that for Mahe, but closely comparable to the probability of an increase in the DJF season rainfall (Fig 8.2.2). This also means that rainfall is also likely to increase in the DJF season. The probability of change in rainfall for the JJA season varies from +0.2 to +0.3. Alternatively, it is unlikely that rainfall will increase over the Aldabra area in the JJA season. It is more likely that rainfall will decrease over the Aldabra area even when compared to the JJA season rainfall over the Mahe area.

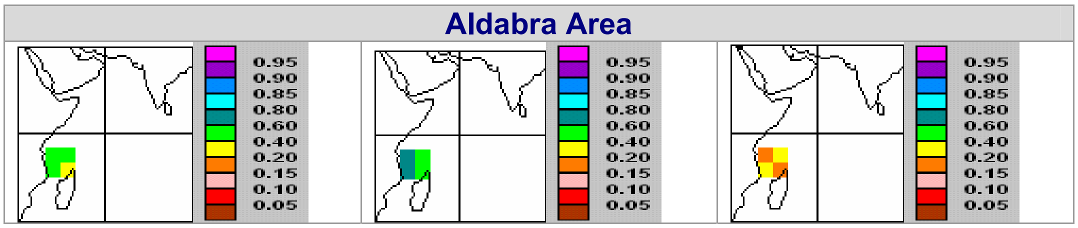

Fig 8.2.2.: Probability of an increase in precipitation for the DJF and JJA seasons and annually for the Aldabra area

Chapter 9

Summary, Conclusion and Recommendations

9.1 Summary

The MAGICC SCENGEN tool is used extensively to construct two climate scenarios for Mahe and the Aldabra area based on the A1 high-range emission with a high climate sensitivity and the B2 mid-range emission with a mid climate sensitivity at seasonal and annual time scales. A range of seven General Circulation Models (GCMs) at 5° (~500 km) resolution are employed to assess the regional climate change patterns. The GCM-Guided Perturbation Method (GPM) and the Regional Climate-Change Projection from Multi-Model Ensembles (RCPM) technique provide an alternative assessment for comparing with the different scenario results. Scenario uncertainties are also explored as a means of quantifying regional climate change patterns and the choice of model selection. This will offer a range of policies and strategies for climate change adaptation. The local parameters assessed are rainfall, maximum and minimum temperatures, and regional sea level.

Mahe Rainfall

Individual GCM output shows a maximum increase in rainfall of +5.9 % (+19 mm) for the year 2025; +9.3 % (+25.4 mm) for the year 2050 and +12.4 % (+38.6 mm) for the year 2100. In contrast, models shows that the JJA season will be characterized by a deficit of -12.7 % (-9.9 mm) in rainfall for the year 2025, but surprisingly rainfall is expected to increase in the JJA season by +22.7 % (+18.4 mm) for 2050. A decrease of -36.3 % (-31.1 mm) is expected for the JJA season in the year 2100. It is not clear what may cause an increase in the JJA season rainfall in the 2050s. However, it may be linked to the upward trend in the multi-decadal 30-year cycle in rainfall variability in the Seychelles (Chang-Seng, 2007).

Similar results are obtained using GCMs composite (average) analyses. The composite change in rainfall for the DJF, MAM, JJA and the SON seasons for the year 2025 is +3.7 %, +2.0 %, -3.3% and +3.8 % respectively. The year 2050 composite change in rainfall for the same respective months is +5.3%, + 4.3%,

+7.3 % and +2.4 %. The year 2100 composite rainfall changes are +4.9%, +10.5%, -10.8 %, and +11.8 % for the DJF, MAM, JJA and SON seasons respectively.
The annual maximum change in rainfall is predicted by the ECH4 model with +4.9 %, +8.5 %, +16.3 % in the years 2025, 2050 and 2100 respectively. The lowest change in rainfall is predicted by the Had3 model with -2.4 %, -4.8 % and -8.6 % respectively for the years 2025, 2050 and 2100. The projected change in average annual rainfall are +1.7 % (+37.9 mm), +2.7 %(+58.2 mm), and 5.5% (+118.7 mm) respectively for the years 2025, 2050 and 2100.

Mahe Temperature

The individual- extreme GCMs scenario of seasonal temperature for the DJF season shows a warming between +0.5 to +0.6 °C for the year 2025; +0.9 to +1.1 °C for the year 2050 and +1.6 to +2.5 °C for the year 2100. The range of temperature warming is from +0.5 to +0.8 °C for the year 2025, +0.8 to +1.6 °C for the year 2050 and +1.6 to +2.9 °C for the JJA season in the year 2100.

On the other hand, the GCMs seasonal average temperature changes for the year 2025 are +0.5 and +0.6 °C respectively. The average temperature warming for these respective months for the year 2050 is +1.0, +1.1 °C and +2.0 and +2.1 °C respectively for the year 2100. The composite temperature pattern also shows warming up to 2100, particularly during the MAM and JJA seasons. This implies the future climate during the southeast monsoon will be characterized by relatively warmer conditions.

The extreme annual warming is predicted by the ECH4 model with +0.7, +1.3, and +2.6 °C respectively for the years 2025, 2050 and 2100. The CSM model shows lower temperature change of +0.5, +0.9 and +1.8 °C respectively for the years 2025, 2050 and 2100. The annual average temperature shows warming of +0.6, +1.1 and +2.1 °C respectively for the above mentioned years.

Comparison between the two Climate Scenarios

In general, the comparison between the two climate scenarios shows clearly that the A1 high-range emission with a high climate sensitivity scenario simulates extreme climate changes compared to the B2 mid-range emission with mid-range climate sensitivity.

The Aldabra Area Rainfall

The Aldabra area extreme seasonal rainfall for the DJF season shows an increase of +7.2 % for the year 2025; +12.6 % for the year 2050 and +19.5 % for the year 2100.The GCMs projection for the JJA season shows a significant decrease in rainfall of -17.4 % for the year 2025, -30.1 % for the year 2050 and -44.6 % for the year 2100. On the other hand, the GCM average simulations of rainfall show a slightly wetter-climate for the DJF season and a significantly dryer climate of up to -21.1 % below normal for the Aldabra area rainfall by the year 2100.

Thus, a major deficit in rainfall is projected for the Aldabra area during the southeast monsoon; however, the annul changes in rainfall for the projected years are not significant. The same results were tested in the case of the P50 emission -business as usual scenario. Individual GCMs show further deficit of -53.7% in the Aldabra area rainfall during the JJA season in the year 2100. Thus, a critical climatic threshold is identified that may threaten the sustainability of the Aldabra ecosystem. Therefore, the Aldabra environmental eco-system is classified as highly vulnerable to climate changes.

Aldabra Area Temperature

The GCMs projected change in extreme seasonal temperature for the DJF season shows warming ranging between +0.5 to +0.6 °C for the year 2025, +0.8 to +1.1 °C for the year 2050 and +1.6 to +2.1 °C for the year 2100. A warming between +0.5 to +0.8 °C is expected for the JJA season of the year 2025, +0.8 to +1.5 °C for the year 2050 and +1.5 to +2.9 °C for the year 2100. On the other hand, the GCMs composite (average) shows relatively warmer temperatures during the JJA season compared to the DJF season. The average temperature changes for the year 2025 are +0.5, and +0.7 °C for the DJF and JJA seasons respectively. The year 2050 temperature changes for these respective months are +1.0 and +1.2 °C. The individual model of seasonal temperature change for the year 2100 is +1.9 and +2.2 °C for the DJF and JJA seasons respectively. The annual extreme temperature warming ranges from +0.4 to +0.6 °C for the year 2025; from +0.9 to +1.4 °C for the year 2050 and from

+2.0 to +2.9 °C for the year 2100. On the other hand, the GCM predicted average temperature warming for the years 2025, 2050 and 2100 are +0.6, +1.2, and +2.6 °C respectively.

General Circulation Model (GCM)-Guided Perturbation Method (GPM)

Overall NACR-PCM and NCAR-CSM GCM-Guided Perturbation Method (GPM) shows significantly wetter-like climate for most of the months, especially during the rainy season. The other models tend to be insensitive and there are large model differences. The GCM-GPM indicates the complete absence of droughts in the future. Most GCM-GPM temperature scenarios show that the southeast monsoon would become warmer than the northwest monsoon (DJF) with the exception of the NACR-CSM model. This suggests a total shift in the temperature patterns. However, the GCM-GPM rainfall scenarios are out of phase with the thermodynamic -temperature scenarios. Thus, only NACR-CSM results should be considered as meaningful.

Regional Climate-Change Projection from Multi-Model Ensembles (RCPM)

The DJF season precipitation rate shows a 45 to 55% chance of up to +0.8 mm per day for the years 2025 and 2050. However, it is not very clear if the JJA season will become dryer or wetter. The associated temperature change shows a 50%-80% *likely* chance of a warming, ranging from +0.5 to +1.2 °C and from +1.1 to +1.7 °C respectively.

In the case of the year 2090, RCPM results suggest close to 50 % chance of an increase in precipitation rate of up to +1.0 mm per day for the DJF season. In contrast, it is *unlikely* (15%) that precipitation rate will decrease for the same period. There is a 55 % chance of a slight decrease in precipitation rate of -0.2 mm per day in the JJA season in the year 2090. On an annual basis, there is a high probability of 80% for an increase in rainfall exceeding 0.5 mm per day from the years 2030 to 2100. Overall, it is *likely* (80%) that the climate will be wetter by the year 2100. There is a *likely* chance (80%) of warming between +2.2 and +2.7 °C in the year 2090 for both seasons. On an annual basis there is a *more likely than not* chance (60 %) for a warming between +0.5 and +1.3 °C, +1.0 to +1.7 °C and 2.0 to +2.7 °C respectively for the years 2030, 2050 and 2090.

Scenario Uncertainties

Climate scenario uncertainties are important for a wide range of policy and decision making. The assessment also includes uncertainties in regional climate change patterns and GCMs selection. There are rather large changes in variability ranging from 25% to 32 % for the two seasons; hence models tend to agree for a wetter DJF season and a dryer JJA season by the year 2100.

The model-to-model pattern correlations for normalized variability change fields for the selected models show some disagreement in terms of the seasonal comparison. ECH4D and the HAD3D tend to have the greater differences with the other models. ECH4 model tends to predict maximum rainfall changes while HAD3D predicts minimum change in rainfall.

Model Error

ECH3 and ECH4 have the lowest model error and mean difference in simulating current climate patterns with observed climate at an annual scale. ECH3 also turns out to have the model with the least error in simulating present DJF season rainfall. In contrast, MODBAR followed by the CSM, ECH4 models have the least error in simulating current JJA seasonal rainfall.

Probability of Increase in Rainfall

It is *likely (*50-80 %) that the DJF season and the annual rainfall will increase and it is *unlikely* to increase in the JJA season (20-40%). The probability of an increase in the Aldabra area annual rainfall is lower than Mahe and it is more *likely* that the Aldabra area rainfall will decrease compared to the Mahe area in the JJA season up to the year 2100.

Regional Sea Level

Thus global sea level is expected rise from 7-8, 15-17 and 35-40 cm respectively according to the policy best guess scenario for the years 2025, 2050 and 2100. The HadCM2 and HadCM3 with the IS92 or P50 business as usual emission scenario shows annual sea level rise ranging from +0.4 to +0.6 meter for the 2070-2100 period.

Tropical cyclone

On the other hand, despite advances in computer numerical modeling of the global climate using various scenarios of greenhouse gas emissions, making projections of how tropical cyclones may change in frequency and intensity remain a significant challenge. Since tropical cyclone activity is modulated by the El Niño Southern Oscillation (ENSO) and wind shear, projections of cyclone frequency will partly depend on the projections of future ENSOs. It is uncertain how ENSO will change in a warmer world. Some studies have suggested that peak winds may increase by 5 to 10 % and peak rainfall rates may rise by 20 to 30 %.

9.2 Conclusion

A1 high range emission and high climate sensitivity simulates more extreme climate changes compared to the B2 mid-range emission with mid-range climate sensitivity (BM). The BM climate scenario shows that the mean air temperature for both Mahe and the Aldabra area is *more likely than not* to warm by +3.0°C by the end of this century. The relative rate of warming will occur mainly during the cooler southeast monsoon. The warming ranges are +0.4 to +0.7; +0.9 to +1.4 and +1.8 to +2.9°C respectively for the years 2025, 2050 and 2100. Consequently, the maximum increase in seasonal rainfall for Mahe is +12.4 %(+38.6 mm) in the DJF season while a decrease of -36.3% (-31.1 mm) is expected during the southeast monsoon of the year 2100. The range of percentage change in annual rainfall is -2.4 to +5.0 %; -4.8 to +8.5 %; -8.6 to +16.3 % respectively for the years 2025, 2050 and 2100. Thus, the rainy season is *more likely than not* to be wetter, while the dry season is *more likely than not* to be dryer with the exception of the JJS season of the year 2050. It is suggested that the projected upward trend in the multi-decadal 30 year-cycle in rainfall variability (Chang-Seng, 2007) could possibly balance the expected deficit during the JJA season of the year 2050 forced by anthropogenic climate changes. Scenario uncertainties methods such as change in model variability and probability of an increase in precipitation analyses support quantitatively that the DJF season will *likely* be wetter while the JJA season is *unlikely* to be wetter and the annual rainfall will *likely* be higher than the 1972-1990 base periods.

The Regional Climate-Change Projection from Multi-Model Ensembles RCPM shows seasonal precipitation rates are *more likely than not* (45-55%) to increase in the rainy season of up to +1.0 mm per day by the year 2100.On an annual basis it is *likely* (80%) that rainfall rate will be greater and equal to +0.5 mm per day.

A critical rainfall threshold of a deficit of -44% (B2 mid-range emission and mid range climate sensitivity) and -53.7 % (P50 business as usual emission) in the JJA season rainfall is identified for the Aldabra area by the year 2100. However, the annual rainfall is unlikely to change significantly. The major deficit in the JJA season by the turn of this century threatens the sustainability of the Aldabra Atoll. Thus, the Aldabra Atoll, one of the world's greatest surviving natural wonders which has remained fairly isolated and preserved (Attenborough, 1995) is now potentially most vulnerable to anthropogenic climate changes in the Seychelles.

The climate can be characterised by *more than likely than not* with more extreme dry, wet, and hot episodes.The increase in precipitation is through the thermodynamic warming and the potential increase in atmospheric water vapour (FAR, 2007). The expected dryness particularly in the JJA season of the year 2100 is likely to be linked to the expected extreme warming in the northern hemisphere which would drive a stronger southeast monsoon, thus inhibiting cloud and rainfall formation in the southwest Indian Ocean.

Model evaluation shows that ECH3 and ECH4 general circulation models have the least error in simulating current climate pattern to observed climate. However, MODBAR model has the least error in simulating the JJA season climate. Overall, model performance is dependent on the choice of time scale selected.

Global sea level is expected to rise from +7-8, +15-17 and +35-40 cm according to the policy best guess scenario by the years 2025, 2050 and 2100 respectively. Regional sea level in the southwest Indian Ocean is expected to rise between +40 to +60 cm according to the UK Meteorological Office model. On the other hand, tropical cyclone scenario remains a major challenge, but recent modeling studies in the US, have suggested that peak winds may increase by 5 to 10 % and peak rainfall rates may rise by 20 to 30 %.

9.3 Recommendations

It is recommended that future climate change scenario assessment should consider higher resolution model to provide more skillful island-type of climate scenarios. It is also envisaged that climate downscaling can be applied to achieve far better results at a national level. Future work should also focus on verifying the ‘critical’ climate changes identified here in this assessment.

A detailed climate change–ecological-environment impact assessment should follow through in the case of the Aldabra area for possible mitigation and adaptation of the impacts.

Reference

Chang-Seng, S. D., 2007: Climate Variability and Climate Change Assessment for the Seychelles, Second National Communication (SNC), Under the United Nations Framework Convention on Climate Change (UNFCCC).

Chang-Seng, S. D., 2005: Marine Weather Systems, Tropical Cyclone Prediction and Impacts in the Southwest Indian Ocean, MSc. Thesis, Department of Geography and Environmental Studies, University of Zululand.

Chang-Seng, S. D., 2002: El Nino and Indian Ocean Dipole Mode and its Impact on Sea Level and Rainfall in the Seychelles, Seychelles National Meteorological Services.

Climate Change, 2007: The Physical Science Base, Summary for Policy Makers. Contribution of Working Group 1 to the Fourth Assessment Report (FAR) of the IPCC, 5th February 2007.

Gray, W., 1984a: Atlantic Seasonal Hurricane Frequency. Part I: El Nino and 30 mb Quasi-Biennial Oscillation Influences. *Mon. Wea. Rev.*, **112**: 1649-1668.

Gray, W., 1984b; Atlantic Seasonal Hurricane Frequency. Part II: Forecasting its Variability. *Mon. Wea. Rev.,* 112: 1669-1683.

Hoareau, K., 1999: La Fréquence des Cyclones Tropicaux Intenses dans le Sud-Ouest de L'ocean Indien (1970-1999). *Publications de l'Association Internationale de Climatologie,* **12**: 405-413.

Hulme. M., Wigley et al, 2000: Using a Climate Scenario Generator for Vulnerability and Adaptation Assessments: Magicc Scengen V2.4 workbook

Jury, M. R., and Parker B. A., 1999: Synoptic Environment of Composite Tropical Cyclones in the South-West Indian Ocean. *S. A. J. Marine Sci.*, **21**: 99-115.

Lajoie, F. R., 2004: WMO/CLIVAR ETCCDMI African Workshop on Extremes, Report for Seychelles

Leuliette, E. W., Nerem. R. S., and Mitchum, G., 2004: Results of TOPEX/Poseidon and Jason Calibration to Construct a Continuous Record of Mean Sea Level, *Mar.Geod,* In Press.

Marguerite., T. M., 2001: Solar activity long term influence on Seychelles rainfall, Meteorological Services, Seychelles